Hydrodynamics of colloids in a narrow channel: An analytical and simulation study

D i s s e r t a t i o n

zur

Erlangung des Doktorgrades(Dr. rer. nat.)

der

Mathematisch-Naturwissenschaftlichen Fakultät

der

Rheinischen Friedrich-Wilhelms-Universität Bonn

vorgelegt

von

Fatemeh Tabatabaei

aus

Teheran

2008

Angefertigt mit Genehmigung der Mathematisch-Naturwissenschaftlichen Fakultät der Rheinischen Friedrich-Wilhelms-Universität Bonn

1.Gutachter: Prof. Dr. Gunter M. Schütz
2.Gutachter: Prof. Dr. U.-G. Meißner

Tag der Promotion: 4th August 2008

Diese Dissertation ist auf dem Hochschulschriftenserver der ULB Bonn unter http://hss.ulb.uni-bonn.de/diss_online elektronisch publiziert

Erscheinungsjahr: 2009

Contents

1 Introduction

1.1 Introduction

Many biological and chemical systems consist of particles under varying degrees of confinement which can affect their dynamical behaviour [1]. There is a wide range of examples of such systems from porous media and nozzles to microfluidic devices [2]. One can also include examples of those processes which are partially confined as the movement of hydrophobic ions in biological channels (see Fig. 1.1), or particle separation and catalysis through microscopic channels of zeolites [3–5].

Sometimes, confinement restricts the motion of the particles to a lower dimension than that of the system. Such dynamics are referred to as "reduced dimensional" dynamics. For example, colloids that are trapped between two planar walls in a three dimensional system, move in effectively two dimensions (quasi-two-dimensional), or a particle in a two dimensional porous medium whose diffusion is a quasi-one-dimensional process.

The effect of confinement on the dynamics of particles in a parallel-wall channel — a quasi-two-dimensional system— has been the subject of many recent theoretical and computational investigations, including studies of the dynamics of rigid particles [6–8], deformable drops [9], and macromolecules [10] in creeping flow. New confinement-induced phenomena such as macromolecular aggregations away from the walls [11] and stability of strongly extended drops in a confined shear flow [10], have been revealed by these studies. Quasi-two-dimensional (Q2D) suspensions have also been investigated experimentally using video-microscopy [12] or optical tweezers [13], e.g. in the investigation of particle dynamics between two walls [14] and in a linear channel [15]. These studies have highlighted flow-mediated effects of the boundaries on particle dynamics. It has been demonstrated that these effects are due to the hydrodynamic interactions in a restricted geometry, which are drastically different from those in a medium without confinement.

Moreover, the collective dynamics of confined mutiparticle systems is reported to be very different from the dynamics of unconfined systems. Consider the ex-

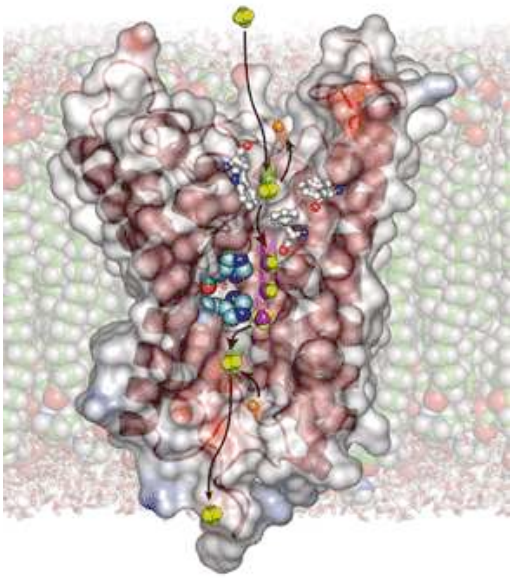

Figure 1.1: A stereo view of membrane proteins which provide molecular-sized entry and exit portals for the various substances that pass into and out of cells. Two vestibules reside at the top and bottom of the channel. Amino acid residues (blue, red, and gray ball-and-stick models) that line the pore of the outer vestibule stabilize $NH4+$ (green and yellow). After a proton (orange) departs, the channel narrows midway through the membrane for a $20 - A^\circ$ distance and is hydrophobic. Here, two pore-lining histidine residues (light and dark blue) stabilize three $NH3$ molecules through hydrogen bonding. Farther on, with the addition of a proton (orange), the molecules return to equilibrium as $NH4+$ in the inner vestibule [16].

ample of the far-field form of the flow which is produced by the particles moving in the channel [17–19]. Confinement causes this flow to differ qualitatively from that in a free space. Differences arise because the fluid-volume has a strong conservation constraint, caused by the presence of the wall and from the fact that momentum vanishes at the wall boundary. Absorption of momentum at the wall makes the velocity field decays too fast to produce a nonzero fluid flux through

the boundary at infinity. Therefore, to ensure fluid incompressibility, the fluid which is displaced by a moving particle forms a dipole flow pattern. In contrast, the momentum in a free space is transferred from the particle to the fluid and diffuses away to infinity. The surrounding fluid moves in the same direction as the particle, without forming a dipole flow pattern. This far-field form of the flow produced by movement of the particles in a channel give rise to specific hydrodynamic interactions, which in turn produce specific collective phenomena of particles in confinement, such as pattern formation and re-arrangement of particle lattice in two-dimensional regular particle arrays [20].

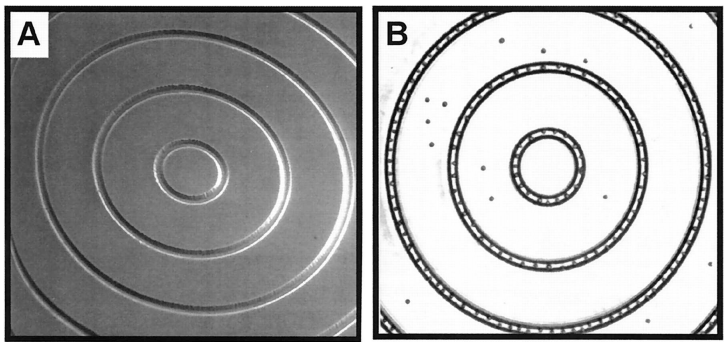

Figure 1.2: (A) Scanning electron microscop image of the 1D trenches fabricated on the photoresist polymer film by photolithography. (B) Optical microscope image of three concentric circular channels with colloidal particles confined in them [21].

The dynamics of particles in a narrow channel where particles effectively move in one dimension, have also been considered. This problem has been investigated theoretically, e.g. Markov chains [22], and has recently become a focus of experimental interest, e.g. in the study of molecular diffusion in zeolites [23], diffusion of colloidal particles in confined geometries [21] or optical lattices [24] and granular diffusion [25]. Diffusion of particles in quasi-one-dimensional geometry is usually referred to as single-file diffusion (SFD). Particles represent random-walk motion in very narrow channels that mutual passage of particles has been blocked (see Fig. 1.2). The single-file effect also occurs in biologi-

cal systems, examples being the motion of ribosomes along the m-RNA during protein synthesis [26, 27]. Here, similarly to the Q2D, motion in a 'reduced dimension' yields differences compared to the case without confinement. For example, single-file motion leads to subdiffusive behaviour [28,29]. This behaviour is due to blockage of mutual passage, which preserves the initial ordering of the particles. The motion of individual particles is correspondingly impeded and modified to such an extent that Fick's law, which predicts that the mean-square displacement is proportional to time, is no longer obeyed for long times. For these systems, mean-squared displacement of particles for times much longer than the direct interaction time, is reported to be proportional to the square root of the time, in contrast to the linear increase with time in systems that allow mutual passage [30–32]. Among other things the single-file effect is responsible for effectively low reaction rates in microporous catalysts [33] and is thus of technical importance in chemical engineering.

The problem becomes even more interesting when the confined particles move in an external force. A typical example of motion in an external force is sedimentation, where the mass of the solute particles cause them to move in a solvent in the presence of a gravitational field; this problem has been considered in many recent works [34, 35]. However, few of these tackle the problem in a specific geometry like narrow channels [36]. It is natural to ask how an external force influences the behaviour of particles that are placed in a restricting geometry. Investigation of this question is the objective of this thesis.

The scope of this thesis is the investigation of systems in quasi-one-dimensional geometries using two different approaches: an analytical approach based on one-dimensional reaction-diffusion systems, and a simulation model. Since in single-file systems the longitudinal motion is the most important dynamical mode, that makes such processes amenable to treatment by one-dimensional models [37, 38]. The best-studied example of these kind of models is asymmetric exclusion process (ASEP), which serves as a starting point for modeling of molecular motors along microtubuli or actin filaments [39]. In order to extend ASEP, we include two possible states of particles. We consider two-component models

which satisfy some specified conservation laws. For the second approach, we perform numerical simulations to model a suspension of colloidal particles in a narrow channel. We use a hybrid simulation scheme which couples a Molecular Dynamics simulation method to a multi-particle collision (MPC) fluid which is a coarse-grained model to describe fluid dynamics.

Systems of diffusing and reacting particles are usually described macroscopically by hydrodynamic equations for coarse-grained quantities like the particle density [40]. These equations are generally non-linear and can exhibit shocks. This means that the solution of the macroscopic equations may develop a discontinuity even if the initial particle density is smooth. We investigate this discontinuity in our reaction-diffusion model, as well as the colloidal simulation model.

1.2 Outline

The outline of this work is as follows. In chapter 2, stochastic reaction-diffusion processes is investigated. Here we considered three-state lattice gas models. We explain symmetries and conservation laws which are required for the models. This yields three distinct groups of models, two of which are studied in this chapter. The families of models which belong to the first group are investigated. The boundary condition is defined for particles entering or leaving the system. The Master equation for probability vectors is considered for the time evolution of the particles. In the stationary distribution, the probability vector satisfies an eigenvalue equation. Hence we find the constraints on bulk rates as well as boundary rates in order to satisfy an eigenvalue equation with zero modes. We calculate the current of particles in the stationary state. The possibility of the existence of a discontinuity in the density (shock solution) is investigated. Solving a random-walk equation for shock solutions imposes new restrictions on the bulk rates. In the second group of models, a two species asymmetric simple exclusion process is studied. Similarly the system in stationary state has been considered and a fugacity gradient which represents a shock solution has been

found.

In the third chapter a simulation technique for modeling colloidal particles suspended in a solvent and located between two planar walls is described. The first section of this chapter describes a mesoscale simulation technique which has been used recently for modeling fluid dynamics. Here the basic algorithms are explained and the units are defined. In order to test the accuracy of the simulation method, a parabolic velocity profile for fluid flow in the presence of gravitational force is considered and the fluid parameters calculated from this profile are compared with the theoretical values. To model the force field between colloidal particles, a molecular dynamics simulation is performed. Then a coupling algorithm is introduced to obtain the desired model. Parameters and units are defined and boundary conditions are discussed. Some methods to test the accuracy of the simulation are explained.

Chapter 4 considers investigation of the colloidal suspension in an external force. The special case of a gravitational field as the external force is considered. In this case, the colloidal particles undergo sedimentation. The relationship between the average colloidal particles velocity and the volume fraction is discussed. These investigations include the variation in the size of the system or in the number of colloidal particles. Then the effect of hydrodynamic interaction (HI) in the behaviour of sedimenting colloids is investigated by using two different proposed methods which model a system without hydrodynamic interaction. In order to identify the laminar flow regime, the sedimentation velocity is obtained as a function of gravitational field. The existence of a density discontinuity in a macroscopic scale due to applying an external force is studied by investigation of the collective behaviour of colloidal particles in the channel. A comparison to the case without an external force is shown.

Chapter 5 summarizes the results concerning the density discontinuity and compares the shock solution of the system in the two approaches which are explained in chapter 2 and chapter 4.

2 A three states lattice gas model; an analytical approach

2.1 Introduction

In this chapter we consider one-dimensional reaction-diffusion systems as a theoretical approach, to investigate the model of particles in a narrow channel. The best-studied example of stochastic lattice models being the asymmetric simple exclusion process (ASEP) [41, 42] which has often been called the Ising model of nonequilibrium statistical physics. In ASEP particles move randomly with a bias onto neighboring lattice sites, provided the target site is empty. Even its most-studied one-dimensional version which describes driven single-file diffusion exhibits rich phenomena, in particular boundary-induced phase transitions, [43–47] and has a wide range of applications in different branches of physics.

Low-dimensional diffusive particle systems are of great interest also from a thermodynamic point of view. In open boundary systems, *kept far from equilibrium* by maintaining a steady state particle current, various unexpected kinds of critical phenomena have been discovered in recent years, including boundary-induced phase transitions, phase separation and spontaneous symmetry breaking, see [37, 38] and references therein for a review. These finite-temperature critical phenomena have no counterpart in thermal equilibrium since in one-dimensional systems with short range interactions there is no mechanism that could prevent the creation and growth of an island of the minority phase inside a domain of the majority phase. Therefore it is not possible to have a phase-separated equilibrium state with a stable and microscopically sharp interface between two fluctuating domains characterized by different values of the order parameter.

Most of these nonequilibrium critical phenomena are not yet well-understood. Given the interesting diffusion properties as well as the potential for applications to catalytic reactions it would thus be interesting to explore critical phenomena in low-dimensional reaction-diffusion systems in more detail. Specifically, in this chapter on one-dimensional reaction-diffusion systems we would like to investigate the existence and microscopic properties of interfaces between coexisting

nonequilibrium domains which are macroscopically different.

In the hydrodynamic approach to traffic flow [48] using partial differential equations traffic jams correspond to shock solutions. A shock is a density discontinuity on moving with some deterministic speed, determined by mass conservation. It is therefore no surprise that on macroscopic Euler scale the time evolution of the particle density of the ASEP is described by the inviscid Burgers equation [49, 50] which develops shocks for generic initial data. With a view on applications of the ASEP to systems for which a hydrodynamic description is too coarse-grained it would thus be of interest to understand what fluctuating microscopic structure (on lattice scale) is underlying the phenomenon of shocks.

In fact, a great deal is known about shocks in the ASEP due to the exact solubility of the model. In the stationary regime the shock structure has been studied as seen from a so-called second-class particle which serves as microscopic marker of the shock position. The particle density decays away from the shock exponentially (on lattice scale) to the respective constant bulk values $\rho_{1,2}$ of the two branches of the shock [51–53]. The shock position itself has been proved to perform Brownian motion on coarse grained diffusive scale [54]. For a particular strength of the driving field the associated decay constant of the particle density vanishes, corresponding to a "minimal" intrinsic shock width. For this special value of the driving field also the motion of the shock simplifies greatly. It performs a biased random walk on microscopic *lattice* scale with explicitly known hopping rates [55, 56].

Moreover, there are a number of exact results about shocks in lattice gas models for driven diffusive systems [51–53, 55–62], in reaction-diffusion systems [56,62–66] (where shocks appear as Fisher waves on the macroscopic scale) and in spin-flip systems [56,62,66] where shocks correspond to domain walls [67]. It has emerged that in all these models the macroscopic shock discontinuity originates from a microscopically sharp increase of the local particle density, i.e., a decrease of the mean distance between particles that can be observed on the scale of a few lattice units (which typically represents the size of particles). The discontinuity itself performs a biased random motion with a constant

mean speed and diffusive mean square displacement. The existence, structure, and dynamical properties of microscopically sharp shocks in lattice models for reaction-diffusion systems are the issues on which the present work focuses. It is natural to ask whether this special feature of the ASEP survives in more complicated models of driven diffusive systems. In particular, one would like to investigate exclusion processes with nonconserved internal degrees of freedom, where particles may have different velocities, charges, masses or other distinguishing properties that they can gain or lose e.g. in a collision or chemical reaction. Here we address this question in the simplest case of two possible internal states that each particle can posses. Such models have been investigated recently for various biological and vehicular transport phenomena [39, 68, 69]. Studying the microstructure of a shock illuminates the role of finite-size effects in first-order boundary-induced phase transitions that are associated with the motion of traffic jams [70–72] in finite systems.

In order to set the stage and sharpen the question we begin with some remarks of general nature and mention some results relevant to our approach. Systems of diffusing and reacting particles are usually described macroscopically by hydrodynamic equations for coarse-grained quantities like the particle density [40]. The density then represents the local order parameter specifying the spatial evolution of the macroscopic state of the system. Such equations are usually proposed on a phenomenological basis, paradigmatic examples being the Burgers equation for driven diffusive systems with particle conservation [49] or the Fisher equation for reactive systems without conservation law [73, 74]. These equations are in general non-linear and exhibit shocks in some cases. This means that the solution of the macroscopic equations may develop a discontinuity even if the initial particle density is smooth. This means that in these systems phase separation may occur. The shock represents the interface between the two thermodynamically distinct phases. This hydrodynamic description of phase separation is, however, not fully satisfactory. It provides no insight into the microscopic origin of the phenomenon, and it gives no information about the internal structure of the shock. It could very well happen that

in a particle system described on hydrodynamic (Eulerian) time scale by an equation which has shock solutions no corresponding microscopic discontinuity would be observable on less coarse-grained space or time scales which are experimentally relevant particularly for the quasi one-dimensional systems referred to above. In order to understand the structure of shocks and the emergence of such nonlinear behaviour from the microscopic laws that govern the stochastic motion and interaction of particles it is therefore necessary to *derive* the macroscopic equations from the microscopic dynamics rather than postulating them on phenomenological grounds.

After this survey we are finally in a position to precisely state the objective of the work in this chapter. All the reaction-diffusion systems studied so far allow only for the presence of a single species of particles. No exact results have been reported so far for non-stationary travelling waves in open two-component systems, i.e., where two diffusive particles species A, B react with each other to form an inert reaction product or undergo a cracking or coagulation reaction ($B \rightleftharpoons 2A$). In order to address this question we adapt the strategy suggested in [56] to two-component systems: We take as initial distribution of particles a shock distribution with given microscopic properties and look for families of models for which the shock distribution evolves into a linear combination of similar distributions with different shock positions. Thus the information of the microscopic structure of the shock that one has initially is preserved for all times. Remarkably it will transpire that such families of reaction-diffusion systems exist for strong external field that drives the particles and keeps them in a nonequilibrium state. We remark that in a similar treatment for a different family of two-component processes we have found such a phenomenon at some specific finite driving strength [75, 76].

This chapter is organized as follows: In the following section we define the class of models that we consider and according to the conservation laws which we require in the system, we distribute this class of models into two groups. In Sec. (2.2), we investigate the families of models which belong to the the first group and we also determine the models with travelling shock solutions on the finite

lattice. In Sec. (2.4), as the second group, we study the ASEP in a case where there is an internal degree of freedom. In Sec. (2.5), we summarize our results and draw some conclusions. Some mathematical details of the calculations are given in the appendices.

2.2 Stochastic reaction-diffusion processes

2.2.1 Three-states lattice gas models

In order to keep the physics that lead to phase-separated nonequilibrium states as transparent as possible we study the simplest possible setting for a stochastic two-component reaction-diffusion process. We consider a lattice gas model defined on a lattice with L sites. The state of the system at any given time is described by a set of "occupation numbers" $\underline{n} = n_1, \ldots, n_L$ where $n_k = 0, 1, 2$ is the local occupation number at site k. These occupation numbers are abstract objects and serve as mathematical labels for three possible local states of each lattice site.

The bulk stochastic dynamics are defined by nearest neighbor transitions between the occupation variables which occur independently and randomly in continuous time after an exponentially distributed waiting time. The mean $\tau(n'_k, n'_{k+1}; n_k, n_{k+1})$ of this waiting time depends on the transition $(n_k, n_{k+1}) \to (n'_k, n'_{k+1})$. For later convenience we introduce an integer label

$$i = 3n_k + n_{k+1} + 1 \tag{2.1}$$

in the range $1 \leq i \leq 9$ for the occupation variables on two neighboring sites k and $k+1$. The inverse mean transition times are the transition rates w_{ij}. Here $i = 3n'_k + n'_{k+1} + 1$ labels the target configuration and j is the respective label of the initial configuration (n_k, n_{k+1}). We assume the bulk dynamics to be spatially homogeneous. The transition rates then do not explicitly depend on the site k.

At the boundary sites $1, L$ we assume the system to be connected to some external reservoir with which the system can exchange particles. For injection and extraction of particles at the left boundary we introduce the rates :

$$\begin{aligned} 0 &\rightleftharpoons 1 \qquad \alpha_1,\ \gamma_1, \\ 0 &\rightleftharpoons 2 \qquad \alpha_2,\ \gamma_2, \\ 1 &\rightleftharpoons 2 \qquad \alpha_3,\ \gamma_3, \end{aligned} \tag{2.2}$$

and for the right boundary

$$\begin{aligned} 0 &\rightleftharpoons 1 \qquad \delta_1,\ \beta_1, \\ 0 &\rightleftharpoons 2 \qquad \delta_2,\ \beta_2, \\ 1 &\rightleftharpoons 2 \qquad \delta_3,\ \beta_3. \end{aligned} \tag{2.3}$$

Here and below the left rate refers to the process going from left to right, while the right rate is for the reversed process.

2.2.2 Symmetries and conservation laws

Within this setting one could describe 72 different bulk transitions, corresponding to the 72 mathematically possible changes of configurations on a pair of sites. However, one shall reduce this large number by imposing various physically motivated constraints. We use the method has been proposed in [75] where a local conservation law is required. Generally, the physical interpretation of the conservation law depends on the physical interpretation of the occupation numbers n_k and will become clear below. Mathematically this means that in a periodic system some function $\sum_k C(n_k)$ of the local occupation numbers should remain invariant under the stochastic dynamics, i.e.,

$$C(n'_k) + C(n'_{k+1}) = C(n_k) + C(n_{k+1}) \tag{2.4}$$

for any local transition between configurations i, j. This constraint forces a large number of transition rates w_{ij} to vanish. Physically $C(n)$ is some observable property (such as mass or charge) of the state n.

The conservation condition (2.4) does not uniquely define the function $C(n)$. In order to analyse these constraints we set $C(0) = 0$ and $C(1) = 1$. This involves no loss of generality since adding a constant to $C(n)$ or multiplying $C(n)$ by an arbitrary factor leaves (2.4) invariant. From inspection of (2.4) one can then see that there are three distinct families of solutions: (i) degenerate case, represented by $C(2) = C(1) = 1$ (or equivalently $C(2) = C(0) = 0$), which is treated in section (2.4) (ii) linear nondegenerate case, represented by $C(2) = 2$

(or equivalently $C(2) = -1$, $C(2) = 1/2$), (iii) two independent conservation laws, represented by any other value of $C(2)$. This case was studied in detail in [59,61]. The degenerate conservation law will be discussed later in (2.4) while the non-degenerate linear conservation law is studied in the next subsection.

2.3 The nondegenerate linear conservation law

As it is discussed before, here we require a single conservation law where $C(2) = 2$. It is straightforward to check that this allows for 10 nonvanishing rates w_{ij}. The physical interpretation of this conservation law as charge-, mass-, or particle conservation respectively depends on the physical interpretation of the occupation numbers n_k and will be given below. We present the following three families of models which are mathematically equivalent, but have rather different physical interpretations.

Diffusion without exclusion

In its most obvious interpretation the abstract occupation number n represents the number of particles on a given site. Requiring particle conservation where $C(n) = n$ allows for 10 hopping processes with rates given as follows:

$$\begin{aligned} 10 &\rightleftharpoons 01 \qquad w_{24},\ w_{42} \\ 20 &\rightleftharpoons 02 \qquad w_{37},\ w_{73} \\ 12 &\rightleftharpoons 21 \qquad w_{86},\ w_{68} \\ 11 &\rightleftharpoons 02 \qquad w_{35},\ w_{53} \\ 20 &\rightleftharpoons 11 \qquad w_{57},\ w_{75}. \end{aligned} \tag{2.5}$$

Here there is no distinction between different particles, only the total number is recorded. Physically this process describes diffusion of a single species of particles in a pore system large enough to accommodate two particles in each pore. Thus the three states do not describe a two-component, single-file particle system, but a one-component system where particles can pass each other.

This makes this process different from the previously studied two-state single-component systems which describe single-file diffusion [55–57]. For definiteness we shall focus in this paper on two-component reaction-diffusion systems and hence not make use of this one-component interpretation of the three local states.

Two-species annihilation $A + B \rightleftharpoons 0$

We define

$$C(n) = 1 - n \tag{2.6}$$

as charge associated with the state n of a lattice. The "occupation number" therefore denotes an internal degree of freedom in a single-file particle system. The value $n = 0$ corresponds to a positively charged particle (denoted as type A), $n = 1$ corresponds to a vacant site (denoted 0), and $n = 2$ corresponds to occupation by a negatively charged particle (denoted as type B). As conservation law we require charge conservation, or, equivalently, conservation of the difference of particle numbers (of positively and negatively charged particles).

Since this process is mathematically equivalent to the particle conserving process (2.5) the dynamics of the process can be represented by the following ten transitions

$$\begin{aligned} 0A &\rightleftharpoons A0 \qquad w_{24},\ w_{42} \\ BA &\rightleftharpoons AB \qquad w_{37},\ w_{73} \\ 0B &\rightleftharpoons B0 \qquad w_{86},\ w_{68} \\ 00 &\rightleftharpoons AB \qquad w_{35},\ w_{53} \\ BA &\rightleftharpoons 00 \qquad w_{57},\ w_{75} \end{aligned} \tag{2.7}$$

This is the well-studied two-component creation/annihilation process, see [77] for a review of some important properties and experimental significance of the one-dimensional pure annihilation case. The main results of this paper are given in terms of this process.

Cracking $B \to 2A$

One may switch the role of A and 0. The "occupation number" $n = 0$ then corresponds to a vacant site 0, $n = 1$ corresponds to a particle of type A, and $n = 2$ corresponds to occupation by a particle of type B. We drop the assignment of charges to particles and instead introduce

$$C(n) = n =: M \tag{2.8}$$

as mass of the particles (in suitable units). A-particles thus have mass 1 and B-particles to have mass 2; the conservation law describes mass conservation. Under this mapping the process (2.7) read

$$\begin{aligned} A0 &\rightleftharpoons 0A \qquad w_{24},\ w_{42} \\ B0 &\rightleftharpoons 0B \qquad w_{37},\ w_{73} \\ AB &\rightleftharpoons BA \qquad w_{86},\ w_{68} \\ AA &\rightleftharpoons 0B \qquad w_{35},\ w_{53} \\ B0 &\rightleftharpoons AA \qquad w_{57},\ w_{75} \end{aligned} \tag{2.9}$$

The last two reactions corresponds to cracking of a molecule B with mass 2 into two identical parts A (mass 1 each), with coagulation as reversed process. The third process in this list is a recombination reaction between neighboring reactands.

2.3.1 Boundary conditions

For definiteness we consider here and below charge conservation. Thus by assigning A to state 0 and B to state 2 we rewrite the process (2.2) for the rates at the left boundary:

$$\begin{aligned} A &\rightleftharpoons 0 \qquad \alpha_1,\ \gamma_1, \\ A &\rightleftharpoons B \qquad \alpha_2,\ \gamma_2, \\ 0 &\rightleftharpoons B \qquad \alpha_3,\ \gamma_3, \end{aligned} \tag{2.10}$$

and (2.2) for the right boundary

$$\begin{aligned} A &\rightleftharpoons 0 \qquad \delta_1,\ \beta_1, \\ A &\rightleftharpoons B \qquad \delta_2,\ \beta_2, \\ 0 &\rightleftharpoons B \qquad \delta_3,\ \beta_3. \end{aligned} \tag{2.11}$$

The corresponding processes for mass conservation are obtained by changing $A \leftrightarrow 0$.

The boundary rates are a further set of model parameters. Below we define them such that they are parametrized by 2 independent boundary chemical potentials which fix boundary densities for the conserved order parameter.

2.3.2 Continuity equation and PT-invariance

The presence of the bulk conservation law implies a lattice continuity equation

$$\frac{d}{dt}C_k = j_{k-1} - j_k \tag{2.12}$$

for the expectation $C_k = \langle\, C(n_k)\,\rangle$. This quantity plays the role of a conserved local order parameter. The quantity j_k is the current associated with the conservation law. It is given by the expectation of some combination of local occupation numbers, depending on the model under investigation, see below. Since we do not study here periodic systems we do not require the boundary sites where the system is connected to the reservoir to respect the conservation law. The quantities j_0, j_L entering the continuity equation for $k = 1$ and $k = L$ respectively are source terms resulting from the reservoirs. They are functions of the reservoir densities. The lattice continuity equation is the starting point for a coarse-grained hydrodynamic description of the time evolution of the local order parameter.

Second, in addition to the conservation law we require PT-invariance, i.e., the bulk dynamics should be symmetric under combined time reversal and space reflection. Time reversal symmetry means to have detailed balance

$$p^*(\underline{n})w(\underline{n} \to \underline{n}') = p^*(\underline{n}')w(\underline{n}' \to \underline{n}). \tag{2.13}$$

In order to combine this relation with the parity (space reflection) operation we change the position of neighboring sites with each other in the initial configuration and final configuration on the left-hand side of the detailed-balance relation. This physical input generalizes the equilibrium condition of detailed balance to allow for external driving forces which lead to a bias in the hopping rates. In such a case the system is forced into a nonequilibrium steady state with a stationary current flowing in the system. Well-known examples for models of this kind are exclusion processes satisfying pairwise balance [78]. As a result of PT-invariance, there are pairwise relations between some of the transition rates, see below.

2.3.3 Master equation

The time evolution defined above can be written in terms of a continuous-time master equation for the probability vector

$$|\, P(t)\,\rangle = \sum_{\underline{n}} P(n_1, \cdots, n_L; t) |\, \underline{n}\,\rangle, \tag{2.14}$$

where $P(n_1, \cdots, n_L; t)$ is the distribution for the probability of finding particles at sites 1 to L and $|\, \underline{n}\,\rangle$ is the basis vector in the space of configurations [42]. The probability vector is normalized such that $\langle s|P\rangle = 1$ with the summation vector $\langle\, s\,| = \sum_{\underline{n}} \langle\, \underline{n}\,|$. The time evolution is generated by the stochastic Hamiltonian H whose offdiagonal matrix elements $H_{\underline{n},\underline{n}'}$ are the negative transition rates between configurations. As required by conservation of probability, the diagonal elements are the negative sum of transition rates in the respective column.

Therefore the master equation is now described by the Schrödinger equation in imaginary time:

$$\frac{d}{dt} |\, P(t)\,\rangle = -H |\, P(t)\,\rangle. \tag{2.15}$$

with the formal solution

$$|\, P(t)\,\rangle = \mathrm{e}^{-Ht} |\, P(0)\,\rangle. \tag{2.16}$$

Since only nearest-neighbour interactions are included, the quantum Hamiltonian H defined above has the structure

$$H = b_1 + \sum_{k=1}^{L-1} h_{k,k+1} + b_L. \tag{2.17}$$

Here b_1 and b_L are the boundary matrices:

$$b_1 = - \begin{pmatrix} -(\alpha_1+\alpha_2) & \gamma_1 & \gamma_2 \\ \alpha_1 & -(\gamma_1+\alpha_3) & \gamma_3 \\ \alpha_2 & \alpha_3 & -(\gamma_2+\gamma_3) \end{pmatrix}_1 , \tag{2.18}$$

$$b_L = - \begin{pmatrix} -(\delta_1+\delta_2) & \beta_1 & \beta_2 \\ \delta_1 & -(\beta_1+\delta_3) & \beta_3 \\ \delta_2 & \beta_3 & -(\beta_2+\beta_3) \end{pmatrix}_L . \tag{2.19}$$

The local bulk transition matrix $h_{k,k+1}$ with offdiagonal matrix elements $-w_{ij}$ acts non-trivially only on sites k and $k+1$. Below we give $h_{k,k+1}$ explicitly.

2.3.4 Nonequilibrium steady states

We stress that our family of models is defined in terms of transition rates, not in terms of an internal energy $E(\underline{n})$ that would determine the stationary distribution of the process as equilibrium distribution $P^*(\underline{n}) \propto \exp(-\beta E(\underline{n}))$. Instead, the stationary distribution is an *a priori* unknown and in general complicated function of the transition rates. It does not in general satisfy detailed balance and thus represents a nonequilibrium steady state. In order to be able to carry out explicit computations we restrict ourselves to systems such that the stationary distribution of the stochastic dynamics factorizes, i.e., one has a product measure without correlations between the occupation numbers at different sites.

Requiring the existence of a stationary product measure imposes constraints both on the boundary rates and on the bulk rates. Physically, the constraints on the boundary rates essentially means that the chemical potentials in the two reservoirs are equal, allowing the bulk to relax into a current-carrying stationary

state with a chemical potential determined by the reservoirs. In this case the origin of the current is not a gradient in the external chemical potential of the reservoirs, but a constant bulk driving force. The conditions on the bulk rates have a less transparent and model-dependent physical interpretation. Once these conditions are determined the model is fully defined and its stationary distribution is given for equal chemical potentials in the reservoir.

In the quantum Hamiltonian formalism introduced above a product measure is given by a tensor product

$$|\, P \,\rangle = |P_1) \otimes |P_2) \otimes ... \otimes |P_L). \tag{2.20}$$

Here the three-component single-site probability vectors $|P_k)$ has as its components the probabilities $P(n_k)$ of finding state n at site k. In the stationary distribution these probabilities are position-independent, $|P_k) \equiv |P)$, and the stationary probability vector thus has the form

$$|\, P^* \,\rangle = |P)^{\otimes L}. \tag{2.21}$$

By definition of stationarity the stationary probability vector satisfies the eigenvalue equation

$$H|\, P^* \,\rangle = 0. \tag{2.22}$$

We shall parametrize the one-site marginals $P(n_k)$ by a generalized fugacity z associated with the conserved quantity and an interaction parameter determined by the transition rates, see below. In formal analogy to equilibrium systems we shall refer to the logarithm of the fugacity as chemical potential.

2.3.5 Initial conditions

The objective of this paper is the analysis of the family of models which is defined by having a stationary product measure if the chemical potentials in the reservoir are equal. However, as physical boundary conditions to be studied we envisage *different* chemical potentials in the reservoirs. The product measure is then no longer stationary and the questions arises what new properties the

stationary distribution exhibits and how the system relaxes to its stationary distribution. Indeed, in order to avoid misunderstanding we stress that the product requirement on the stationary distribution with *equal* reservoir chemical potentials does not imply the absence of correlations during the time evolution of the more general open system with different reservoir chemical potentials.

Specifically, we prepare the system initially in a state described by a (nonstationary) shock measure of the form

$$|\, k \,\rangle = |P_1)^{\otimes k} \otimes |P_2)^{\otimes L-k}. \tag{2.23}$$

These shock measures have single-site probabilities given by $|P_1)$ in the left chain segment up to site k (chosen to match the chemical potential of the left reservoir) and single-site probabilities given by $|P_2)$ in the remaining chain segment from site $L-k$ up to site L (chosen to match the chemical potential at the right reservoir).

Such a shock measure defines fully the internal structure of the shock. Since there are no correlations in a shock measure one may regard the lattice unit as the intrinsic shock width. A typical configuration has a sharp decrease of the mean interparticle distance across the lattice point k. In the course of time the measure $|\, P(t) \,\rangle = \exp(-Ht)|\, k \,\rangle$ changes and it is interesting to investigate this time evolution. For the models studied below $|\, P(t) \,\rangle$ is computed explicitly and allows for a detailed explicit calculation of all correlations that develop with time.

2.3.6 Stationary distribution

Following the ideas outlined above we first search for stationary product solutions of the model with spatially constant single-site probabilities. By choosing the basis of three states as follows

$$|A) = \begin{pmatrix} 1 \\ 0 \\ 0 \end{pmatrix}, \quad |0) = \begin{pmatrix} 0 \\ 1 \\ 0 \end{pmatrix}, \quad |B) = \begin{pmatrix} 0 \\ 0 \\ 1 \end{pmatrix}, \tag{2.24}$$

one can conveniently write the product measure for the periodic model in terms of a generalized fugacity z and arbitrary constant r

$$| P^* \rangle = \frac{1}{\nu^L} \begin{pmatrix} 1 \\ z \\ rz^2 \end{pmatrix}^{\otimes L} \tag{2.25}$$

Here

$$\nu = 1 + z + rz^2 \tag{2.26}$$

is the local "partition function". The quantity r parametrizes the density ratio of the two particle species, $\rho^B/\rho^A = rz^2$. The fugacity z is associated with the conservation law, i.e., in a periodic system where the charge is conserved $| P^* \rangle$ would be stationary for any value of z. This probability measure is grand-canonical. The charge $\sigma = \rho^A - \rho^B$ in this ensemble has mean

$$\sigma = 1 - z\frac{d}{dz} \ln \nu = \frac{1 - rz^2}{\nu}. \tag{2.27}$$

The corresponding canonical distributions with a definite value of the charge can be constructed in standard fashion, but we do not consider them here since we are dealing with an open system where the bulk fugacity is fixed by the generalized chemical potentials of the reservoirs. The nonconserved particle density $\rho = \rho^A + \rho^B$ in this ensemble is given by

$$\rho = \frac{1 + rz^2}{\nu}. \tag{2.28}$$

The stationary distribution of the model is not known in full generality and we have to determine constraints on the bulk rates such that the product measure (2.25) is stationary. The transition matrix $h_{k,k+1}$ for the bulk stochastic dynamics is given by

$$-h_{k,k+1} =$$

$$\begin{pmatrix}
0 & 0 & 0 & 0 & 0 & 0 & 0 & 0 & 0 \\
0 & -w_{42} & 0 & w_{24} & 0 & 0 & 0 & 0 & 0 \\
0 & 0 & -(w_{53}+w_{73}) & 0 & w_{35} & 0 & w_{37} & 0 & 0 \\
0 & w_{42} & 0 & -w_{24} & 0 & 0 & 0 & 0 & 0 \\
0 & 0 & w_{53} & 0 & -(w_{35}+w_{75}) & 0 & w_{57} & 0 & 0 \\
0 & 0 & 0 & 0 & 0 & -w_{86} & 0 & w_{68} & 0 \\
0 & 0 & w_{73} & 0 & w_{75} & 0 & -(w_{37}+w_{57}) & 0 & 0 \\
0 & 0 & 0 & 0 & 0 & w_{86} & 0 & -w_{68} & 0 \\
0 & 0 & 0 & 0 & 0 & 0 & 0 & 0 & 0
\end{pmatrix}_{k,k+1} \tag{2.29}$$

and stationarity of the product measure implies

$$h_{k,k+1}|\, P^* \,\rangle = [F(\hat{n}^A_{k+1} - \hat{n}^A_k) + F'(\hat{n}^B_{k+1} - \hat{n}^B_k)]|\, P^* \,\rangle. \tag{2.30}$$

Here F and F' are arbitrary constants and $\hat{n}^A_k$ and $\hat{n}^B_k$ are number operators which take value 1 if there is a particle of the respective species at site k and zero otherwise, i.e., $\rho^A = \langle\, n^A_k \,\rangle$ and $\rho^B = \langle\, n^B_k \,\rangle$ independently of k due to homogeneity of the measure.

In order to satisfy the relation (2.30) for systems with open boundaries we can write for b_1 and b_L, using another arbitrary constant g

$$b_1|\, P^* \,\rangle = (F\hat{n}^A_1 + F'\hat{n}^B_1 + g)|\, P^* \,\rangle, \tag{2.31}$$

$$b_L|\, P^* \,\rangle = -(F\hat{n}^A_L + F'\hat{n}^B_L + g)|\, P^* \,\rangle. \tag{2.32}$$

As detailed in Appendix A one may solve the eigenvalue Eq. (2.22) and find F and F':

$$F = w_{24} - w_{42}, \tag{2.33}$$

$$F' = w_{86} - w_{68}. \tag{2.34}$$

Therefore the bulk rates and densities satisfy two relations due to the eigenvalue equation (2.22):

$$r = \frac{w_{35} + w_{75}}{w_{53} + w_{57}}, \tag{2.35}$$

$$w_{24} - w_{42} + w_{68} - w_{86} + w_{73} - w_{37} = \frac{w_{35}w_{57} - w_{53}w_{75}}{w_{35} + w_{75}}. \tag{2.36}$$

The first equation (2.35) expresses the constant r in terms of the reaction rates. The second equation (2.36) is a constraint on the transition rates which we impose on the model.

For the boundaries one needs to satisfy

$$g = \frac{1}{\nu}(F + F' r z^2). \tag{2.37}$$

This leaves two equations for the left boundary:

$$(w_{42} - w_{24})z(1 + rz) - (w_{68} - w_{86})rz^2 + (\alpha_1 + \alpha_2)\nu - \gamma_1 z\nu - \gamma_2 r z^2 \nu = 0, \tag{2.38}$$

$$(w_{68} - w_{86})rz^2(1 + z) - (w_{42} - w_{24})rz^2 - \alpha_3 z\nu + (\gamma_3 + \gamma_2)rz^2\nu - \alpha_2\nu = 0, \tag{2.39}$$

and for the right boundary one has

$$(w_{42} - w_{24})z(1 + rz) - (w_{68} - w_{86})rz^2 - (\delta_1 + \delta_2)\nu + \beta_1\nu + \beta_2\mu = 0, \tag{2.40}$$

$$(w_{68} - w_{86})rz^2(1 + z) - (w_{42} - w_{24})rz^2 + \delta_3 z\nu - (\beta_3 + \beta_2)rz^2\nu + \delta_2\nu = 0. \tag{2.41}$$

These equations relate the boundary rates to the fugacity and moreover impose some constraints on the the boundary rates which are required for a proper interpretation as boundary reservoirs with fixed chemical potential.

We remark that the given choice of nonvanishing rates is only determined by the conservation law and requiring stationarity of the product measure. Many physical processes satisfy PT-invariance, i.e., the bulk dynamics should be symmetric under combined time reversal and space reflection. Following (2.13) we find that PT-invariance imposes the following further relations

$$\begin{aligned} w_{75} &= r w_{53}, \\ w_{35} &= r w_{57}. \end{aligned} \tag{2.42}$$

In the calculations of the next section we do not make use of these extra relations. We have merely listed them for possible applications of our general results to specific PT-symmetric systems.

2.3.7 Stationary Current and Hydrodynamics

As remarked above the conservation law implies a lattice continuity equation (2.12) for the charge current. To calculate the charge current we use the equation of motion for the expected local charge density

$$\frac{d}{dt}\sigma_k(t) = \frac{d}{dt}[\langle n_k^A\rangle - \langle n_k^B\rangle] = j_{k-1} - j_k. \tag{2.43}$$

One finds for the expected local density of A-particles

$$\begin{aligned}\frac{d}{dt}\langle n_k^A\rangle = \quad & -w_{24}\langle n_{k-1}^0 n_k^A\rangle + w_{42}\langle n_{k-1}^A n_k^0\rangle - w_{37}\langle n_{k-1}^B n_k^A\rangle + w_{73}\langle n_{k-1}^A n_k^B\rangle \\ & -w_{57}\langle n_{k-1}^B n_k^A\rangle + w_{75}\langle n_{k-1}^0 n_k^0\rangle + w_{24}\langle n_k^0 n_{k+1}^A\rangle - w_{42}\langle n_k^A n_{k+1}^0\rangle \\ & +w_{37}\langle n_k^B n_{k+1}^A\rangle - w_{73}\langle n_k^A n_{k+1}^B\rangle + w_{35}\langle n_k^0 n_{k+1}^0\rangle - w_{53}\langle n_k^A n_{k+1}^B\rangle,\end{aligned} \tag{2.44}$$

and for B-particles

$$\begin{aligned}\frac{d}{dt}\langle n_k^B\rangle = \quad & w_{37}\langle n_{k-1}^B n_k^A\rangle - w_{73}\langle n_{k-1}^A n_k^B\rangle - w_{86}\langle n_{k-1}^0 n_k^B\rangle + w_{68}\langle n_{k-1}^B n_k^0\rangle \\ & +w_{35}\langle n_{k-1}^0 n_k^0\rangle - w_{53}\langle n_{k-1}^A n_k^B\rangle - w_{37}\langle n_k^B n_{k+1}^A\rangle + w_{73}\langle n_k^A n_{k+1}^B\rangle \\ & +w_{86}\langle n_k^0 n_{k+1}^B\rangle - w_{68}\langle n_k^B n_{k+1}^0\rangle - w_{57}\langle n_k^B n_{k+1}^A\rangle + w_{75}\langle n_k^0 n_{k+1}^0\rangle\end{aligned} \tag{2.45}$$

This gives the charge current

$$\begin{aligned}j_k = \quad & -w_{24}\langle n_k^0 n_{k+1}^A\rangle + w_{42}\langle n_k^A n_{k+1}^0\rangle - 2w_{37}\langle n_k^B n_{k+1}^A\rangle + 2w_{73}\langle n_k^A n_{k+1}^B\rangle \\ & -w_{68}\langle n_k^B n_{k+1}^0\rangle + w_{86}\langle n_k^0 n_{k+1}^B\rangle - w_{35}\langle n_k^0 n_{k+1}^0\rangle + w_{53}\langle n_k^A n_{k+1}^B\rangle \\ & -w_{57}\langle n_k^B n_{k+1}^A\rangle + w_{75}\langle n_k^0 n_{k+1}^0\rangle.\end{aligned} \tag{2.46}$$

In the steady state we can compute the current using the stationary distribution. One finds

$$j^* = (-w_{24}+w_{42})\frac{z}{\nu^2} + [2(-w_{37}+w_{73})+w_{53}-w_{57}]\frac{rz^2}{\nu^2} + (w_{86}-w_{68})\frac{rz^3}{\nu^2} + (w_{75}-w_{35})\frac{z^2}{\nu^2}, \tag{2.47}$$

and by using (2.35) and the stationary condition (2.36)

$$j^* = \frac{1}{2}(w_{42} - w_{24})(\rho + \sigma)(1 - \sigma) + \frac{1}{2}(w_{86} - w_{68})(\rho - \sigma)(1 + \sigma), \tag{2.48}$$

where σ and $\rho \equiv \langle n_k^A \rangle + \langle n_k^B \rangle$ are the stationary density of charges (2.27) and particles (2.84) respectively.

Since the individual particle densities are not conserved the equations of motion for the local densities take the form

$$\frac{d}{dt}\langle n_k^A \rangle = j_{k-1}^A - j_k^A + S_k, \tag{2.49}$$

$$\frac{d}{dt}\langle n_k^B \rangle = j_{k-1}^B - j_k^B + S_k, \tag{2.50}$$

with source term

$$\begin{aligned} S_k = \; & -\tfrac{1}{2}w_{57}(\langle n_{k-1}^B n_k^A \rangle + \langle n_k^B n_{k+1}^A \rangle) + \tfrac{1}{2}w_{75}(\langle n_{k-1}^0 n_k^0 \rangle + \langle n_k^0 n_{k+1}^0 \rangle) \\ & + \tfrac{1}{2}w_{35}(\langle n_{k-1}^0 n_k^0 \rangle + \langle n_k^0 n_{k+1}^0 \rangle) - \tfrac{1}{2}w_{53}(\langle n_{k-1}^A n_k^B \rangle + \langle n_k^A n_{k+1}^B \rangle). \end{aligned} \tag{2.51}$$

The particle currents are given by

$$\begin{aligned} j_k^A = \; & - \; w_{24}\langle n_k^0 n_{k+1}^A \rangle + w_{42}\langle n_k^A n_{k+1}^0 \rangle - w_{37}\langle n_k^B n_{k+1}^A \rangle + w_{73}\langle n_k^A n_{k+1}^B \rangle \\ & - \; \frac{1}{2}w_{35}\langle n_k^0 n_{k+1}^0 \rangle + \frac{1}{2}w_{53}\langle n_k^A n_{k+1}^B \rangle - \frac{1}{2}w_{57}\langle n_k^B n_{k+1}^A \rangle + \frac{1}{2}w_{75}\langle n_k^0 n_{k+1}^0 \rangle, \end{aligned} \tag{2.52}$$

$$\begin{aligned} j_k^B = \; & \quad w_{68}\langle n_k^B n_{k+1}^0 \rangle - w_{86}\langle n_k^0 n_{k+1}^B \rangle + w_{37}\langle n_k^B n_{k+1}^A \rangle - w_{73}\langle n_k^A n_{k+1}^B \rangle \\ & + \; \frac{1}{2}w_{35}\langle n_k^0 n_{k+1}^0 \rangle - \frac{1}{2}w_{53}\langle n_k^A n_{k+1}^B \rangle + \frac{1}{2}w_{57}\langle n_k^B n_{k+1}^A \rangle - \frac{1}{2}w_{57}\langle n_k^0 n_{k+1}^0 \rangle. \end{aligned} \tag{2.53}$$

The resulting charge current $j_k = j_k^A - j_k^B$ is studied above. One may introduce also a particle current $\tilde{j}_k = j_k^A + j_k^B$ and write

$$\frac{d}{dt}\rho_k(t) = \tilde{j}_{k-1} - \tilde{j}_k + 2S_k. \tag{2.54}$$

For a coarse-grained hydrodynamic description of the time-evolution of the system we follow standard arguments [50, 79]. We pass to a continuum description by making the lattice unit a (which until now had been taken to be $a = 1$)

infinitesimal and we consider continuum space as $x = \frac{k}{L}$. The coarse-grained local observables $\sigma(x,t), \rho(x,t)$ in continuous space are averaged over a large but finite lattice interval around the lattice point x and therefore given by the expected local densities $\sigma_x(t), \rho_x(t)$. We consider Eulerian scaling $t' = ta$ with rescaled macroscopic time t'. In the continuum limit the two equations for σ and ρ then take the form (to leading order in the lattice constant a)

$$\partial_{t'}\sigma(x,t') = -\partial_x j(\sigma,\rho), \tag{2.55}$$

$$\partial_{t'}\rho(x,t') = -\partial_x \tilde{j}(\sigma,\rho) + R(\sigma,\rho)/a + \tilde{R}(\sigma,\rho), \tag{2.56}$$

where because of local stationarity

$$R(\sigma,\rho) = -\frac{1}{2}(w_{57}+w_{53})(\rho+\sigma)(\rho-\sigma) + 2(w_{75}+w_{35})(1-\rho)^2, \tag{2.57}$$

$$\tilde{R}(\sigma,\rho) = (w_{57}-w_{53})\frac{1}{4}[(\rho+\sigma)\partial_x(\rho-\sigma) - (\rho-\sigma)\partial_x(\rho+\sigma)]. \tag{2.58}$$

The space-time dependence of R and $\tilde{R}$ is implicit in arguments $\sigma(x,t'), \rho(x,t')$.

In this limit, when time and space are large, the term contained $R(\sigma,\rho)$ in the equation for ρ becomes large enough to make the two other terms negligible. Therefore $\rho(x,t)$ reaches its stationary state very fast, in agreement with the notion that non-conserved local degrees of freedom have attained their stationary values under hydrodynamic scaling. This implies that in the stationary state $R(\sigma,\rho) = 0$, from which we obtain the stationary particle density

$$(\rho^{*2} - \sigma^2) = 4r(1-\rho^*)^2. \tag{2.59}$$

for a given value of charge σ. Therefore ρ takes at any instant of (macroscopic) time a special value ρ^* which is a function of σ. The remaining slow dynamical mode is the charge, the evolution of which is thus governed by the hydrodynamic equation

$$\partial_{t'}\sigma(x,t') = -\partial_x j_x(\rho^*,\sigma) = -\partial_\sigma j(\rho^*,\sigma)\partial_x\sigma(x,t'). \tag{2.60}$$

In the second equation $j(\rho^*,\sigma)$ is the stationary current (2.48). This evolution equation is a nonlinear partial differential equation which can be solved by the method of characteristics. Because of the nonlinearity the solution may develop shocks in the charge distribution and we now turn to the investigation of these shocks on microscopic scale.

2.3.8 Shock measures

We assume that the initial distribution of charges exhibits a shock which on microscopic scale is represented by a shock measure (see Figure 2.1). We represent a shock measure with a shock in the fugacities between sites k and $k+1$ as

$$|\, k \,\rangle = \frac{1}{\nu_1^k \nu_2^{L-k}} \begin{pmatrix} 1 \\ z_1 \\ r z_1^2 \end{pmatrix}^{\otimes k} \otimes \begin{pmatrix} 1 \\ z_2 \\ r z_2^2 \end{pmatrix}^{\otimes L-k} . \tag{2.61}$$

In this model with open boundary condition, the first (second) fugacity matches the fugacity in left(right) boundary.

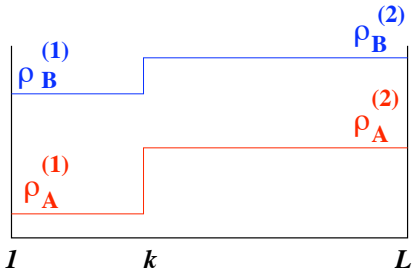

Figure 2.1: Coarse grained density profiles of a shock measure with shock between sites $k, k+1$.

Now we investigate the possibility that in analogy to the processes considered in [56,59,66] the family of shock measures $|\, k \,\rangle$ is closed under the time evolution t. This means that the initial measure evolves into a linear combination of shock measures after time t. This condition requires H which generates the time evolution to satisfy the following equation after an infinitesimal step

$$\frac{d}{dt}|\, k \,\rangle = d_1 |\, k-1 \,\rangle + d_2 |\, k+1 \,\rangle - (d_1 + d_2)|\, k \,\rangle. \tag{2.62}$$

We remark that this equation for the full particle distribution is mathematically equivalent to the evolution equation of a single-particle random walk with hopping rate d_1 to the left and d_2 to the right. Thus, if (2.62) can be satisfied, the shock in the initial distribution remains microscopically preserved at all times,

but its position performs a random walk with shock hopping rates d_1 to the left and d_2 to the right respectively.

For further analysis we define

$$\tilde{h}_{i,i+1} \equiv h_{i,i+1} + F(n_i^A - n_{i+1}^A) + F'(n_i^B - n_{i+1}^B), \tag{2.63}$$

$$\tilde{b}_1 \equiv b_1 - Fn_1^A - F'n_1^B, \tag{2.64}$$

$$\tilde{b}_L \equiv b_L + Fn_L^A + F'n_L^B. \tag{2.65}$$

Using

$$\tilde{h}_{i,i+1}|\,k\,\rangle = 0 \quad for\ \ i \neq k, \tag{2.66}$$

$$\tilde{b}_1|\,k\,\rangle = g_1|\,k\,\rangle, \quad \tilde{b}_L|\,k\,\rangle = -g_2|\,k\,\rangle. \tag{2.67}$$

with

$$g_1 = -F\frac{1}{\nu_1} - F'\frac{rz_1^2}{\nu_1}, \tag{2.68}$$

$$g_2 = -F\frac{1}{\nu_2} - F'\frac{rz_2^2}{\nu_2}, \tag{2.69}$$

yields

$$-H|\,k\,\rangle = -(\sum_i \tilde{h}_{i,i+1} + \tilde{b}_1 + \tilde{b}_L)|\,k\,\rangle = (-\tilde{h}_{k,k+1} - g_1 + g_2)|\,k\,\rangle. \tag{2.70}$$

Together with (2.62) we thus find

$$(-\tilde{h}_{k,k+1} + d_1 + d_2 - g_1 + g_2)|\,k\,\rangle - d_1|\,k-1\,\rangle - d_2|\,k+1\,\rangle = 0. \tag{2.71}$$

The quantities $g_{1,2}$ are obtained from the boundary conditions (Appendix B).

This is a set of 9 equations for the bulk rates. We have found a solution (see Appendix B) with $w_{24} = 0$. Putting this into the 9 equations (2.155)-(2.163) one finds after some straightforward algebra

$$d_2 = z_2 = 0, \tag{2.72}$$

$$d_1 = \frac{S}{\nu_1} = \frac{w_{42}}{\nu_1}, \tag{2.73}$$

$$w_{57} = w_{37} = 0, \tag{2.74}$$

$$w_{86} = w_{68}. \tag{2.75}$$

In this model there is a strong driving force for the positive particles that leads them to move only to the right as in the totally asymmetric simple exclusion process. $z_2 = 0$ means that in the right branch of the shock the lattice is completely filled with positive particles (see Fig. 2.2). Hence incoming A-particles which react with B particles in the left branch of the shock hit the pure A-domain where they stop because of the single-file (exclusion) condition. The shock that separates the two domain moves only to the left with rate d_1. Hence its mean velocity v_s and diffusion coefficient D_s are determined by the density and hopping rate only of the A-particles in the left domain

$$v_s = 2D_s = w_{42}\rho_1^A. \tag{2.76}$$

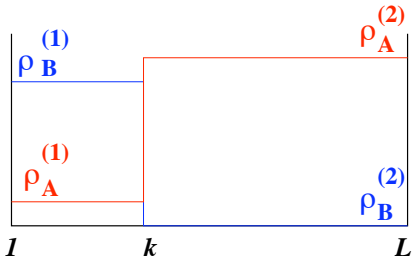

Figure 2.2: Density profile of a shock measure in the case $z_2 = 0$.

The interpretation of this result for the cracking process is readily available by interchanging the role of positive particles and vacancies. The right branch of the shock is the empty lattice where no reactions are going on. The left branch is active. All particles are driven to the left so that the inactive region grows diffusively with drift and fluctuations determined by (2.76) and ρ_1^A replaced by the vacancy density in the active domain.

We note that PT-invariance of the special model with $w_{24} = 0$ leads to

$$w_{35} = 0, \tag{2.77}$$

and to the stationary state condition

$$w_{42} = w_{73} + w_{53}. \tag{2.78}$$

The properties of the shock are not effected by PT-invariance.

2.4 Exclusion process with binary internal degree of freedom

Here we investigate the degenerate conservation law. The degenerate function $C(n)$ in (2.4) has a natural interpretation as counting the number of particles at a given site irrespective of its internal state. Here we assign state 0 to an empty lattice site, state 1 to a particle of type A and state 2 to a particle of type B. The labels A and B represent two possible internal states of a particle. As in the first model in section (2.3) there are 3 states but the conservation law on particles leads to different dynamics. Eq.(2.4) forces to 48 transitions rates to vanish. The following 24 transitions remain:

$$\begin{array}{llll}
0A \to A0 & w_{42}, & A0 \to 0A & w_{24}, \\
0B \to B0 & w_{73}, & B0 \to 0B & w_{37}, \\
AB \to BA & w_{86}, & BA \to AB & w_{68}, \\
B0 \to A0 & w_{47}, & 0A \to 0B & w_{32}, \\
0B \to A0 & w_{43}, & 0A \to B0 & w_{72}, \\
A0 \to B0 & w_{74}, & 0B \to 0A & w_{23}, \\
B0 \to 0A & w_{27}, & A0 \to 0B & w_{34}, \\
BA \to AA & w_{58}, & AA \to AB & w_{65}, \\
AB \to AA & w_{56}, & AA \to BA & w_{85}, \\
BB \to AA & w_{59}, & AA \to BB & w_{95}, \\
BB \to BA & w_{89}, & AB \to BB & w_{96}, \\
BB \to AB & w_{69}, & BA \to BB & w_{98}.
\end{array} \tag{2.79}$$

We represent the single-site basis vectors for this model as

$$|0) = \begin{pmatrix} 1 \\ 0 \\ 0 \end{pmatrix}, \quad |A) = \begin{pmatrix} 0 \\ 1 \\ 0 \end{pmatrix}, \quad |B) = \begin{pmatrix} 0 \\ 0 \\ 1 \end{pmatrix} \tag{2.80}$$

and parametrize the stationary one-site marginal

$$|P) = \frac{1}{\nu} \begin{pmatrix} 1 \\ z \\ cz \end{pmatrix} \tag{2.81}$$

by a fugacity z and the ratio c of A and B concentrations. The normalization factor

$$\nu = 1 + z + cz \tag{2.82}$$

is the local partition function. Thus one has for this grandcanonical ensemble

$$\rho^A = \frac{z}{\nu}, \quad \rho^B = c\frac{z}{\nu} \tag{2.83}$$

and for the total conserved particle density

$$\rho := \rho^A + \rho^B = z\frac{d}{dz}\ln\nu = (1+c)\frac{z}{\nu}. \tag{2.84}$$

In formal analogy to systems in thermal equilibrium we shall refer to the logarithm of the fugacity as chemical potential.

Parity-time invariance leads to pairwise relations between some of the rates of (2.79). Using (2.81) this yields the following symbolic relations for the rates

$$w(A \to\ B) = cw(B \to A) \tag{2.85}$$

for each particle on a pair of neighboring sites.In order to illustrate how this equation leads to some relations between rates, we calculate one of them explicitly. For example the reaction process $AB \to\ AA$ with the rate w_{56} changes to $AA \to\ AB$ after applying time reversal symmetry and by operating space reflection one obtains $AA \to\ BA$ with the rate w_{86}. By using (2.85) for every single site we obtain $w_{85} = cw_{56}$. With the relation (2.85) we can reduce

the number of independent rates in the process (2.79) to only 15 nonstationary rates, viz. 6 hopping rates and 9 "reaction rates" for changes of the internal states of the particles. For clarity we represent all of the hopping rates by h's and reaction process by r's and write the rates as

$$\begin{aligned}
w_{47} = r_1,\ w_{32} = cr_1,\\
w_{43} = r_2,\ w_{72} = cr_2,\\
w_{23} = r_3,\ w_{74} = cr_3,\\
w_{27} = r_4,\ w_{34} = cr_4,\\
w_{58} = r_5,\ w_{65} = cr_5,\\
w_{56} = r_6,\ w_{85} = cr_6,\\
w_{59} = r_7, w_{95} = c^2 r_7,\\
w_{89} = r_8,\ w_{96} = cr_8,\\
w_{69} = r_9,\ w_{98} = cr_9,\\
w_{42} = h_1,\ \ w_{73} = h_2,\\
w_{24} = h_3,\ \ w_{86} = h_4,\\
w_{68} = h_5,\ \ w_{37} = h_6.
\end{aligned} \tag{2.86}$$

In the quantum Hamiltonian formalism, the bulk transition matrix is then given by

$$h_{k,k+1} = -\begin{pmatrix}
. & 0 & 0 & 0 & 0 & 0 & 0 & 0 & 0\\
0 & . & r_3 & h_3 & 0 & 0 & r_4 & 0 & 0\\
0 & cr_1 & . & cr_4 & 0 & 0 & h_6 & 0 & 0\\
0 & h_1 & r_2 & . & 0 & 0 & r_1 & 0 & 0\\
0 & 0 & 0 & 0 & . & r_6 & 0 & r_5 & r_7\\
0 & 0 & 0 & 0 & cr_5 & . & 0 & h_5 & r_9\\
0 & cr_2 & h_2 & cr_3 & 0 & 0 & . & 0 & 0\\
0 & 0 & 0 & 0 & cr_6 & h_4 & 0 & . & r_8\\
0 & 0 & 0 & 0 & c^2 r_7 & cr_8 & 0 & cr_9 & .
\end{pmatrix}_{k,k+1} . \tag{2.87}$$

We consider an open boundary model with injection and extraction rates in the left and the right boundary defined exactly as in the previous model. The boundary matrices h_1 and h_L in the Hamiltonian (2.17) are then given by (2.18) and (2.19).

2.4.1 Product measure

With (2.81) the homogeneous product measure has the form

$$|\, P^* \,\rangle = \frac{1}{\nu^L} \begin{pmatrix} 1 \\ z \\ cz \end{pmatrix}^{\otimes L} . \tag{2.88}$$

It is convenient to define

$$\hat{h}_{i,i+1} = h_i - [E(\hat{n}_i^A - \hat{n}_{i+1}^A) + E'(\hat{n}_i^B - \hat{n}_{i+1}^B)] \tag{2.89}$$

where E, E' are arbitrary constants and $\hat{n}_A$ and $\hat{n}_B$ are number operators with eigenvalue 1 if a particle of the respective species is present and 0 otherwise. Furthermore we define modified boundary matrices

$$\hat{b}_1 = b_1 + E\hat{n}_1^A + E'\hat{n}_1^B, \quad \hat{b}_L = b_L - E\hat{n}_L^A - E'\hat{n}_L^B. \tag{2.90}$$

This allows us to rewrite the quantum Hamiltonian as

$$H = \hat{b}_1 + \sum_{i=1}^{L-1} \hat{h}_{i,i+1} + \hat{b}_L. \tag{2.91}$$

The eigenvalue equation (2.22) may be rewritten

$$0 = \hat{h}_{i,i+1}|\, P^* \,\rangle = (\hat{b}_1 + g)|\, P^* \,\rangle = (\hat{b}_L - g)|\, P^* \,\rangle. \tag{2.92}$$

with a further arbitrary constant g.

This trick allows us to determined the conditions on the rates that ensure that (2.88) actually is stationary. For the bulk rates (2.92) yields

$$\begin{aligned} E &= h_3 - h_1 + c(r_3 + r_4 - r_1 - r_2), \\ E' &= h_6 - h_2 + r_1 + r_4 - r_2 - r_3. \end{aligned} \tag{2.93}$$

Furthermore, some algebra shows that the bulk rates must satisfy the following condition for stationarity

$$h_6-h_2+h_1-h_3+h_4-h_5+(1+c)(r_1-r_3)+(1-c)(r_4-r_2)+c(r_8-r_9)+r_6-r_5=0. \tag{2.94}$$

In order to satisfy the eigenvalue equation at the boundaries the terms involving E, E' must cancel. For the left boundary this yields the two relations

$$\begin{aligned}[h_1-h_3+c(2(r_2-r_4)+h_2-h_6)]z &= \gamma_1 z\nu+\gamma_2 cz\nu-(\alpha_1+\alpha_2)\nu \\ &= -\beta_1 z\nu-\beta_2 cz\nu+(\delta_1+\delta_2)\nu,\end{aligned} \tag{2.95}$$

and similarly at the right boundary

$$\begin{aligned}[(-r_5+r_6+c(r_8-r_9)+h_4-h_5)z-r_1+r_2+r_3-r_4+h_2-h_6]cz& \\ =(\gamma_2+\gamma_3)cz\nu-\alpha_2\nu-\alpha_3 z(1+z)\nu& \\ =-(\beta_2+\beta_3)cz\nu+\delta_2\nu+\delta_3 z(1+z)\nu.&\end{aligned} \tag{2.96}$$

These relations define a model for which the product measure with constant fugacity z is stationary. The fugacity is determined by its boundary value encoded in the boundary rates.

2.4.2 Fugacity gradient

Now we generalize the model to allow for different fugacities z_1, z_2 at the two boundaries. The product measure is then no longer stationary and there is no general principle that would constrain the form of the stationary distribution. However, in principle its properties can be calculated from the studying the time evolution of the system starting from some initial distribution.

In general, solving for the dynamics of a many-particle system is a much harder task than determining its stationary distribution. However, guided by previous experience [56] we make as ansatz an initial distribution which is a shock measure connecting the two boundary fugacities. The representation of

the shock measure here is

$$|\, k \,\rangle = \frac{1}{\nu_1^k \nu_2^{(L-k)}} \begin{pmatrix} 1 \\ z_1 \\ cz_1 \end{pmatrix}^{\otimes k} \otimes \begin{pmatrix} 1 \\ z_2 \\ cz_2 \end{pmatrix}^{\otimes L-k} . \tag{2.97}$$

On a coarse-grained scale the density profile corresponding to this measure has a jump discontinuity, see Fig. 2.1. We search for conditions on the rates such that 2.62 is satisfied. This implies that the family of shock measures labelled by the shock position k is closed under the time evolution of the many-particle system. Physically this behaviour corresponds to a random walk of the shock with hopping rates d_1, (d_2) to the left (right).

In order to have the random walk equation (2.62) for the shock, one replaces the left hand side by the (negative) quantum Hamiltonian in the form (2.91). Then in each branch of the shock one has $\hat{h}_{i,i+1}|\, k \,\rangle = 0$, except for $i = k$. Stationarity at the boundaries implies

$$b_1|\, P^* \,\rangle = (-E\hat{n}_1^A - E'\hat{n}_1^B + g_1)|\, P^* \,\rangle, \tag{2.98}$$

$$b_L|\, P^* \,\rangle = (E\hat{n}_L^A + E'\hat{n}_L^B - g_2)|\, P^* \,\rangle, \tag{2.99}$$

where g_1 and g_2 are obtained using (2.93) as

$$\begin{aligned} g_1 &= E\frac{z_1}{\nu_1} + E'\frac{cz_1}{\nu_1} = (1+c)(p-q)\frac{z_1}{\nu_1} \\ &= \alpha_1 + \alpha_2 - (\gamma_1 + c\gamma_2)z_1, \end{aligned} \tag{2.100}$$

$$\begin{aligned} g_2 &= E\frac{z_2}{\nu_2} + E'\frac{cz_2}{\nu_2} = (1+c)(p-q)\frac{z_2}{\nu_2} \\ &= -(\delta_1 + \delta_2) + (\beta_1 + c\beta_2)z_2. \end{aligned} \tag{2.101}$$

The random walk condition for the shock thus leads to 9 equations for the bulk rates represented in the last section in Eq.(2.71) for the bulk rates. Three of these conditions are fulfilled without any constraint on the rates, leaving the

following 6 equations :

$$S - d_1\frac{\nu_1}{\nu_2} - d_2\frac{\nu_2}{\nu_1} = 0, \tag{2.102}$$

$$(cr_4 + h_3)(z_1 - z_2) + Sz_2 - d_1 z_2\frac{\nu_1}{\nu_2} - d_2 z_1\frac{\nu_2}{\nu_1} = 0, \tag{2.103}$$

$$(r_4 + h_6)(z_1 - z_2) + Sz_2 - d_1 z_2\frac{\nu_1}{\nu_2} - d_2 z_1\frac{\nu_2}{\nu_1} = 0, \tag{2.104}$$

$$(cr_2 + h_1)(z_2 - z_1) + Sz_1 - d_1 z_2\frac{\nu_1}{\nu_2} - d_2 z_1\frac{\nu_2}{\nu_1} = 0, \tag{2.105}$$

$$S - d_1\frac{z_2\nu_1}{z_1\nu_2} - d_2\frac{z_1\nu_2}{z_2\nu_1} = 0, \tag{2.106}$$

$$(r_2 + h_2)(z_2 - z_1) + Sz_1 - d_1 z_2\frac{\nu_1}{\nu_2} - d_2 z_1\frac{\nu_2}{\nu_1} = 0, \tag{2.107}$$

where

$$S = d_1 + d_2 + g_2 - g_1. \tag{2.108}$$

Solving the above equations leads to three independent relations between bulk rates and densities

$$h_3 + cr_4 = h_6 + r_4 \equiv p, \tag{2.109}$$

$$h_1 + cr_2 = h_2 + r_2 \equiv q, \tag{2.110}$$

$$\frac{p}{q} = \frac{z_2}{z_1}, \tag{2.111}$$

and two relations

$$d_1 = q\frac{\nu_2}{\nu_1}, \tag{2.112}$$

$$d_2 = p\frac{\nu_1}{\nu_2}, \tag{2.113}$$

that express the shock hopping rates in terms of the hopping rates of the model and the fugacities of the shock. On this parameter manifold the stationarity condition (2.94) reduces to

$$h_4 - h_5 + (1 + c)(r_1 - r_3) + c(r_8 - r_9) + r_6 - r_5 = 0. \tag{2.114}$$

The shock performs a random walk for a specific ratio of the boundary fugacities, or, equivalently, at some specific strength of the driving force encoded in the particle hopping rates. Thus shock mean velocity v_s in terms of vacancy density and hopping rates is

$$v_s = \frac{q\nu_2^2 - p\nu_1^2}{\nu_1\nu_2}, \tag{2.115}$$

and its diffusion coefficient as long as the shock is far from the boundaries is

$$D_s = \frac{p\nu_1^2 + q\nu_2^2}{2\nu_1\nu_2}. \tag{2.116}$$

From the shock hopping rates and its biased random walk dynamics we can read off the stationary distribution of the system for different boundary densities. This is a linear combination of shock measures

$$|\, P^* \,\rangle \propto \sum_k \left(\frac{d_1}{d_2}\right)^k |\, k \,\rangle. \tag{2.117}$$

For $d_1 > d_2$ (bias to the right) the stationary shock position is in the vicinity of the right boundary, leaving the system in a phase of low density. Conversely, for $d_1 < d_2$, the system is in a high-density phase. At $d_1 = d_2$ the system undergoes a first-order nonequilibrium transition [46]. Here the shock has no bias and can be found with equal probability anywhere on the lattice. The stationary density profile is linear, but a typical particle configuration has two different regions of constant (but fluctuating) density. The density jumps quickly from one density to another in some small region of the lattice.

2.4.3 Steady state current

In order to make contact with the ASEP we calculate the stationary current for this model. In order to identify the current we first calculate the equation of motion for the expected local particle densities,

$$\begin{aligned}
\frac{d}{dt}\langle n_k^A\rangle \;=\; & -(h_1 + cr_1 + cr_2)\langle n_{k-1}^0 n_k^A\rangle + h_3\langle n_{k-1}^A n_k^0\rangle + (h_4 - r_6)\langle n_{k-1}^A n_k^B\rangle \\
& -(h_5 + cr_9)\langle n_{k-1}^B n_k^A\rangle + r_3\langle n_{k-1}^0 n_k^B\rangle + r_4\langle n_{k-1}^B n_k^0\rangle \\
& -c(r_5 + cr_7)\langle n_{k-1}^A n_k^A\rangle + (r_7 + r_8)\langle n_{k-1}^B n_k^B\rangle + h_1\langle n_k^0 n_{k+1}^A\rangle \\
& -(h_3 + cr_3 + cr_4)\langle n_k^A n_{k+1}^0\rangle - (h_4 + cr_8)\langle n_k^A n_{k+1}^B\rangle \\
& +(h_5 + r_5)\langle n_k^B n_{k+1}^A\rangle + r_1\langle n_k^B n_{k+1}^0\rangle - r_2\langle n_k^0 n_{k+1}^B\rangle \\
& -c(r_6 + cr_7)\langle n_k^A n_{k+1}^A\rangle + (r_7 + r_9)\langle n_k^B n_{k+1}^B\rangle,
\end{aligned} \tag{2.118}$$

$$\begin{aligned}\frac{d}{dt}\langle n_k^B\rangle &= -(h_2+r_2+r_3)\langle n_{k-1}^0 n_k^B\rangle + h_6\langle n_{k-1}^B n_k^0\rangle - (h_4+r_6)\langle n_{k-1}^A n_k^B\rangle \\ &+(h_5+cr_9)\langle n_{k-1}^B n_k^A\rangle + cr_1\langle n_{k-1}^0 n_k^A\rangle + cr_4\langle n_{k-1}^A n_k^0\rangle \\ &+c(r_5+cr_7)\langle n_{k-1}^A n_k^A\rangle - (r_7+r_8)\langle n_{k-1}^B n_k^B\rangle + h_2\langle n_k^0 n_{k+1}^B\rangle \\ &-(h_6+r_1+r_4)\langle n_k^B n_{k+1}^0\rangle + (h_4+cr_8)\langle n_k^A n_{k+1}^B\rangle \\ &-(h_5+r_5)\langle n_k^B n_{k+1}^A\rangle + cr_2\langle n_k^0 n_{k+1}^A\rangle + cr_3\langle n_k^A n_{k+1}^0\rangle \\ &+c(r_6+cr_7)\langle n_k^A n_{k+1}^A\rangle - (r_7+r_9)\langle n_k^B n_{k+1}^B\rangle.\end{aligned} \tag{2.119}$$

This can be written in terms of A and B particle current

$$\frac{d}{dt}\langle n_k^A\rangle = j_{k-1}^A - j_k^A + S_k, \tag{2.120}$$

$$\frac{d}{dt}\langle n_k^B\rangle = j_{k-1}^B - j_k^B - S_k, \tag{2.121}$$

where the source term

$$\begin{aligned}S_k &= (cr_1 - \frac{cr_2}{2})\langle n_{k-1}^0 n_k^A\rangle + (\frac{r_2}{2}+r_3)\langle n_{k-1}^0 n_k^B\rangle + \frac{r_4}{2}\langle n_{k-1}^B n_k^0\rangle \\ &-\frac{cr_4}{2}\langle n_{k-1}^A n_k^0\rangle - (cr_5+c^2r_7)\langle n_{k-1}^A n_k^A\rangle + r_6\langle n_{k-1}^A n_k^B\rangle \\ &+(r_7+r_8)\langle n_{k-1}^B n_k^B\rangle - cr_9\langle n_{k-1}^B n_k^A\rangle + (r_1+\frac{r_4}{2})\langle n_k^B n_{k+1}^0\rangle \\ &+\frac{r_2}{2}\langle n_k^0 n_{k+1}^B\rangle - \frac{cr_2}{2}\langle n_k^0 n_{k+1}^A\rangle - (cr_3+\frac{cr_4}{2})\langle n_k^A n_{k+1}^0\rangle \\ &+r_5\langle n_k^B n_{k+1}^A\rangle - (cr_6+c^2r_7)\langle n_k^A n_{k+1}^A\rangle + (r_7+r_9)\langle n_k^B n_{k+1}^B\rangle \\ &-cr_8\langle n_k^A n_{k+1}^B\rangle.\end{aligned} \tag{2.122}$$

expresses the fact that the individual particle densities are not conserved. The particle currents are given by the expectations

$$\begin{aligned}j_k^A &= -(h_1+\frac{cr_2}{2})\langle n_k^0 n_{k+1}^A\rangle + (h_3+\frac{cr_4}{2})\langle n_k^A n_{k+1}^0\rangle + h_4\langle n_k^A n_{k+1}^B\rangle \\ &-h_5\langle n_k^B n_{k+1}^A\rangle - \frac{r_2}{2}\langle n_k^0 n_{k+1}^B\rangle + \frac{r_4}{2}\langle n_k^B n_{k+1}^0\rangle,\end{aligned} \tag{2.123}$$

$$\begin{aligned} j_k^B &= -(h_2 + \frac{r_2}{2})\langle n_k^0 n_{k+1}^B\rangle + (h_6 + \frac{r_4}{2})\langle n_k^B n_{k+1}^0\rangle - h_4\langle n_k^A n_{k+1}^B\rangle \\ &\quad + h_5\langle n_k^B n_{k+1}^A\rangle - \frac{cr_2}{2}\langle n_k^0 n_{k+1}^A\rangle + \frac{cr_4}{2}\langle n_k^A n_{k+1}^0\rangle. \end{aligned} \tag{2.124}$$

By adding the two individual currents we find the total particle current to be given by

$$\begin{aligned} j_k &= j_k^A + j_k^B \\ &= -h_1\langle n_k^0 n_{k+1}^A\rangle + h_3\langle n_k^A n_{k+1}^0\rangle - h_2\langle n_k^0 n_{k+1}^B\rangle + h_6\langle n_k^B n_{k+1}^0\rangle \\ &\quad -r_2\langle n_k^0 n_{k+1}^B\rangle - cr_2\langle n_k^0 n_{k+1}^A\rangle + cr_4\langle n_k^A n_{k+1}^0\rangle + r_4\langle n_k^B n_{k+1}^0\rangle. \end{aligned} \tag{2.125}$$

In the steady state we obtain

$$j^* = \frac{h_3 - h_1 + c(h_6 - h_2) + 2c(r_4 - r_2)}{1 + c}\rho(1 - \rho), \tag{2.126}$$

where ρ is the average density (2.84). This can be written in terms of E and E'

$$j^* = \frac{E + cE'}{1 + c}\rho(1 - \rho). \tag{2.127}$$

This is the well-known parabolic current-density relation of the ASEP [41, 42] where the density-independent pre-factor plays the role of the hopping bias. In fact, on the special manifold which gives rise to the random walk of the shock we find, using (2.109)-(2.110), the simpler expression

$$j^* = (p - q)\rho(1 - \rho). \tag{2.128}$$

2.5 Conclusions

In this chapter we have found that three-states lattice gases with a single local conservation law can be classified into two families, one where the function is degenerate, i.e., takes the same value for two different states, another where the conserved quantity is a linear nondegenerate function of the occupation

variable. The nonlinear nondegenerate functions lead to two independently conserved quantities.

In the case of nondegenrate conservation law we have studied the dynamics of a family of one-dimensional driven two-component reaction-diffusion processes with open boundaries on microscopic *lattice scale* and derived a hydrodynamic description on coarse grained Eulerian scale. This is the first main result, see Eqs. (2.48), (2.59), (2.60). The hydrodynamic equation is nonlinear and therefore admits shock solutions, corresponding to phase-separated states of the system. This generalizes one-dimensional field-induced phase separation that has been studied in some detail for lattice fluids in thermal equilibrium [80].

The degenerate linear conservation describes a class of asymmetric exclusion processes with a binary internal degree of freedom. We have identified constraints on the transition rates such that the stationary distribution is a product measure, parametrized by the nonequilibrium analog of the fugacity. Also for open systems with different boundary fugacities we have found a complete list of models where the shock performs a biased random walk on the lattice. For these systems we have detailed knowledge about the microscopic structure of the shock. these shocks are intrinsically maximally sharp and behave like collective single-particle excitations already on the lattice scale – not only after coarse-graining where all the microscopic features of the shock are lost. Apparently this enormous reduction in the number of dynamical degrees of freedom in a subspace of the stochastic dynamics appears more frequently than previously suggested [58].

An immediate consequence of the random walk dynamics of the shock is the existence of a first order boundary-induced phase transition which occurs if the boundary fugacities reverse the mean shock velocity. Away from this special manifold our result for the sharpness of the shock suggest that finite systems with lattice size of the order 10 can be well described by the domain wall theory for first order boundary-induced phase transitions, [46, 47], with limitations analogous to those obtained from the exact results of Ref. [72].

It is intriguing that the maximal sharpness appears at some specific value

of the driving force or, equivalently, ratio of boundary fugacities. It would be interesting to investigate whether such a field-induced sharpening of the interface is a special property of lattice models or can appear also in continuum systems such as the recently studied mass transfer models [81, 82]. It is also an open problem whether there can be an analogous reduction of the shock dynamics to a random walk problem in exclusion processes where the stationary distribution does not factorize. [83, 84]

2.6 Appendix A: Stationarity condition

Assuming product measure as stationary solution, we have

$$|\, P^* \,\rangle = \frac{1}{\nu^L} \begin{pmatrix} 1 \\ z \\ rz^2 \end{pmatrix}^{\otimes L} . \tag{2.129}$$

With (2.63)-(2.65), where n_i^A and n_i^B are number operators

$$n_i^A = \begin{pmatrix} 1 & 0 & 0 \\ 0 & 0 & 0 \\ 0 & 0 & 0 \end{pmatrix}_i , \qquad n_i^B = \begin{pmatrix} 0 & 0 & 0 \\ 0 & 0 & 0 \\ 0 & 0 & 1 \end{pmatrix}_i , \tag{2.130}$$

and eigenvalue equation

$$H|\, P^* \,\rangle = 0, \tag{2.131}$$

we write

$$\tilde{h}_{i,i+1}|\, P^* \,\rangle = (\tilde{b}_1 + \tilde{b}_L)|\, P^* \,\rangle = 0. \tag{2.132}$$

$\tilde{h}_{i,i+1}$ in terms of arbitrary constants F and F' is given by

$$\tilde{h}_{i,i+1} =$$

$$-\begin{pmatrix} 0 & 0 & 0 & 0 & 0 & 0 & 0 & 0 & 0 \\ 0 & -F-w_{42} & 0 & w_{24} & 0 & 0 & 0 & 0 & 0 \\ 0 & 0 & -\Theta_1 & 0 & w_{35} & 0 & w_{37} & 0 & 0 \\ 0 & w_{42} & 0 & F-w_{24} & 0 & 0 & 0 & 0 & 0 \\ 0 & 0 & w_{53} & 0 & -(w_{35}+w_{75}) & 0 & w_{57} & 0 & 0 \\ 0 & 0 & 0 & 0 & 0 & F'-w_{86} & 0 & w_{68} & 0 \\ 0 & 0 & w_{73} & 0 & w_{75} & 0 & -\Theta_2 & 0 & 0 \\ 0 & 0 & 0 & 0 & 0 & w_{86} & 0 & -F'-w_{68} & 0 \\ 0 & 0 & 0 & 0 & 0 & 0 & 0 & 0 & 0 \end{pmatrix}_{i,i+1} , \tag{2.133}$$

where

$$\Theta_1 = F - F' + w_{53} + w_{73}, \tag{2.134}$$

$$\Theta_2 = -F + F' + w_{37} + w_{57}. \tag{2.135}$$

Substituting $\tilde{h}_{i,i+1}$ in the Eq. (A-7) yields 5 independent equations. One gets F and F' by solving following equations

$$(F + w_{42} - w_{24})z = 0, \tag{2.136}$$

$$(-F' + w_{86} - w_{68})rz^2 = 0. \tag{2.137}$$

Hence F and F' are

$$F = w_{24} - w_{42}, \tag{2.138}$$

$$F' = w_{86} - w_{68}. \tag{2.139}$$

Three remained equations which have to be satisfied are

$$(w_{37} - \Theta_1)rz^2 + w_{35}z^2 = 0, \tag{2.140}$$

$$(w_{73} - \Theta_2)rz^2 + w_{75}z^2 = 0, \tag{2.141}$$

$$(w_{53} + w_{57})rz^2 - (w_{35} + w_{75})z^2 = 0. \tag{2.142}$$

From Eq. (A-17) we obtain

$$r = \frac{w_{35} + w_{75}}{w_{53} + w_{57}}. \tag{2.143}$$

Subtracting Eq. (A-15) from Eq. (A-16) yields second stationary state condition

$$w_{24} - w_{42} + w_{68} - w_{86} + w_{73} - w_{37} = \frac{w_{35}w_{57} - w_{53}w_{75}}{w_{35} + w_{75}}, \tag{2.144}$$

where the sum of (A-15) and (A-16) is already satisfied.

This model is assumed to have open boundaries, therefore b_1 and b_L in terms of injection and extraction rates are given by Eq. (2.18) and Eq. (2.19). For satisfying Eq. (A-6) for the model with open boundaries one writes

$$b_1|\, P^* \rangle = (F\hat{n}_1^A + F'\hat{n}_1^B + g)|\, P^* \rangle, \tag{2.145}$$

$$b_L|\, P^* \rangle = -(F\hat{n}_L^A + F'\hat{n}_L^B + g)|\, P^* \rangle. \tag{2.146}$$

where g is an arbitrary constant. Eq. (A-22) for the left boundary leads to three equations

$$(\alpha_1 + \alpha_2) - \gamma_1 z - \gamma_2 rz^2 = F + g, \tag{2.147}$$

$$-\alpha_1 + (\gamma_1 + \alpha_3)z - \gamma_3 rz^2 = gz, \tag{2.148}$$

$$-\alpha_2 - \alpha_3 z + (\gamma_2 + \gamma_3)rz^2 = (F' + g)rz^2. \tag{2.149}$$

We then obtain g

$$\begin{aligned} g &= -\frac{F + F' r z^2}{\nu} \\ &= \gamma_1 + \alpha_3 - \frac{\alpha_1}{z} - r z \gamma_3. \end{aligned} \tag{2.150}$$

One also can obtain two conditions for boundary rates, which for the left one

$$(w_{42} - w_{24}) z (1 + rz) - (w_{68} - w_{86}) r z^2 + (\alpha_1 + \alpha_2)\nu - \gamma_1 z \nu - \gamma_2 r z^2 \nu = 0, \tag{2.151}$$

$$(w_{68} - w_{86}) r z^2 (1 + z) - (w_{42} - w_{24}) r z^2 - \alpha_3 z \nu + (\gamma_3 + \gamma_2) r z^2 \nu - \alpha_2 \nu = 0, \tag{2.152}$$

and for the right boundary

$$(w_{42} - w_{24}) z (1 + rz) - (w_{68} - w_{86}) r z^2 - (\delta_1 + \delta_2)\nu + \beta_1 \nu + \beta_2 \mu = 0, \tag{2.153}$$

$$(w_{68} - w_{86}) \mu (1 - \mu) - (w_{42} - w_{24}) \nu \mu - (\beta_3 + \beta_2)\mu + \gamma_3 \lambda + \delta_2 \nu = 0. \tag{2.154}$$

2.7 Appendix B: Random walk conditions for the shock

Explicitly the equations (2.71) that solve the random-walk condition for the shock are given by

$$S - d_1 \frac{\nu_1}{\nu_2} - d_2 \frac{\nu_2}{\nu_1} = 0, \tag{2.155}$$

$$(S - w_{35} - w_{75}) z_1 z_2 + w_{53} r z_2^2 + w_{57} r z_1^2 - d_1 \frac{\nu_1}{\nu_2} z_2^2 - d_2 \frac{\nu_2}{\nu_1} z_1^2 = 0, \tag{2.156}$$

$$S - d_1 \frac{z_2^2}{z_1^2} \frac{\nu_1}{\nu_2} - d_2 \frac{z_1^2}{z_2^2} \frac{\nu_2}{\nu_1} = 0, \tag{2.157}$$

$$(S - w_{24}) z_2 + w_{24} z_1 - d_1 z_2 \frac{\nu_1}{\nu_2} - d_2 z_1 \frac{\nu_2}{\nu_1} = 0, \tag{2.158}$$

$$(S - w_{42}) z_1 + w_{42} z_2 - d_1 z_2 \frac{\nu_1}{\nu_2} - d_2 z_1 \frac{\nu_2}{\nu_1} = 0, \tag{2.159}$$

$$(S - w_{68}) z_2 + w_{68} z_1 - d_1 \frac{z_2^2}{z_1} \frac{\nu_1}{\nu_2} - d_2 \frac{z_1^2}{z_2} \frac{\nu_1}{\nu_2} = 0, \tag{2.160}$$

$$(S - w_{86}) z_1 + w_{86} z_2 - d_1 \frac{z_2^2}{z_1} \frac{\nu_1}{\nu_2} - d_2 \frac{z_1^2}{z_2} \frac{\nu_1}{\nu_2} = 0, \tag{2.161}$$

$$(S - w_{37} - w_{53} - \Delta) r z_2^2 + w_{35} z_1 z_2 + w_{37} r z_1^2 - d_1 r z_2^2 \frac{\nu_1}{\nu_2} - d_2 r z_1^2 \frac{\nu_2}{\nu_1} = 0, \quad (2.162)$$

$$(S - w_{73} - w_{57} + \Delta) r z_1^2 + w_{75} z_1 z_2 + w_{73} r z_2^2 - d_1 r z_2^2 \frac{\nu_1}{\nu_2} - d_2 r z_1^2 \frac{\nu_2}{\nu_1} = 0, \quad (2.163)$$

where for compact notation we have introduced

$$S = d_1 + d_2 - g_1 + g_2; \quad \Delta = w_{24} - w_{42} + w_{68} - w_{86} + w_{73} - w_{37}. \quad (2.164)$$

These relations can be rewritten as 4 independent relations between the hopping rates and the fugacities

$$w_{24} = w_{68} \equiv p, \quad (2.165)$$

$$w_{42} = w_{86} \equiv q, \quad (2.166)$$

$$\frac{p}{q} = \frac{z_2^2}{z_1^2} \equiv X^2, \quad (2.167)$$

$$S = p + q. \quad (2.168)$$

and two equations for the shock hopping rates

$$d_1 = q \frac{\nu_2}{\nu_1}, \quad (2.169)$$

$$d_2 = p \frac{\nu_1}{\nu_2}. \quad (2.170)$$

To be more specific, solving Eq. (2.155) and (2.158)-(2.159) yields Eq. (2.169) and Eq. (2.170) for d_1 and d_2, from these two and Eq. (2.157) and (2.160)-(2.161), we obtain (2.167), a relation between rates and densities, then using Eq. (2.155) with above results yields Eq. (2.165), (2.166) and (2.168).

Using these 6 relations (2.165)-(2.170), equations (2.162), (2.163) and Eq. (2.156) respectively lead to the following relations for the so far undetermined rates

$$(p - q)(1 - \frac{w_{37}}{p}) r + w_{35} (\sqrt{\frac{q}{p}} - 1) = 0, \quad (2.171)$$

$$(q - p)(1 - \frac{w_{73}}{q}) r + w_{75} (\sqrt{\frac{p}{q}} - 1) = 0, \quad (2.172)$$

$$(p + q) r^{-1} + w_{53} (\sqrt{\frac{p}{q}} - 1) + w_{57} (\sqrt{\frac{q}{p}} - 1) = 0. \quad (2.173)$$

Simplifying Eq. (2.168) by using Eqs. (2.68)-(2.69) for g_1 and g_2 yields following more explicit relation between r and X

$$r = \frac{X}{(1+X)^2}. \tag{2.174}$$

This relation on r together with Eqs. (2.171)-(2.173) and the stationary state equation (2.36), implies that $X = 0$. This solved by $p = z_2 = 0$.

The boundary equations (2.68)-(2.69) lead to

$$\begin{aligned} g_1 &= \frac{p-q}{\nu_1}(rz_1^2 - 1) \\ &= -\alpha_1 \frac{1}{z_1} - \gamma_3 r z_1 + (\gamma_1 + \alpha_3), \end{aligned} \tag{2.175}$$

$$\begin{aligned} g_2 &= \frac{p-q}{\nu_2}(rz_2^2 - 1) \\ &= \delta_1 \frac{1}{z_2} + \beta_3 r z_2 - (\beta_1 + \delta_2), \end{aligned} \tag{2.176}$$

for g_1 and g_2 respectively.

3 A simulation model of colloidal dispersions in a MPC solvent

3.1 Introduction

In this chapter we present simulations of a model of a narrow long channel which contains colloidal particles suspended in a solvent. Recently, the structure, transport properties and hydrodynamics of suspensions have received a lot of research attention [85–88]. However, calculating the nonequilibrium properties of colloidal particles suspended in a solvent is a highly nontrivial problem, since their dynamics depend on both the short-time thermal Brownian motion and the long-time hydrodynamic behaviour of the solvent [89].

It is a fundamental problem to fully including the detailed solvent dynamics in a computer simulation. This becomes more apparent when one considers the huge differences between the time- and length-scale of the dynamics of the mesoscopic colloidal particles and the microscopic solvent particles. For example a typical colloidal particle has a diameter 10-1000 nm which displaces on the order of 10^{10} water molecules each with the diameter of about 0.2 nm. Moreover, to describe the intermolecular forces between the solvent molecules, an MD scheme would need to resolve time scales on the order of $10^{-10}s$, while a colloidal particle with the diameter of $1\mu m$ takes about $1s$ to diffuses in water over its own diameter [90, 91].

Obviously, simulating even an extremely crude molecular model for the fluid particles on the time scales of interest is a difficult task. Therefore a form of coarse-graining is required, i.e., it is necessary to integrate out some degrees of freedom of the solvent particles. The object of this chapter is to describe in detail one such coarse-graining scheme which is based on the coupling of the Molecular Dynamic simulation method to a so-called MPC method. The Multi-Particle Collision dynamics (MPC) or stochastic rotation dynamics derived by Malevanets and Kapral [92] is a method to enhance the efficiency of simulation of a solvent by a coarse-grained collision step. In MPC, space is partitioned into a rectangular grid, and at a discrete time-step the particles inside each cell exchange momenta by rotating their velocity vectors relative to the center of mass velocity of the cell. Here to enforce Galilean invariance it is necessary to

include a grid-shift procedure, which was first pointed out by Ihle and Kroll [93].

After the coarse-graining of the solvent particles, a coupling between the MPC solvent and the suspended colloidal particles is required. Malevanets and Kapral [94] derived such a hybrid algorithm that combines a full MD scheme of the solute-solute and solute-solvent interactions, while treating the solvent-solvent interactions via MPC. This algorithm was applied to a two-dimensional many-particle system [95] and to the aggregation of colloidal particles [96]. The method of Malevanets and Kapral [94] has been extended and applied to the sedimentation of up to hundreds hard-sphere-(HS)-like colloids as a function of volume fraction for different Peclet numbers [97]. In this chapter, we describe the simulation of our model of colloidal suspension, based on the extended method which is proposed by Padding *et al.* in [97].

We model colloidal suspensions in confinement, which requires including geometrical restrictions into simulation [17, 86, 98]. This makes the simulation of such systems a rather challenging task [98–101]. As seen in [18, 102], the collective dynamics of particles in confinement is very different from the dynamics of the unconfined system.

We would like to restrict the motion of interacting particles such that they represent a Single-File Diffusion (SFD) [28, 29]. SFD occurs when the particles are located in a confined geometry and are unable to pass each other [21]. To this end, we set the diameter of every colloid to be comparable to the width of the channel such that the spatial sequence of the colloidal particles remains unchanged.

The Model

Here we briefly explain the model under consideration. The solvent is modeled by point-like particles and colloids represented by spherical particles with a finite diameter value. The diameter of every colloid is chosen comparable to the width of the system, in order to model SFD. Colloids are considered as hard-sphere-(HS-)like colloids, i.e, fluid particles are not allowed to penetrate

the surface of the colloidal particles. This represents one of the boundaries in the system. The channel is another boundary which is introduced in the system using different methods for the solvent and the colloidal particles: the solvent particles are treated with the bounce-back rule while colloids "sense" the wall by a determined potential.

The simulation is in two dimensions. However the movement of colloidal particles is limited in one dimension because of the confinement due to SFD. In the case when an external force is applied (see next chapter), the colloidal particles effectively move in one direction and the system is therefore effectively quasi-one-dimensional. After this introductory review, in section (3.2) we present a detailed description of the properties of a pure MPC fluid and the implementations which are required to complete an MPC simulation for a solvent located between two walls. In section (3.3) the requirements of a Molecular Dynamics simulation are explained. In section (3.4) we describe our final simulation model of colloidal suspensions in a channel, by using these two methods.

3.2 Multi-particle Collision Dynamics simulation

The Multi-particle Collision Dynamics (MPC) or Stochastic rotation dynamics (SRD) is a mesoscale simulation technique in which binary collisions are replaced by multi-particle collisions in a prescribed collision volume [103–107]. It employs a discrete time dynamics with continuous velocities and local multi-particle collisions. Mass, momentum, and energy are locally conserved quantities by construction and it has been demonstrated that the hydrodynamic equations are satisfied. MPC is also a very recent mesoscale simulation technique which was first introduced by Malevants and Kapral [92,94] in 1999. The fluid particles represented in MPC should not be viewed as some kind of composite particles or clusters. Instead the particles are merely a convenient computational device to facilitate the coarse-graining of the fluid particles [108].

3.2.1 Simulation algorithm for an MPC fluid

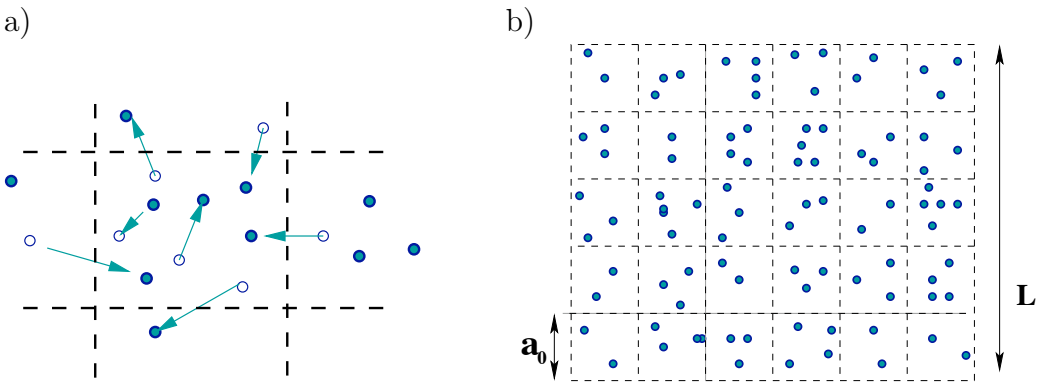

Figure 3.1: Diagram of the MPC dynamics in two dimensions. (a) Streaming step, (b) particles are sorted into collision boxes.

The fluid is modeled by N point particles, each with mass m_f. Each of the particles is characterized by its position r_i and velocities v_i and labeled with $i = 1, ..., N$. Positions and velocities are continuous variables which evolve in

a time increment τ_c by integrating Newton's equations of motion

$$m_f \frac{dv_i}{dt} = f_i, \tag{3.1}$$

$$\frac{dr_i}{dt} = v_i, \tag{3.2}$$

where f_i is the total (external) force on particle i, which may come from an external field such as gravity or a fixed boundary conditions such as suspended colloids. However the internal forces between pair of particles are neglected in the time evolution. Herein lies the main advantage of MPC. Instead of directly treating the interactions between the fluid particles, a coarse-grained collision step is performed at each time step.

In the case of a system with no external force the MPC algorithm consists of two steps, streaming and collision which are sketched in Fig. 3.1. In the streaming step, (see Fig. 3.1a), the particles evolve during time τ_c according to the following rule

$$r_i(t + \tau_c) = r_i(t) + \tau_c v_i(t). \tag{3.3}$$

In the collision step, the particles are sorted into collision boxes (see Fig. 3.1b).

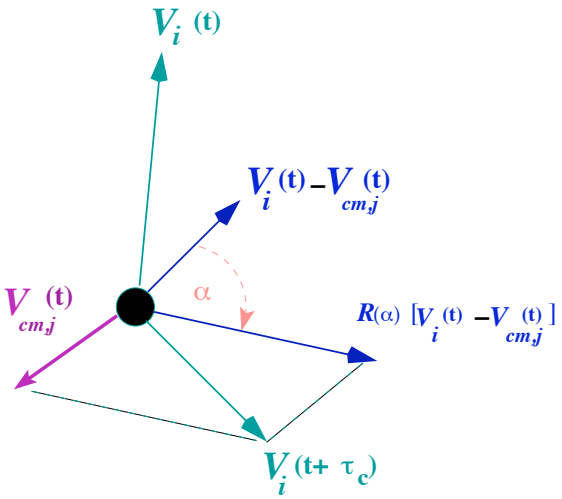

Figure 3.2: Rotation of particle velocity relative to the center of mass.

The collision boxes are typically the unit cells of a d-dimensional cubic lattice

with lattice constant a_0. The collision is then defined as a rotation of the velocities of all particles in a box in a frame co-moving with its center of mass (see Fig. 3.2). Thus the relative velocity of the ith particle after the collision is:

$$v_i(t+\tau_c) = v_{cm,j}(t) + R(\alpha)(v_i(t) - v_{cm,j}(t)), \tag{3.4}$$

while $v_{cm,j}(t)$ is the velocity of center of mass of collision box j

$$v_{cm,j}(t) = \frac{\sum_j^{(i,t)} m_f v_j}{\sum_j m_f}, \tag{3.5}$$

and $R(\alpha)$ is a stochastic rotation matrix. This implies that the magnitude and the direction of the velocity of every particles change during the collision step in a way that the total momentum and kinetic energy will be conserved within every collision box. This is easy to understand since velocity of the center of mass for every collision box $v_{cm,j}(t)$ does not change during collision,

$$\begin{aligned}
\sum_i^{(j,t)} m_f v_i(t+\tau_c) &= \sum_i m_f(v_{cm,j}(t) + R(\alpha)(v_i(t) - v_{cm,j}(t))) \\
&= \sum_i m_f v_{cm,j}(t) + \sum_i R(\alpha)(m_f v_i(t) - m_f v_{cm,i}(t)) \\
&= m_f N v_{cm,j}(t) + R(\alpha)\sum_i (m_f(v_i(t) - v_{cm,j}(t))) \\
&= \sum_i^{(j,t)} m_f v_i(t).
\end{aligned} \tag{3.6}$$

Also for the kinetic energy we obtain

$$\sum_i^{(j,t)} \frac{m_f}{2} v_i^2(t+\tau_c) = \sum_i^{(j,t)} \frac{m_f}{2} v_i^2(t). \tag{3.7}$$

Therefore with the collision rule as in Eq.(3.4), the conservation of mass, local momentum and kinetic energy are guaranteed by construction.

3.2.2 Random rotation vector

Together with the collision step, the stochastic rotation matrix $R(\alpha)$ has been introduced, such that α is a parameter of the model. In two dimension the

rotation of the relative velocity is simply given by an angle $\pm\alpha$, where the sign is independent and randomly chosen for each cell. In three dimensions a random direction is independently generated in each collision cell by selecting two uncorrelated random numbers s_1 and s_2, from an interval [0,1] [103]. The random unity vector R has components,

$$R_x = \sqrt{1-\theta_1^2}cos\theta_2, \qquad R_y = \sqrt{1-\theta_1^2}sin\theta_2, \qquad R_z = \theta_1, \qquad (3.8)$$

where $\theta_1 = 2s_1 - 1$ and $\theta_2 = 2\pi s_2$.

3.2.3 MPC units

For a MPC simulation the following units are used: lengths will be in units of cell size a_0, energies in units of system temperature k_BT and the masses in units of m_f. This is equivalent to setting a_0=1, k_BT=1 and m_f=1. Time is expressed in units of $t_0 = a_0\sqrt{\frac{m_f}{k_BT}}$. Then $\tau_c = \lambda t_0$, where λ is called the mean free path and is the average fraction of a cell size that a fluid particle travels between collisions. In the simulation, N particles are initially located in a square system of linear extension L and with initial velocities that are drawn from the Maxwell-Boltzmann velocity distribution. The average number of particles in a two dimensional system is the number density $n_f = N(\frac{a_0}{L^2})$.

3.2.4 Galilean invariance; Random shift

As already discussed, in order to perform the multi-particle collision, the particles are sorted into cells where the collisions take place. To choose these collision boxes, a preferential grid needs to be defined. A first naive choice would be a fixed grid whose outside borders coincide with the system boundaries (see Fig. 3.3a). Nevertheless, such a fixed grid does not satisfy Galilean invariance. To prove this, suppose the displacement of particle i is smaller than the size of the collision box a_0. The set of particles in the collision box in a moving frame will not be the same as in a frame at rest. This will lead to different dynamics in the two frames and therefore will cause a breakdown of the Galilean invariance.

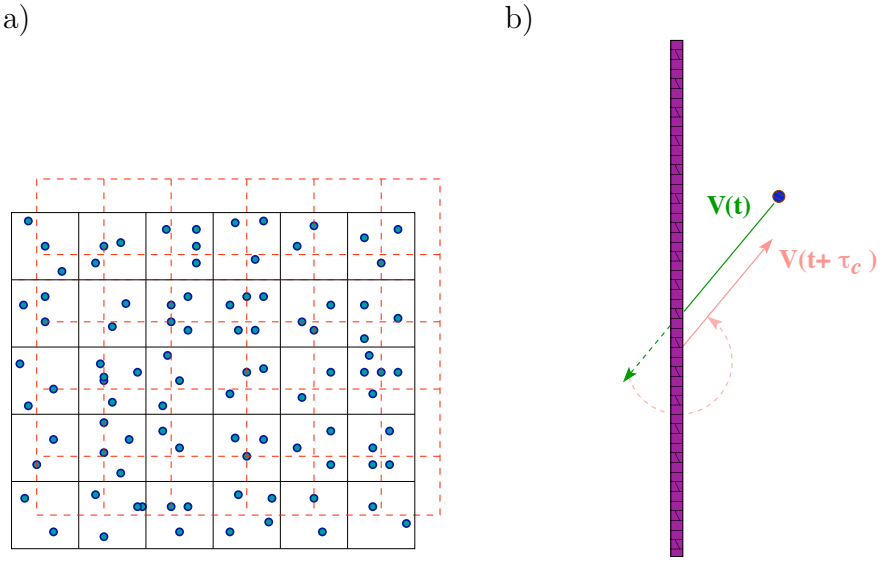

Figure 3.3: (a) Diagram of random shift of the collision grid, (b) Diagram of bounce-back rule.

Hence, a random shift of the collision grid has to be performed in the execution of the collision step [93, 109] in order to restore Galilean invariance. This Random shift is performed by displacing the collision grid by drawing a random number uniformly distributed in the interval (0,1) which is chosen independently in each collision. As a consequence of such a shift no special frame exists and Galilean invariance is restored. Hence two particles placed at a quite small distance but separated in a fixed grid now would interact. The random shift implementation also yields the result that the probability of two particles to interact will be inversely proportional to their relative distance, in a way similar to a soft range potential.

3.2.5 Implementation of walls in a MPC fluid

Modeling of many systems requires the implementation of walls as boundaries. A simple case would be the implementation of a fixed solid wall. This is performed by applying the so-called "stick boundary conditions".

For simulating fixed walls with MPC, standard *bounce-back* is applied during

the streaming step, such that when a particle hits the walls it returns in the incoming direction with equal and opposite velocity (see Fig. 3.3b).

Here we intend to derive clearly the position and the velocity of the particle after colliding with the wall at $y = 0$ for a two dimensional system. In this case, a gravitational field g exists parallel to the wall. We consider three pair of position and time for particle, (see Fig. 3.4) as follows:
The initial position when particle begins to approach the wall is (x_0, y_0) at time $t = 0$,
the position of the particle when it hits the wall at $y = 0$ is $(x_c, 0)$ at time $t = t_c$, and the final position of the particle after hitting the wall is (X, Y) at time step τ_c.

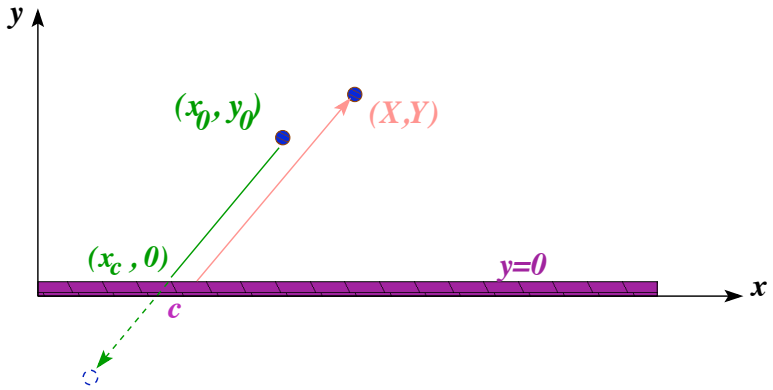

Figure 3.4: Position coordinates of a particle before and after hitting the wall.

First we calculate the colliding time t_c from the equation of motion Eq.(3.1) parallel to y direction,

$$t_c = -\frac{y_0}{v_y}, \tag{3.9}$$

so x component of the position at hitting point

$$x_c = x_0 + v_x t_c + \frac{1}{2} g t_c^2, \tag{3.10}$$

For the particle at colliding point x_c, the time requited to reach (X, Y) with inverted velocities $-v_{xc}$ and $-v_{yc}$, is $(\tau_c - t_c)$. Thus we obtain the equations for

X and Y as

$$X = x_c - v_{x_c}(\tau_c - t_c) + \frac{1}{2}g(\tau_c - t_c)^2,$$
$$Y = -v_{y_c}(\tau_c - t_c). \tag{3.11}$$

After replacing the relations for t_c and x_c, we finally obtains the components of the position of the particle

$$X = x_0 - v_x\tau_c - 2y_0\frac{v_{x_c}}{v_{y_0}},$$
$$Y = -y_0 - \tau_c v_{y_c}, \tag{3.12}$$

where the velocities read as

$$v_{x_c} = v_{x_0} + gt_c,$$
$$v_{y_c} = v_{y_0}. \tag{3.13}$$

The relations for a particle hitting the wall located at L_y can be received similarly, by substituting $y_c = L_y$.

However this will not be enough since the walls will not generally coincide with the cell boundaries, due to random shift (see Fig. 3.5). In this case the cells in the boundary will be generally partially filled, which will not lead to the desired stick boundary conditions. We therefore need a generalization of the bounce-back rule for partially filled cells. Many different schemes are possible. An efficient algorithm has been used in our simulation.

The basic idea is as follows: for all the cells of the channel that are cut by the walls, and therefore have a number of particles n which is smaller than the average number n_f of the bulk cells, "virtual particles" will be added in order to make the effective density equal to the average density. The velocities of the particles at the wall are drawn from a Maxwell-Boltzmann distribution with zero average velocity and the same temperature T as the fluid. The collision step Eq.(3.4) is then carried out with the average velocity of all particles in the cell. Since the sum of the random vectors, each drawn from a Gaussian distribution is again Gaussian, the velocities of the individual particles at the wall need not

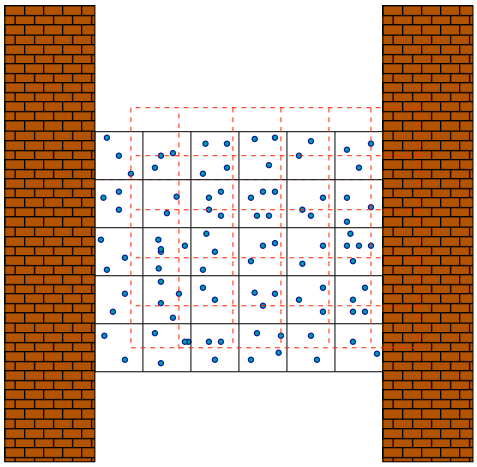

Figure 3.5: Diagram of random shift in the presence of the wall where some cells in the boundary are partially filled.

be determined explicitly. Instead, the center of mass velocity in Eq.(3.4) can be written as

$$v_{cm} = \frac{\sum_{i=1}^{n} v_i + \zeta}{n_f}, \tag{3.14}$$

where ζ is a vector whose components are numbers from the Maxwell-Boltzmann distribution with zero average and variance $(n_f - n)k_BT$.

3.2.6 MPC solvent in gravitational field

Considering a fluid resting between two planar walls, a gravitational field g is applied in one direction parallel to the walls. After a relaxation time, the system reaches a stationary state with a parabolic velocity profile between the walls and the direction of the force. It is known [110] that the measured maximum velocity v_{max} of the parabola is inversely proportional to the kinematic viscosity ν of the fluid like

$$v_{max} = \frac{gL_y^2}{8\nu}. \tag{3.15}$$

This behaviour is reproduced by MPC simulation of fluid [105,107,111]. See an example in Fig. 3.6. This parabolic profile is obtained for a two dimensional square system where $L_x = L_y = 25$. The planar fixed walls are implemented at

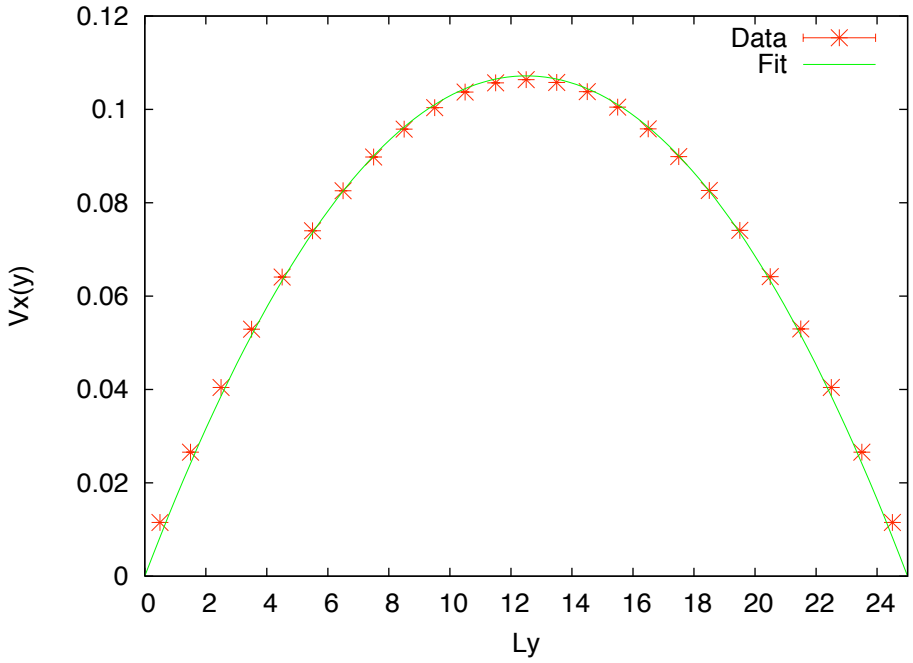

Figure 3.6: Parabolic velocity profile in the presence of gravitational field reproduced by MPC for a 2D square system. The green parabola curve has been fitted to data points to obtain ν.

$y = 0$ and $y = 25$. The simulation parameters are set for time step $\tau_c = 0.1$, particle density $n_f = 10$ and the rotational angle $\alpha = 90\,°$. The viscosity obtained from relation (3.15) for the maximum velocity in Fig. 3.6 in a gravitational field $g = 0.001$ is 0.729. This value should be compared with the value for viscosity obtained from theoretical prediction. The theoretical viscosity relation $\nu = \nu_{coll} + \nu_{kin}$ is a sum over two contributions: the kinetic viscosity ν_{kin} and the collisional viscosity ν_{coll}. The relations for ν_{coll} and ν_{kin} in two dimensions [104, 112] read as

$$\begin{aligned} \nu_{coll} &= \frac{a_0\,(1 - cos\alpha)}{12\tau_c}\left(\frac{\rho_f - 1 + e^{-\rho_f}}{\rho_f}\right), \\ \nu_{kin} &= \frac{k_B T \tau_c}{m_f}\left[\frac{1}{1 - cos2\alpha}\left(\frac{\rho_f}{\rho_f - 1 + e^{-\rho_f}}\right) - \frac{1}{2}\right], \end{aligned} \tag{3.16}$$

where a_0, ρ_f, α and τ_c are the parameters of the solvent (see subsection 3.2.3).

Calculating the theoretical viscosity for the system in Fig. 3.6 yields $\nu_{theory} =$

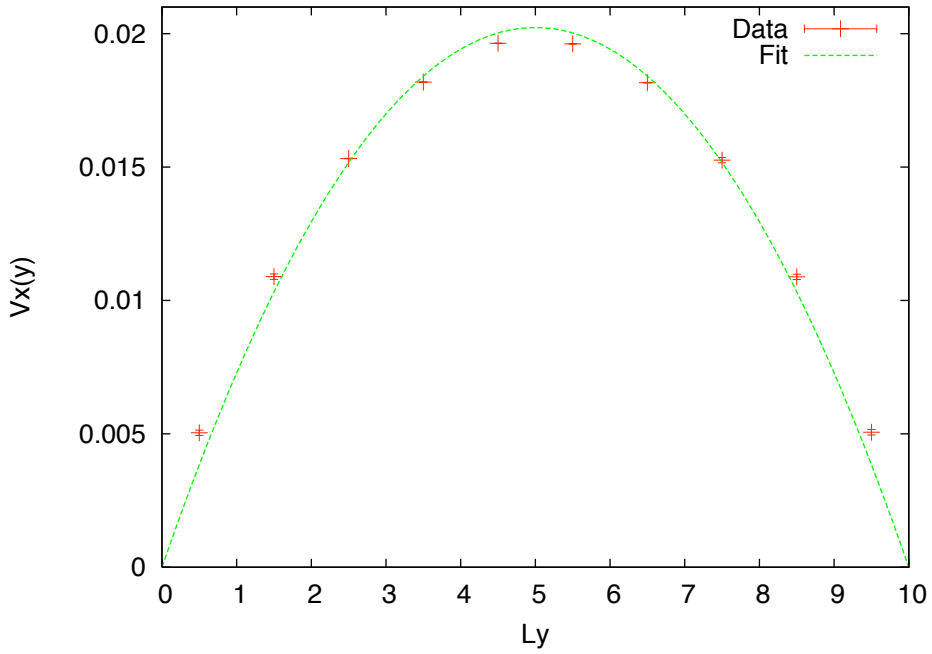

Figure 3.7: Parabolic velocity profile for the system with the width $Ly = 10$. The green curve has been fitted to data points to obtain ν.

0.755, where a good agreement with the result from our simulation can be seen. Another example depicted in Fig. 3.7, has been obtained for a system with length $L_x = 20$. Now walls are located at $y = 0$ and $y = L_y = 10$ which is closer to the representation of our final simulation model of a channel. The parameters are the same as in Fig. 3.6, except the density which is $n_f = 5$. The maximum velocity in parabolic profile of Fig. 3.7 yields viscosity $\nu = 0.6179$, where a reasonable consistency with the theoretical value $\nu_{theory} = 0.6802$ obtained from Eq.(3.16) can be seen. The maximum numerical error bar for Fig. 3.7 is of the order of 10^{-5}.

3.3 Molecular Dynamics simulation

Molecular dynamics simulations generate information on the microscopic level, in particular, atomic positions and velocities as a function of time, i.e., the complete description of the system in the sense of classical mechanics. This

microscopic information has to be translated into macroscopic observable like pressure, heat capacity, diffusion coefficient, etc., by means of statistical mechanics. Molecular dynamics simulations are exploited in a wide range of applications in fundamental and applied science. In the late 1950's [113, 114] which MD method was introduced by Adler and Wainwright to study the interactions of hard spheres. The literature, since then is full of molecular dynamics simulation results ranging from atomic and solid state physics to soft matter applications [115–118].

Today the number of simulation techniques has greatly expanded. Specialized techniques for particular problems, including mixed quantum mechanical-classical simulations,have been developed [119]. To cover the length- and time-scale gap of complex fluids, hybrid simulation techniques are exploited, where MD simulations are one of the components (see next section).

3.3.1 Equations of motion

The basic dynamical equations of classical mechanics are Newton's equations of motion. For a system of N point particles of mass $m_i (i = 1, ..., N)$ at positions r_i and velocities v_i, they are given by

$$m_i \frac{d^2 r_i}{dt^2} = F_i. \tag{3.17}$$

The forces F_i on particle i are obtained from the potential energy $U(\{r\})$ via

$$F_i = - \bigtriangledown_{r_i} U(\{r\}). \tag{3.18}$$

The solutions of these equations provide the complete information of a system for particular initial conditions, say at $t = 0, r_i(0)$ and $\dot{r_i}(0)$. Alternatively, Hamilton's equations of motion for the generalized momenta p_i and positions r_i follow from the Hamiltonian

$$H = \sum_{i=1}^{N} \frac{p_i^2}{2m_i} + U(\{r\}), \tag{3.19}$$

via the canonical equations

$$\begin{aligned} \dot{r_i} &= \bigtriangledown_{p_i} H, \\ \dot{p_i} &= -\bigtriangledown_{r_i} U(\{r\}) = F_i. \end{aligned} \tag{3.20}$$

For cartesian coordinates Hamilton's equations become

$$\begin{aligned} \dot{r_i} &= \frac{p_i}{m_i}, \\ \dot{p_i} &= -\bigtriangledown_{r_i} U(\{r\}) = F_i. \end{aligned} \tag{3.21}$$

We consider systems that are conservative, i.e., there is a potential energy which is independent of time. As a consequence, the total energy of the system $E = H = E_k + U$ is conserved, where $E_k = \sum_i m_i \dot{r_i}^2/2$ is the kinetic energy. Moreover, the systems under consideration are invariant with respect to translations which implies the conservation of the linear momentum, i.e., $\sum m_i \ddot{r_i} = 0$. To obtain a complete description of the system, one should explicitly determine the terms of potential energy in Eq.(3.21) (see below).

3.3.2 Potentials and force fields

All macroscopic properties of materials are strongly dependent on the forces among their elementary building blocks. The spectrum of properties ranges from the spatial structure of solids to the secondary and ternary structure of biological supermolecular systems. Thus, it is desirable to achieve a representation of the actual interactions in terms of the classical potential energy $U(\{r\})$ *(force field)* as accurately as possible. Nevertheless, the potential energy is an empirical quantity. Hence there is no 'correct' functional form. Its functional form is rather a compromise between accuracy and efficiency.

The potential energy of N interacting atoms can be divided into terms which are functions of the coordinates of individual atoms, pairs of atoms or atoms-triplets, etc. A constant term in the potential energy represents the effect of an external field on the system, e.g. gravitational field, electric fields, boundary walls, etc. The pair potential term is the most important. The term of triples

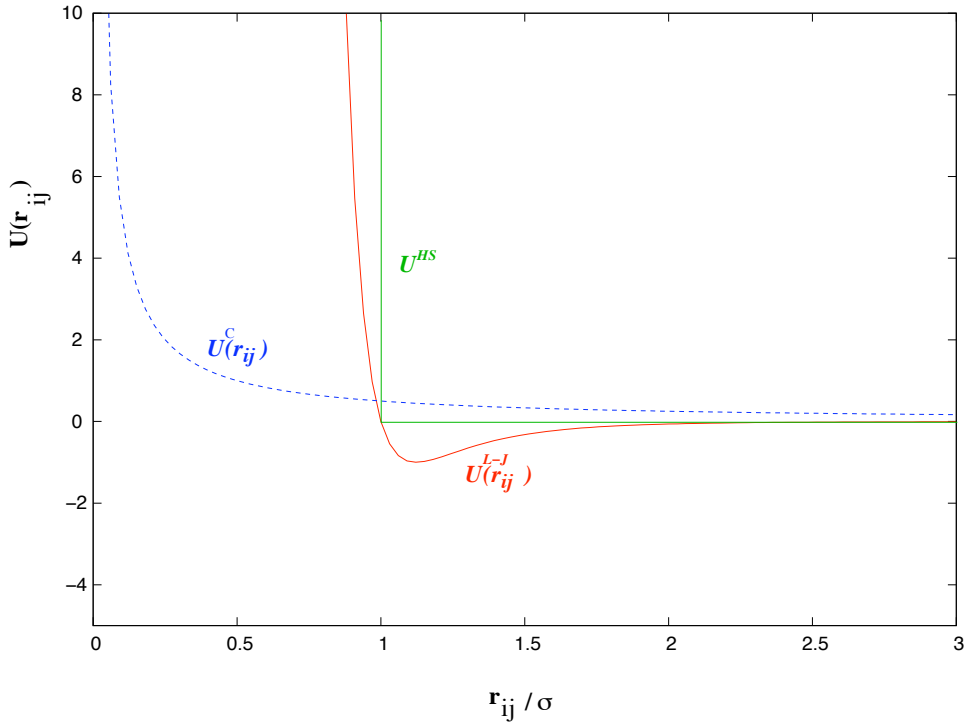

Figure 3.8: Atomic pair potentials $u(r_{ij})$ where r_{ij} represents the distance between the two atoms. The relations for U^{HS}, U^c and U^{L-J} are given in Eq.(3.22), Eq.(3.23) and Eq.(3.24) respectively.

of atoms is significant at liquid densities. Higher order terms are expected to be small. Usually triplet terms are not included in computer simulation because their computation is very time consuming. Generally, the pair potential is chosen such that it includes triplet and higher order interactions. Thus, it has to be regarded as an effective pair potential, representing all the many-body effects. A consequence of this approximation is that the effective pair potential which is needed to reproduce experimental data, may depend on the density, temperature, etc., while the true two-body potential does not.

Typical atomic pair potentials $u(r_{ij})$ where r_{ij} represents the distance between the two atoms i and j are (see Fig. 3.8):

- Hard sphere-potential

$$U^{HS} = \begin{cases} \infty, & r_{ij} < \sigma \\ 0, & r_{ij} > \sigma \end{cases} \tag{3.22}$$

The simplest possible model can be modeled via potential of hard spheres.

- Coulomb potential

$$U^{C}(r_{ij}) = \frac{q_i q_j}{r_{ij}}, \tag{3.23}$$

where the q_is are the charges.

- Lennard-Jones potential

$$U^{LJ}(r_{ij}) = 4\epsilon \left[\left(\frac{\sigma}{r_{ij}} \right)^{12} - \left(\frac{\sigma}{r_{ij}} \right)^{6} \right], \tag{3.24}$$

which is one of the most commonly used form for pair potentials, originally proposed for liquid argon. The parameter ϵ in this potential governs the strength of the interaction and σ, which is called the collision diameter, is defined as the separation of the particles when the potential is zero. The Lennard-Jones potential has a long-range attractive tail coming from r^{-6} and a short-range repulsive tail coming from the term r^{-12}. The attractive tail essentially represents the van der Walls interaction, while the strongly repulsive core arising from unbounded overlap between the electron clouds of particles has a rather arbitrary form. However, in cases where a different steepness for the potential is required, other values of the power law exponent for a general form of repulsion term have been proposed [97, 120]. This consequently renders new functional forms for the potential. An example of this will be presented in subsection (3.4.2).

Finally the potential energy of the N particle interacting system for particle i can be represented as:

$$U_{total} = \sum_{j \neq i} u(r_{ij}), \tag{3.25}$$

where the sum is over all $N-1$ atoms excluding i itself. The term $u(r_{ij})$ in this sum includes all pair potentials that are needed to model the system. Since $u(r_{ij}) = u(r_{ji})$, each atom pair should be considered once.

3.3.3 Molecular Dynamic simulation units

In MD simulations, often suitable units of energy and length are chosen and all other quantities are expressed in terms of these units. In a system with Lennard-Jones interaction the unit of length is usually set equal to σ and the unit of energy to ϵ. As a consequence, the unit of time is $\sigma\sqrt{m/\epsilon}$, where m is the mass of one of atoms, and the unit of temperature T is ϵ/k_B, where k_B is the Boltzmann constant.

For our model, two different simulation methods, MD and MPC, are combined and the units of simulation parameters are also modified accordingly.

3.3.4 Potential truncation

Here and below, we consider the Lennard-Jones potential as the only pair interaction potential. However, Eq.(3.25) still contains very many terms and hence cannot be calculated accurately. The attractive tail of the Lennard-Jones potential in Eq.(3.24) decays like r^{-6}. That means the potential energy of two particles at a distance of 3σ is only half a percent of the minimum value $-\epsilon$. To determine the remaining part is very time-consuming and useless. Since it is sufficient to calculate pair interactions only up to a certain cut-off radius; at larger distances the potential is negligible. According to method proposed by Weeks, *et al,* the potential separation involves splitting the potential at the minimum [121]. The Lennard-Jones potential therefore is often truncated at its minimum as

$$U_{min} = -\epsilon, \qquad r_{min} = r_c = \sqrt[6]{2}\sigma. \tag{3.26}$$

This means that only the reflecting part of the potential is taken into account which simplify the interaction even further. To avoid jumps of the potential at the point of truncation, the potential is shifted by its values at $r = r_c$ (see Fig. 3.9) and it finally reads

$$U_{LJ}^{\text{“truncated”}}(r_{ij}) = \begin{cases} 4\epsilon\left[\left(\frac{\sigma}{r_{ij}}\right)^{12} - \left(\frac{\sigma}{r_{ij}}\right)^{6}\right] + \epsilon & r_{ij} \le r_c \\ 0 & r_{ij} > r_c \end{cases} \tag{3.27}$$

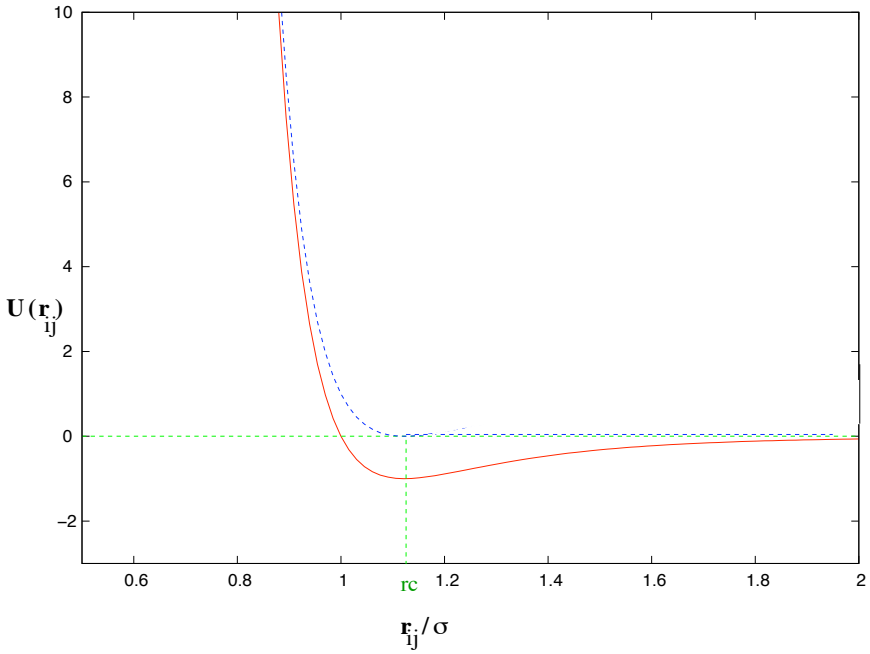

Figure 3.9: Lennard-Jones potential (red line) and truncated Lennard-Jones potential (blue line).

From the above equation, the force between two particles i and j can be obtained

$$\vec{F_{i,j}} = - \bigtriangledown_{i,j} U_{LJ}^{\text{“truncated”}} = \begin{cases} 24\epsilon \left[2 \left(\frac{\sigma}{r_{ij}} \right)^{12} - \left(\frac{\sigma}{r_{ij}} \right)^{6} \right] \frac{1}{r_{i,j}^2} \vec{r}_{i,j}, & r_{ij} \leq r_c \\ 0, & r_{ij} > r_c \end{cases} \tag{3.28}$$

where $r_{i,j}$ is defined as

$$r_{ij}^2 = (x_i - x_j)^2 + (y_i - y_j)^2 + (z_i - z_j)^2. \tag{3.29}$$

3.3.5 Boundary conditions and wraparound effect

We consider a two dimensional system. The boundaries in one of the directions is defined with walls (see next section). In the other direction, a periodic boundary condition has been applied . A periodic boundary condition implies an infinite space-filling array of identical copies of the simulation region (see Fig. 3.10). Consequently, an atom that leaves the simulation region through a particular boundary immediately re-enters the region through the opposite side.

It is important to make sure that the properties of the small, infinitely periodic system and those of the macroscopic system that it represents are the same. For this, one should consider the range of interacting potentials and the the properties of interest. For a fluid represented by Leonard-Jones potential it should be possible to perform a simulation in a square box of side length $L \backsim 6\sigma$, without a particle "feeling" the symmetry of periodic boundary. On the other hand, for the potentials of this kind, atoms lying within a distance r_c of a boundary interact with atoms in an adjacent copy of the system. In this case the minimum image convention or a *wraparound effect* can be applied. This means that only interactions among the closest neighbouring particles are calculated.

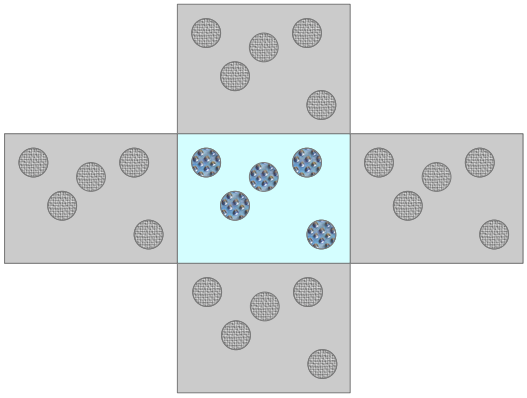

Figure 3.10: Diagram of periodic boundary condition in two directions.

The wraparound effect of the periodic boundaries must be taken into account in integration of equations of motion and also in the computations of interaction. After each integration step, the coordinates must be examined, and if an atom is found to move outside the simulation box through a boundary, then its coordinates must be adjusted to bring it back through the opposite boundary. Then the interaction potential must be updated according to the new coordinates. Since the cut-off radius has to be smaller than half of the simulation box, the $x-$ component of the particles' positions is defined within the range of $[-L_x/2, L_x/2]$. Thus if the $x-$ components of distance between a pair of atoms be x_{ij},

then for $|x_{ij}| > L_x/2$, we replace it by $x_{ij} - L_x$ for $x_{ij} > 0$, and by $x_{ij} + L_x$ if $x_{ij} < 0$.

3.3.6 Lennard-Jones potential at the walls

We implement walls to cause the boundaries in the second direction (see Fig. 3.11). Using the method proposed in [122, 123], we assume that the walls of the channel contain an infinite number of particles. In order to prevent particles leaving the system, a Lennard-Jones potential between the particles in the wall and the particles in the system has been applied.
In order to calculate the total force between particles of the wall and a particle in the channel we determine the sum over all small L-J contributions, and obtain the total wall potential

$$U_{wall} = \sum_{x=0}^{N} U_x^{L-J}. \tag{3.30}$$

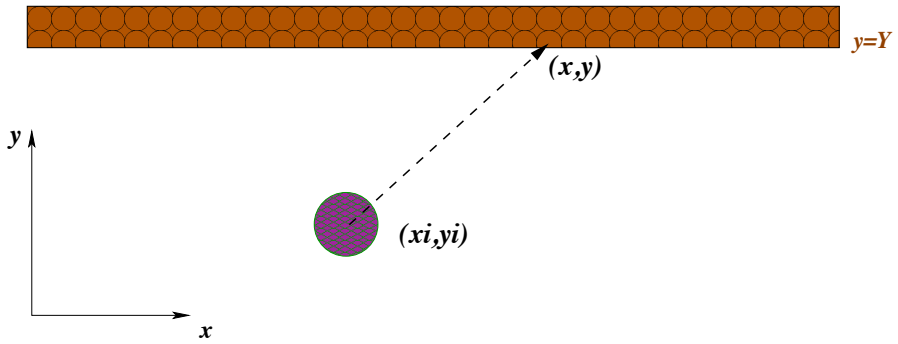

Figure 3.11: Diagram of the wall of the channel which contains many number of particles and each of them has a contribution in the total L-J potential.

Here the walls are located along the x direction and it is assumed that the walls are continuous. Thus the sum in Eq.(3.30) is replaced by the following integration

$$U_{wall} = \int_{-\infty}^{+\infty} \rho U^{L-J}(x) dx + K, \tag{3.31}$$

where $\rho = \frac{q}{\sigma}$ is the density at the wall and q is a constant depending on the properties of the wall. Substituting Eq.(3.27) in the above relation, one gets

$$U_{wall}(y_i) = \frac{4\epsilon q}{\sigma} \int_{-\infty}^{+\infty} \left[\frac{\sigma^{12}}{[(x_i - x)^2 + (y_i - y)^2]^6} - \frac{\sigma^6}{[(x_i - x)^2 + (y_i - y)^2]^3} \right] dx + K. \tag{3.32}$$

Accordingly, we need to perform the following integration

$$\int_{-\infty}^{+\infty} \frac{dx}{[(a - x)^2 + b^2]^n}, \tag{3.33}$$

for $n = 3$ and $n = 6$ where $a = x_i$ and $b = y_i - y$. This integration is determined for the required values of n as

$$\begin{aligned} \frac{3\pi}{8b^5}, \quad & for \quad n = 3, \\ \frac{315\pi}{1280b^{11}}, \quad & for \quad n = 6. \end{aligned} \tag{3.34}$$

Using the above expressions, we obtain the final expression for the potential at the wall-position at $y = Y$

$$U_{wall}(y_i) = \frac{3\epsilon q\pi}{2} \left[\frac{21}{32} \left(\frac{\sigma}{y_i - Y} \right)^{11} - \left(\frac{\sigma}{y_i - Y} \right)^5 \right] + K. \tag{3.35}$$

Here the repulsive tail of L-J potential will be taken into account (see subsection (3.3.4)). The cut-off radius has been found as follows

$$\frac{\partial U_{wall}}{\partial y_i} = 0 \qquad \Longrightarrow \qquad r_{min} = r_c = \sqrt[6]{1.444375}\sigma. \tag{3.36}$$

The value of the truncation distance r_c is required to calculate the minimum potential U_{min}. The truncated wall-potential finally reads

$$U_{wall}^{truncated} \begin{cases} \frac{3\epsilon q\pi}{2} \left[\frac{21}{32} \left(\frac{\sigma}{y_i - Y} \right)^{11} - \left(\frac{\sigma}{y_i - Y} \right)^5 + \frac{6}{11} \frac{1}{1.44375^{\frac{5}{6}}} \right], & r \leq r_c \\ 0. & r > r_c \end{cases}$$

Finally calculating the derivative of the potential yields the force along the y direction

$$F_{wall}(y_i) = \frac{15\epsilon q\pi}{2} \left[\frac{231}{160} \left(\frac{\sigma}{y_i - Y} \right)^{11} - \left(\frac{\sigma}{y_i - Y} \right)^5 \right] \frac{1}{y_i - Y}. \tag{3.37}$$

We typically set the parameter value $q = 1$ in our simulation.

3.3.7 MD algorithms, velocity Verlet algorithm

A number of algorithms have been suggested to integrate Newton's equations of motion. A simple but efficient algorithm, which has been used in the present thesis, is the velocity Verlet algorithm [124–126]. Starting from the Liouville equation of motion [127], one obtains the integration scheme for positions and velocities

$$r_i(\tau_{MD}) = r_i(0) + \tau_{MD}\dot{r}_i(0) + \frac{\tau_{MD}^2}{2m_i}F_i(0), \tag{3.38}$$

$$\dot{r}_i(\tau_{MD}) = \dot{r}_i(0) + \frac{\tau_{MD}}{2m_i}\left(F_i(0) + F_i(\tau_{MD})\right), \tag{3.39}$$

which is called *velocity Verlet algorithm.*

The steps for integration of Newtons equations of motion in the simulation code are as follows :

- 1.Providing initial conditions by generating initial position $r(t_0)$, velocities $\dot{r}(t_0)$ and forces $F(t_0)$.
- 2. Calculation of new positions at time $t + \tau_{MD}$ according to Eq.(3.38)

$$r_i(t + \tau_{MD}).$$

- 3. Calculation of velocities at time $t + \tau_{MD}/2$

$$\dot{r}_i(t + \tau_{MD}/2) = \dot{r}_i(0) + \frac{\tau_{MD}}{2m_i}F_i(t).$$

- 4. Calculation of forces using positions $r(t + \tau_{MD})$ and Eq.(3.28)

$$F_i(t + \tau_{MD}) = F_i(r(t + \tau_{MD})).$$

- 5. Calculation of velocities at time $t + \tau_{MD}$ by using velocities at time $t + \tau_{MD}/2$

$$\dot{r}_i(t + \tau_{MD}) = \dot{r}_i(t + \tau_{MD}/2) + \frac{\tau_{MD}}{2m_i}F_i(t + \tau_{MD}),$$

3.3.8 Microcanonical ensemble; thermostats algorithm

The MD simulation described so far applies to a closed system with a given number of particles N in a fixed volume V at constant energy E. Thus the averages obtained in such a simulation are equivalent to ensemble averages in the microcanonical ensemble or NVE ensemble. However, various physical situations require the simulation of other ensembles by inclusion of the environment into the simulation. One example of this is canonical ensemble. In the canonical ensemble, the number of particles N, the temperature T, and the volume V are constant. The energy is no longer a conserved quantity, only the mean of the energy is constant over time.

In order to obtain a canonical ensemble in a molecular dynamics simulation, one has to couple the system under consideration to a heat bath. There are various methods to implement such a coupling (see below).

The Andersen scheme, stochastic method

The stochastic method proposed by Andersen [126,128] is a thermostat in which the coupling to the environment is achieved by random "collisions" with imaginary heat bath particles. These collisions lead to instantaneous momentum changes. Here, at each step, a prescribed number of particles is selected, and their momenta (actually, their velocities) are drawn from a Maxwell-Boltzmann distribution at the prescribed temperature [129]. The strength of the coupling to the heat bath is specified by a collision frequency ν. For each particle, a random variable is selected between 0 and 1. If this variable is less than $\nu\Delta t$, then that particle's velocities are updated. Between the collisions, the particles move according to Newtons equations of motion. The time correlation functions can be calculated inside this interval.

Velocity rescaling

An alternative method to simulate constant temperature is *velocity rescaling*. Here the velocities of all particles are rescaled such that at any integration

step the desired kinetic energy and hence the temperature is obtained [130]. According to the equipartition theorem for a canonical ensemble one can write

$$\left\langle \sum_i m_i v_i^2 \right\rangle = 3Nk_BT. \tag{3.37}$$

On the other hand, if E_k is the kinetic energy at a certain time and $v' = v/c$ is the scaled velocity, using Eq.(3.37), we have

$$E_k = \frac{1}{2}\sum_{i=1}^{N} m_i v_i^2 = \frac{1}{2}\sum_{i=1}^{N} m_i c^2 v_i'^2 = c^2 \frac{1}{2}\sum_{i=1}^{N} m_i v_i'^2 = c^2 \frac{3}{2} N k_B T. \tag{3.38}$$

Hence one finds the rescaling factor c and therefore the rescaled velocity:

$$v' = v\sqrt{\frac{3Nk_BT}{2E_k}}. \tag{3.39}$$

The pre-factor 3 in Eq.(3.39) represents the degree of freedom for a three dimensional system. For a two dimensional system the rescaling factor c is given by

$$c = \sqrt{\frac{Nk_BT}{E_k}}. \tag{3.40}$$

Since the same factor is used for all the particles, there is no effect on the center of mass motion. Usually, the velocities are periodically rescaled after every few time steps, during equilibration. Rescaling the velocities at certain intervals may add some periodic perturbation to the system, which is in general undesirable, but sometimes such a perturbation can serve as a tool to study system dynamics. The rescaling is also performed when the kinetic energy falls outside a certain error-bar around the desired value or it is used to equilibrate the system during the the first few hundred MD steps before the production run starts and data are collected.

3.4 A colloidal dispersion; simulation method

After considering the implementation and characteristic behaviour of two simulation methods, MD and MPC, the next question is how the system of a colloidal suspension in a channel can be modeled using these two methods. To this end, the strategy is to define a hybrid algorithm where the solvent is simulated with the MPC technique and the solute is modelled with standard molecular dynamics. Malevants and Kapral first showed how to implement a hybrid MD scheme that couples a set of colloidal particles to a bath of MPC particles [94]. In their model, both the solute-solute and solute-solvent interactions were taken into account through excluded-volume potentials with MD, and only the solvent-solvent interactions were macroscopically described through MPC. In this section we illustrate their method, describing in detail how their implemented algorithm used to model our system. We restrict ourselves to hard-sphere(HS)-like colloids with steep interparticle repulsions by using truncated L-J potential (see section 3.3), although attractions between colloids can easily be added on. The colloid-colloid and colloid-fluid interactions $\phi_{cc}(r)$ and $\phi_{cf}(r)$, respectively, are integrated via a normal MD procedure while the fluid-fluid interactions are coarse-grained using MPC. The advantage of this model comes from the fact that fluid particles vastly outnumbers HS colloids and approximating their interactions using MPC greatly speeds up the simulations.

3.4.1 Units and simulation parameters

Before describing the details of the simulation model, it is useful to introduce the units and parameters which we use in the program. We define lengths in units of a MPC cell size a_0, energies in units of k_BT and masses in units of fluid particle mass m_f. In other words, we set $a_0 = 1$, k_BT=1, m_f=1. Other units can be derived from these basic units. For example time in terms of basic units is $t_0 = a_0\sqrt{\frac{m_f}{k_BT}}$. The dimensionless mean free path is then

$$\lambda = \frac{\tau_c}{a_0}\sqrt{\frac{k_BT}{m_f}} = \frac{\tau_c}{t_0}, \tag{3.41}$$

which provides a measure of the average fraction of a cell size that a fluid particle travels between collisions. Two independent parameter sets, have been used to simulate the fluid particles and the colloids (see Table 3.1). However, since the fluid particles play the role of MD particles in the simulation program as well, few parameters are common between them and colloids and these are presented in the colloid column below.

MPC particle simulation parameters

m_f: fluid particle mass

Lx : MPC box length along x

Ly: MPC box length along y

α : stochastic rotation angle

n_f: fluid number density (average number of particles per cell)

N_f: number of fluid particles

τ_c: MPC collision time step

Colloid simulation parameters

M_c : colloid mass

N_c : number of colloids

τ_{MD} : MD time step

r_c : colloid radius

σ_{cc} : colloid-colloid collision diameter (a colloid diameter)

ϵ_{cc} : colloid-colloid energy scale

σ_{cf} : colloid-fluid collision diameter

ϵ_{cf} : colloid-fluid energy scale

σ_w : colloid-wall collision diameter

ϵ_w : colloid-wall energy scale

r_{cc} : cutoff radius of colloid-colloid repulsive potential

r_{cf} : cutoff radius of colloid-fluid repulsive potential

r_{cf} : cutoff radius of colloid-fluid repulsive potential

r_w : cutoff radius of colloid-wall repulsive potential

g_c : gravitation field exerted on colloid

Table 3.1: Simulation parameters for the colloidal suspension model

Some parameters above have been set to following values:
the energy scales, $\epsilon_{cc} = \epsilon_{cf} = \epsilon_w = k_B T$,
the width of the channel or y component of MPC box, $Ly = 10$,
the number density of fluid particle, $n_f = 10$,
the mass colloid density $\rho_c = 10$. We choose the mass density of colloids equal to n_f, in order to have a homogeneous system. Hence the mass of every spherical colloid may be calculated as $M_c = \pi r_c^2 n_f = 125.664$.
We set $r_c = 2$ in most of the cases, which means the surface of every colloid occupies few MPC cells. The diameter of the colloidal particles and the width of the channel are chosen such that the colloidal particles exhibit SFD. The value of r_c determines collision diameters as $\sigma_{cc} = 2\sigma_{cf} = 2r_c$ and $\sigma_w = \sigma_{cc}$. The last one has been chosen to guarantee that the spatial sequence of colloids remains constant in the channel.
The value of gravitational force exerted on colloids is set to $g_c = 0.1$.

It is noted that the number of colloids is one of the parameters which may vary in different cases. Thus the number of fluid particles N_f will be altered consequently to keep the total mass density constant. We use $N_f = n_f(L_x L_y - N_c \pi r_c^2)$ to obtain the number of fluid particles.

3.4.2 Colloid-colloid and colloid-fluid interaction

For the colloid-fluid interaction we take a repulsive Lennard-Jones potential as explained in subsection (3.3.4)

$$\phi_{cf}(r) = \begin{cases} 4\epsilon \left[\left(\frac{\sigma_{cf}}{r}\right)^{12} - \left(\frac{\sigma_{cf}}{r}\right)^{6} + \frac{1}{4} \right], & r < r_{cf} \\ 0. & r > r_{cf} \end{cases} \tag{3.42}$$

We approximate pure HS colloids by another repulsive interaction of the truncated Lennard-Jones form

$$\phi_{cc}(r) = \begin{cases} 4\epsilon \left[\left(\frac{\sigma_{cc}}{r}\right)^{48} - \left(\frac{\sigma_{cc}}{r}\right)^{24} + \frac{1}{4} \right], & r < r_{cc} \\ 0. & r > r_{cc} \end{cases} \tag{3.43}$$

For the colloid-colloid interaction $\phi_{cc}(r) = 4\epsilon[(\sigma_{cc}/r)^{2n} - (\sigma_{cc}/r)^{n} + 1/4]$, we choose $n = 24$ because that makes the $\phi_{cc}(r)$ rather steep, almost like hard spheres, but still soft enough to allow the time step to be set by the colloid-fluid interaction (see subsection 3.4.6). Since the mass m_f of a fluid particle is much smaller than the mass M_c of a colloid, the average thermal velocity of the fluid particles is larger than that of the colloid particles by a factor of $\sqrt{M_c/m_f}$. Therefore the time step τ_{MD} is usually restricted by the fluid-colloid interaction Eq.(3.42), allowing fairly large exponents n for the colloid-colloid interaction $\phi_{cc}(r)$.

3.4.3 Particles at boundaries

A periodic boundary condition has been applied for both the solvent and solute particles as explained in section (3.3.5). In our simulation, the walls of the channel are located in the x-direction, along which the periodic boundary condition is applied.

For the y direction, the wall of the channel effectively acts as a boundary for colloids and fluid particles. However, we use two slightly different algorithms: for MPC point particles of the fluid we use the bounce-back rule as explained in

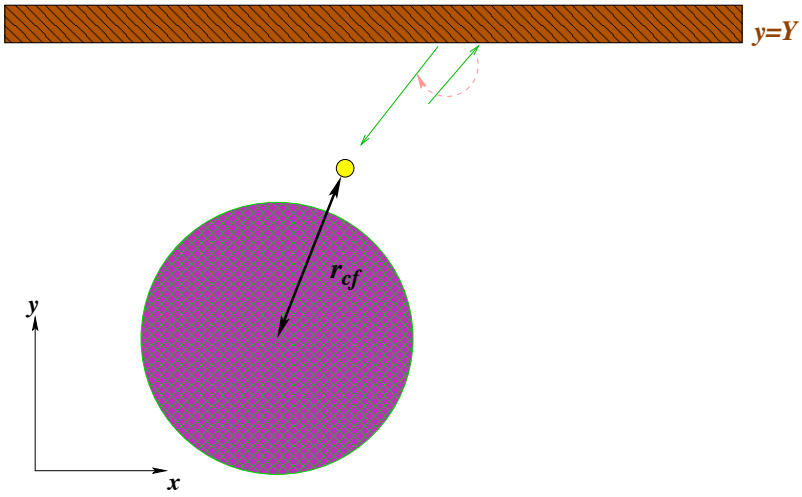

Figure 3.12: Diagram of a case where fluid particle hit at wall enters within the cut-off distance from a colloid.

subsection (3.2.5), while an integrated potential has been proposed (see subsection 3.3.6), in order to keep MD colloids within the channel walls.

The bounce-back relations which have been calculated in Sec.(3.2.5) correspond to the case of pure solvent. Including colloids in the model requires to modify the relations slightly. We imagine a case where a colloid is propelled close to the wall and is accidentally within the cutoff distance r_{cf} from a fluid particle (see Fig. 3.12). This yields a nonzero $\phi_{cf}(r)$ in Eq.(3.42) and consequently a force along y direction which alters the equations of motion for fluid particles. In order to calculate the new collision time t_c in Eq.(3.9), we write the equation of motion for the y coordinate of a fluid particle at the point it hits the wall

$$y_c = y_0 + v_{y_0} t_c + \frac{F_y t_c^2}{m_f}, \tag{3.44}$$

where F_y is the force perpendicular to the wall exerted by a colloid. y_c can take two values, 0 or L_y, which represent the location of channel walls. The only possible force inserted from a colloid nearby is repulsive, hence the coefficient of t_c^2 in Eq.(3.44) is negative. Hence the polynomial equation (3.44) has one possible solution, which is the positive one. Substituting new relation for t_c

yields new X and Y in Eq.(3.12), for the final position of a fluid particle after hitting the wall.

Slip boundary condition

The surface of a colloid is never perfectly smooth. Therefore the collisions with fluid particles transfer angular momentum as well as liner momentum. Nevertheless, here as described in Eq.(3.42), colloids and fluid particles are assumed to have radial interactions. The fluid particles do not transfer angular momentum to a spherical colloid and hence give rise to effective slip boundary conditions.

3.4.4 Initial state

In a numerical simulation, one should be able to sample the entire phase space of the system. Hence we require a simulation where the results after a sufficient 'equilibration' time are not sensitive to the initial state, so any convenient initial state is allowed. A particularly simple choice is to start with the colloids located at the sites of a regular lattice. Then the positions of the solvent particles can be fixed by drawing random numbers from a uniform distribution and excluding the space occupied by the colloids. The initial velocities are assigned random directions drawn from a Maxwell-Boltzmann distribution with the magnitudes of $\sqrt{\frac{k_B T_0}{m}}$, where $k_B T_0$ is initial temperature. In order to ensure that the center of mass of the system is at the rest, the initial velocities should be adjusted to eliminate any overall flow.

3.4.5 Integration

After initializing the positions and the velocities, the integration of the equations of motion is applied at every time step τ_{MD}. For fluid particles there is another time step for collisions, τ_c. The positions and the velocities of the colloids are updated through the velocity Verlet algorithm, explained in subsection (3.3.7)

after an MD time step:

$$r_c^i(t+\tau_{MD}) = r_c^i(t) + v_c^i(t)\tau_{MD} + \frac{F_c^i(t)}{2M_c}\tau_{MD}^2, \tag{3.45}$$

$$v_c^i(t+\tau_{MD}) = v_c^i(t) + \frac{F_c^i(t) + F_c^i(t+\tau_{MD})}{2M_c}\tau_{MD}, \tag{3.46}$$

r_c^i and v_c^i are the position and velocity of i-th colloid, respectively. F_c^i represents the total force on the colloid, which includes the force exerted by the fluid particles, the force arising from any external field (such as gravity), or from any external potential (such as repulsive walls), as well as other colloids within the range of the interaction potential. The force from j-th fluid particle can be calculated using Eq.(3.42):

$$\vec{F}_{cf}(r_{ij}) = -\vec{\bigtriangledown}\phi_{cf}(r_{ij}), \tag{3.47}$$

and the force from j-th colloid using Eq.(3.43):

$$\vec{F}_{cc}(r_{ij}) = -\vec{\bigtriangledown}\phi_{cc}(r_{ij}). \tag{3.48}$$

The force due to the repulsive wall has been calculated in subsection (3.3.6) and in our case takes the form

$$\vec{F}_{wall}(y_i) = \frac{15q\epsilon\pi}{2}\left[\frac{231}{160}\left(\frac{\sigma_w}{y_i - Y}\right)^{11} - \left(\frac{\sigma_w}{y_i - Y}\right)^{5}\right]\frac{\hat{y}}{y_i - Y}, \tag{3.49}$$

$y_i - Y$ represents the distance of the colloid from the wall.

Hence the total force on a colloid i is given by

$$\vec{F}_c^i = \sum_{j=1}^{N_f}\vec{F}_{cf}(r_{ij}) + \sum_{j=1}^{N_c}\vec{F}_{cc}(r_{ij}) + \vec{F}_{wall}(y_i) + \vec{F}_g, \tag{3.50}$$

where F_g represents an external force.

For fluid particles, as far as they represent MD particles, the positions and velocities are updated similarly with the time step τ_{MD}

$$r_f^i(t+\tau_{MD}) = r_f^i(t) + v_f^i(t)\tau_{MD} + \frac{f_f^i(t)}{2m_f}\tau_{MD}^2, \tag{3.51}$$

$$v_f^i(t+\tau_{MD}) = v_f^i(t) + \frac{f_f^i(t) + f_f^i(t+\tau_{MD})}{2m_f}\tau_{MD}, \tag{3.52}$$

$f_f^i(t)$ is the total force on the i-th fluid particle. It is a sum of the force due to the external field (if any) and due to the interactions with the colloids, which can be calculated from Eq.(3.47). In every time step τ_c, stochastic rotation dynamic propagation rule is used to update the velocities of fluid particles in each MPC cell according to Eq.(3.4).

3.4.6 Accuracy check

To check that our hybrid simulation algorithm is correct, various physical quantities can be monitored. An immediate check is that the conservation laws are properly obeyed, particularly the total energy and momentum should be constant.

In order to control the system temperature, various thermostats can be used, e.g. velocity rescaling method, explained in subsection (3.3.8). One can employ the velocity rescaling technique as a thermostat in the MPC algorithm, explained below. The simulation box is divided into L_y/a_0 layers, parallel to the walls. Suppose that fluid particle i with velocity v_i is placed in the cell j which belongs to layer l_j. In each layer l_j, the new velocity v_i' of each particle of the cell j is obtained by rescaling the velocity relative to the center-of-mass velocity $v_{cm,j}$ of that cell

$$v_i' = v_{cm,j} + (v_i - v_{cm,j})\sqrt{\frac{k_BT}{k_BT'}}. \tag{3.53}$$

Here k_BT' is calculated from the actual velocity distribution for each layer

$$\sum_{j\in lj}\sum_{i}^{N_j}\frac{1}{2}m_f(v_i - v_{cm,j})^2 = (\sum_{j\in lj} N_j - N_{lj})k_BT', \tag{3.54}$$

where N_j denotes the number of particles in cell j and N_{lj} denotes the number of cells which contains particles within the layer lj.

In subsection (3.2.5), we introduced virtual fluid particles at the cells that coincide with the walls. The velocities of the particles are drawn from a Maxwell-Boltzmann distribution with the same temperature T as the fluid. Hence, as in the Anderson thermostat scheme (see subsection 3.3.8), a coupling to a imaginary heat bath for the cells close to the wall is achieved. The virtual wall

particles therefore can also thermalize the colloidal suspension in our model. However, existing virtual particles make fluctuations in the kinetic energy and consequently in the total energy.

In the case where still a temperature gradient is observed, a thermostat can be used with an algorithm based on the stochastic method, previously explained in subsection (3.3.8). Here one may choose an ϵ in the interval $[0, \gamma]$ and apply for ζ one of the values $1+\epsilon$ or $1/(1+\epsilon)$, each with the probability 1/2. With one of these values the velocity is scaled by the Monte Carlo acceptance rate. The mean velocity v_{cm} within one MPC cell defines the velocity field of the fluid. Therefore it should not be modified by the thermostat. One only scales the velocity component relative to the mean velocity:

$$v_i^{new} = \zeta(v_i - v_{cm}) + v_{cm}. \tag{3.55}$$

The Monte Carlo acceptance rate is given by

$$\zeta^{3(n_f-1)} exp(-(n_f-1)(\zeta^2-1)T/T^*), \tag{3.56}$$

with

$$T = \frac{m_f}{2(n_f-1)k_B} \sum_{i=1}^{n_f} (v_i - v_{cm})^2, \tag{3.57}$$

which is the local temperature in the MPC cell and T^* denotes the temperature to which the thermostat will drive the system. n_f is the number of particles in the cell. Note that one has to divide the total thermal energy in the MPC cell by $(n_f - 1)$ instead of n_f to calculate the local temperature. This reflects the fact that the mean velocity u in the cell already contains three degrees of freedom for a 3D system, which the particles in the MPC cell have. The choice of γ and the frequency with which the thermostat is applied determine the relaxation rate, at which the system adapts T^*.

Another parameter that should be chosen carefully is the time step [131]. Choosing a time step too long may cause a slow upward drift of the energy, but a time step which is too small will be very wasteful of computer time. Essentially choosing τ_{MD} and τ_c as large as possible enhances the efficiency of a

simulation. To first order, these time step are determined by different physics: τ_{MD} is determined by the steepness of the potentials and τ_c by the desired fluid properties so there is some freedom in choosing their relative values. We choose $\tau_c/\tau_{MD} = 15$ for our simulation. Particularly, the mass of the colloids has been considered which is much bigger than those of the fluids, so we set the above value for the time steps' ratio in order to provide enough time for colloids to integrate over this time accurately.

In this chapter, we described the algorithms which are used to simulate our model. In the next chapter, we explain the characteristics of the colloidal suspension which we have studied using this simulation program.

4 Colloidal system in an external field: Sedimentation

4.1 Introduction

In the last chapter we described a hybrid algorithm of MPC and MD in order to simulate our colloidal suspension model in a channel. In this chapter, we investigate the colloidal system when an external force is applied to the solute particles. An example of this is electrophoresis where an electric field is present in the system. In our case, a gravitational field is acting on the colloidal particles; this represents sedimentation of a collection of colloidal particles through the solvent [1, 34–36, 89, 132]. If the mass of the fluid particles is assumed to be much smaller than that of the colloids, then the direct gravitational force acting on fluid particles can be neglected.

After a large enough equilibration time, every colloid attains a constant mean velocity v_s which is called the sedimentation velocity or settling speed. In a system containing a mixture of components, any external field causes each component to reach a different sedimentation velocity. Therefore sedimentation can be exploited to separate individual components from a mixture. The sedimentation velocity evidently depends on the size and the mass of Brownian particles. (The colloidal particles are classified as Brownian particles when the random collisions between solvent molecules and colloidal particles yield thermal motion and this motion is referred to as Brownian motion [89]). We assume the collection of colloids to have similar mass and size which means they attain the same mean velocity v_s. To determine v_s in simulation, one calculates a time average of the velocities over all the time steps after reaching equilibrium.

The important point to consider is the non-zero velocity of the fluid surrounding the colloidal particles, which prevents compression of sedimenting material. We assume in an experiment that colloids sediment in a closed container. One considers a cross sectional area of the container perpendicular to the direction of sedimentation. In a laboratory reference frame, the total volume of the colloidal material that sediments through the area of this cross section, must be compensated by fluid flow in the opposite direction, i.e., the total volume flux must be zero [132]. The sedimenting suspension is characterized by the volume

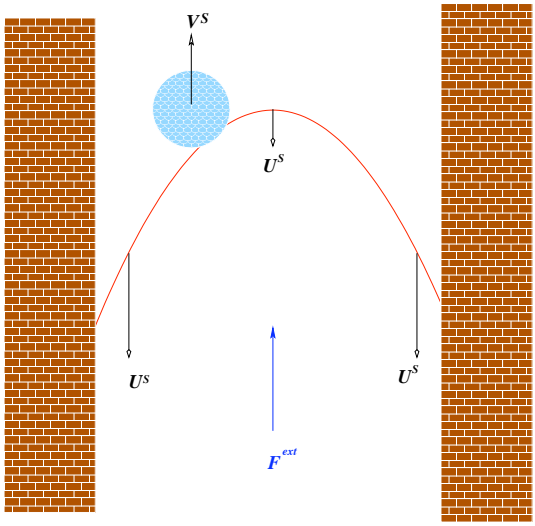

Figure 4.1: Diagram of nonuniform backflow of particles in a container

fraction ϕ, which is the ratio between the volume occupied by the particles and the total volume of the suspension. For a sedimentation velocity v_s, the total volume of the colloidal material that is displaced is compensated by a fluid flow with an average velocity u_s, when

$$u_s(1-\phi) + v_s\phi = 0, \tag{4.1}$$

where ϕ is the volume fraction of the Brownian particles. Hence,

$$u_s = -\frac{\phi}{(1-\phi)} v_s. \tag{4.2}$$

The fluid flow that compensates the volume flow of the Brownian particles is called the *backflow*. The above expression for the backflow velocity is obtained for a case where the fluid is considered to be homogeneous on a local scale. However, at the wall of the container the fluid flow velocity is zero in order to have the stick boundary condition (see Fig. 4.1). Here, one considers a container which is very large compared to the size of Brownian particles. Hence the mean backflow velocity u_s is not position dependent and backflow is uniform.

Settling speed in infinite dilution

We consider a very dilute suspension, where the concentration of the particles is so low that the direct force and the hydrodynamic force (see section 4.3) between the particles are negligible. In the stationary state the Brownian particle reaches a sedimentation velocity that compensates the Brownian force due to friction with the solvent. We denote the sedimentation velocity of a single spherical particle in the infinite dilution as v_s^0. Hence

$$v_s^0 = \frac{1}{\xi} F^g, \tag{4.3}$$

where $\xi = 6\pi\eta_0 r$ is the friction coefficient and r is the radius of the spherical particle.

Using proportionality between the gravitational force F^g and the mass of the colloids, including a correction for buoyancy, one finds

$$F^g = g\frac{4\pi}{3} r^3(\rho_c - \rho_f), \tag{4.4}$$

where ρ_c and ρ_f are the mass density of colloidal material and the fluid, respectively. Substituting this relation into Eq.(4.3) yields

$$v_s^0 = g\frac{2}{9}\frac{r^2}{\eta_0}(\rho_c - \rho_f) \tag{4.5}$$

Hence the sedimentation velocity in a dilute suspension is proportional to the the radius of the colloidal particle. Particles with the same mass density and larger size sediment faster than smaller ones in the solvent.

Studying the case with interacting particles, is rather difficult. Sedimentation velocity in Eq.(4.3) no longer relates to the gravitation force with a simple friction coefficient. Instead macroscopic diffusion matrices D_{ij} are introduced [89, 133]. In this case, the force fields that interacting colloids exert on each other must be taken into account (see below).

Forces present in interacting colloids

There are three types of forces acting on a colloidal particle i suspended in a solvent:

a) The direct force due to direct interactions between particles. For example the hard core of every colloid, which may cause volume exclusion, gives rise to the direct interactions or Lennard-Jones potential between colloidal particles that was discussed in the previous chapter.

b) The hydrodynamic force, which is due to friction with the solvent. When a colloidal particle moves, its motion perturbs the medium. This perturbation propagates through, affecting neighboring particles. This process gives rise to an indirect, long-ranged, complex coupling of the motion of individual particles. This is known as hydrodynamic interaction (HI) (see Fig. 4.2). Equations which describe hydrodynamic interaction are linear for system with small values

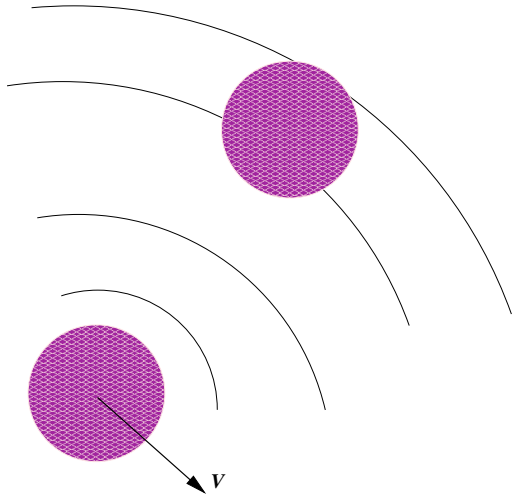

Figure 4.2: The motion of particles perturbs the solvent and causes the hydrodynamic interaction.

of Reynolds number [134, 135]. Hence, the hydrodynamic force F_i^h on particle i is linearly related to the velocities of all particles v_i,

$$F_i^h = -\sum_{i=1}^{N} \Omega_{ij}.v_j, \tag{4.6}$$

where the tensor Ω_{ij} denotes the hydrodynamic friction coefficient tensor [101, 136, 137], which has a complicated dependence on the positions of all the particles.

c) The Brownian force which is due to coarse graining. Consider a very dilute system where any interaction between colloids is absent, i.e, there are no hydrodynamic or direct forces acting on particle i. However, in a suspension which has an inhomogeneous density, the system moves towards a state with a homogeneous density. Thus there should be a driving force in this process which is called Brownian force.

The sum of the three types of forces gives the total force exerted to the particle i.

The sedimentation velocity of colloidal particles is investigated in the next three sections.

4.2 Sedimentation velocity and colloid concentration

Studying the effect of the concentration of Brownian particles on the sedimentation velocity of rigid spherical particles began with Smulochowski in 1912 [138]. Since then, there have been a lot of contributions in order to investigate this effect [35, 97, 139, 140]. In [132], Batchelor considered the problem of classical dispersion of small rigid spheres in a fluid where the dispersion was assumed to be statistically homogeneous. The volume fraction of the spheres was considered small compared to unity, i.e., the dispersion was assumed to be dilute. By means of theoretical calculations, Batchelor showed that the average sedimentation velocity of hard spheres has a correction to the settling speed of single particle v_s^0 (given in Eq. 4.3). Hence the settling speed of spheres or the sedimentation velocity is finally given by [132, 139]

$$v_s = v_s^0(1 - 6.55\phi), \tag{4.7}$$

ϕ is the volume fraction which is the fraction of volume that is occupied by the spheres. The correction term $O(\phi)$ in Eq.(4.7) is due to fluid backflow in the system of sedimenting colloids. An increase in the volume fraction provides a higher volume flux of the material and consequently a larger backflow of the

fluid. The stronger backflow effect finally yields a drop in the settling speed of the hard spheres.

It would be interesting to extend the calculation explained above for systems on systems which do not exactly fulfill the basic and usual assumptions for having a homogeneous dispersion in a sedimentation problems. An example

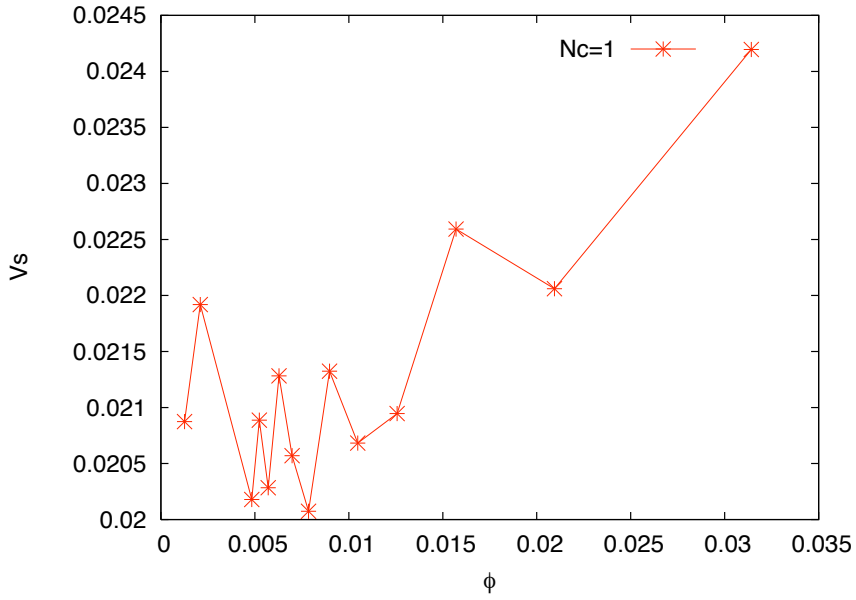

Figure 4.3: The sedimentation velocity of single particles versus volume fraction which is changing due to system size change.

could be our model of confined colloidal dispersion, where the geometry of the channel does not satisfy the condition of obtaining a homogeneous mixture. For our 2D system, the volume fraction is $\phi = \pi r_c^2 n_c$, where $n_c = \frac{N_c}{L_x L_y}$ is the colloid number density. One may consider the system in a reference frame which gives rise to back flow effect. We consider a co-moving frame as the reference frame in our simulation model which is explained below.

Co-moving reference frame

We investigate the model in a frame where the total volume flux is zero. We choose the reference frame that is co-moving with the velocity of the center of mass, i.e., in this frame, the total momentum is zero. If P_t is the actual total

momentum of particles, we write

$$P_t = \sum_{i=1}^{N_f} m_f \tilde{v}_i^f + \sum_{i=1}^{N_c} M_c \tilde{v}_i^c, \tag{4.8}$$

where $\tilde{v}^c$ and $\tilde{v}^f$ are the velocities of colloids and fluid particles respectively at the frame at rest. Therefore, the velocity of colloidal particles in the co-moving frame is given by

$$v_i^c = \tilde{v}_i^c - \frac{P_t}{N_f m_f + N_c M_c}, \tag{4.9}$$

The relation for the average settling speed v_s of colloidal particles

$$v_s = \tilde{v}_s - \frac{N_f m_f v_f + N_c M_c v_s}{N_f m_f + N_c M_c}. \tag{4.10}$$

We first consider a simple case of a single colloid where the suspension is so dilute that the hydrodynamic interactions are negligible. According to Eq.(4.5), the sedimentation velocity of a single colloid depends on its radius (where other parameters are assumed to be constant). In Fig. 4.3 the sedimentation velocity of a single colloid versus the volume fraction is plotted. We determine the mean settling speed v_s of colloid in simulation by calculating a time average for velocities over all the time steps after reaching equilibrium. The equilibration time in our system is evaluated to be $t_{eq} = 10^5$. We change ϕ by changing the system length from $L_x = 40$ to $L_x = 1000$. The width is set to a constant value of $L_y = 10$. Fig. 4.3 shows that the settling velocity v_s fluctuates, and on average is constant for volume fractions ϕ less than about 0.015, which corresponds to system length more than $L_x = 100$. However, v_s increases for smaller length. This can be interpreted as a finite size effect for our system which is periodic in the direction of sedimentation. A single particle which has left the system and re-enters by means of periodic boundary condition experiences the effects of flow induced by the copied particles.

Next, we consider interacting colloidal particles (where HI is not negligible). To investigate such a case, we consider the number of colloidal particles $N_c = 2$ and $N_c = 3$. Fig. 4.4 shows the settling speed in these two cases for the range

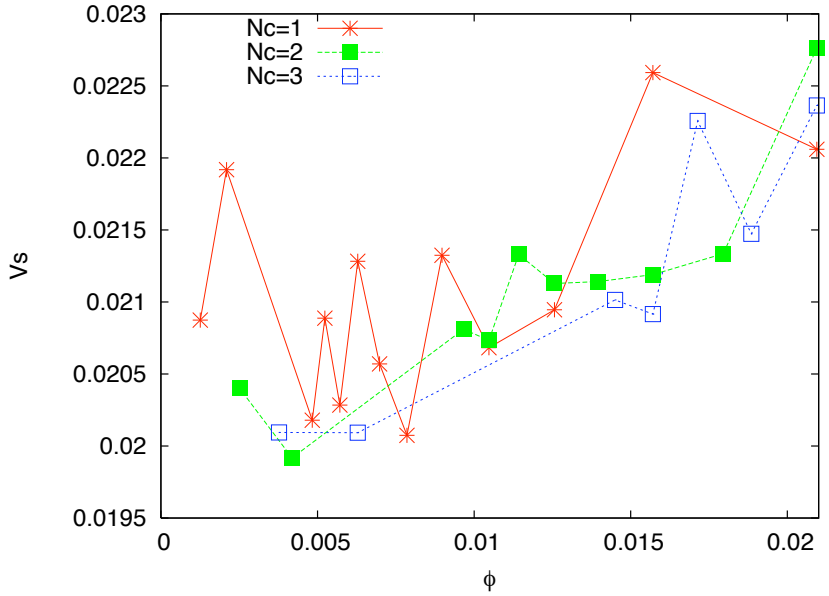

Figure 4.4: Sedimentation velocity as a function of volume fraction for systems with $N_c = 1$, $N_c = 2$ and $N_c = 3$ particles.

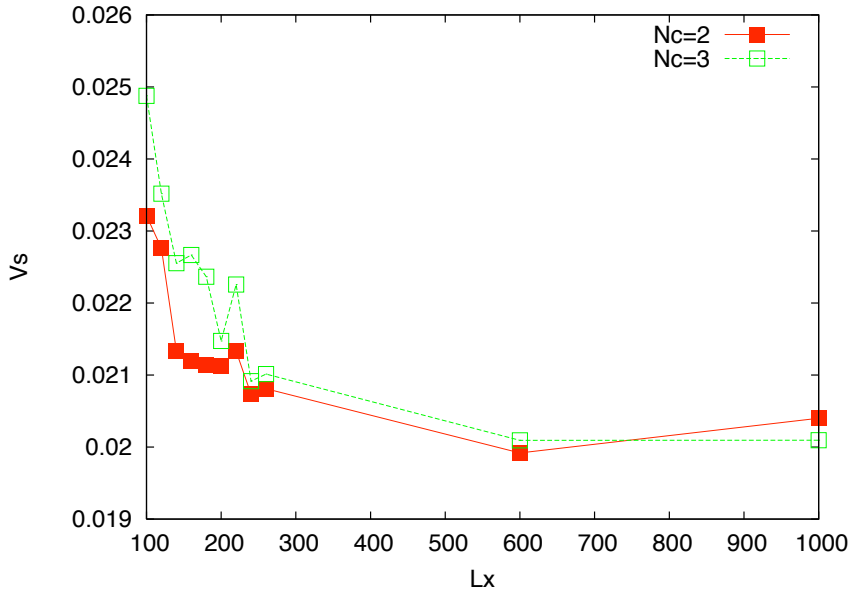

Figure 4.5: Sedimentation velocity as a function of length L_x for systems with two or three colloidal particles.

of ϕ where the settling speed of a single particle on average is constant (see Fig. 4.3). In Fig. 4.4, one finds that the sedimentation velocity of the systems with $N_c = 2$ and $N_c = 3$ increase in this interval of volume fraction. To compare these data points with single particle data makes this observation more clear. One may trace the role of hydrodynamic interaction in the settling speed. However it is hard to make a concrete statement, because ϕ was varied by varying L_x. For small L_x, finite size effects become important and should be taken into account in the behaviour of sedimentation velocity (see Fig. 4.5).

Therefore we consider larger systems and change the volume fraction by including more numbers of colloidal particle into the system while

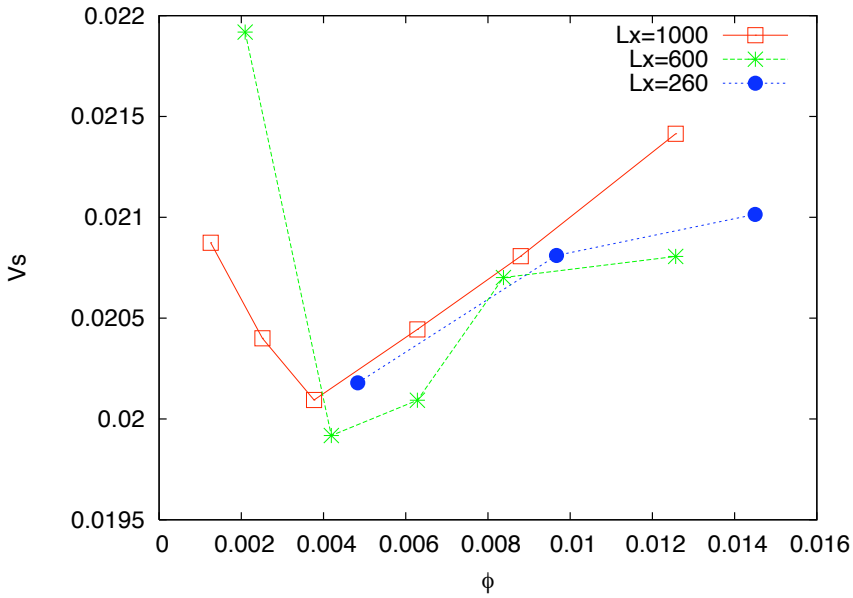

Figure 4.6: Sedimentation velocity as a function of volume fraction in different systems with length L_x =1000, 600 and 260.

the size of the system is kept constant. We consider a system size of length $Lx = 1000$ and width $Ly = 10$. Fig. 4.6 shows the sedimentation velocity of colloids for such a system as a function of volume fraction. Here for small volume fractions, the sedimentation velocity of the colloids shows a reduction, which seems to be consistent with the result obtained by Batchelor shown in Eq. (4.7). However, as the volume fraction increases, the speed of sedimenting

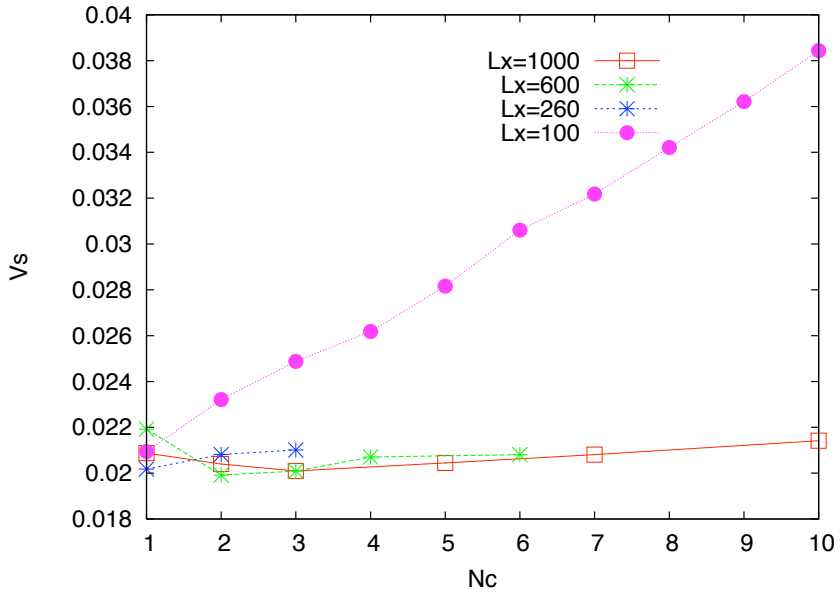

Figure 4.7: Sedimentation velocity as a function of number of colloids in system length ranging from 100 to 1000.

colloids tends to increase linearly as one can see in Fig. 4.6, also for systems with size of 600×10 and 260×10. The increasing of the sedimentation velocity apparently disagrees with what one may expect from Eq.(4.7) for the volume fraction values that we considered.

The explanation for this disagreement could be the Batchelor's basic assumption for a homogeneous suspension, which is not valid in our model. Because of the special geometry of the model, the colloidal particles are confined in the y direction and they move efficiently in the x direction. Hence when we increase the number of colloidal particles aligned in the channel, they form a bead. Sedimentation of this bead of particles in the channel, perturbs the surrounding solvent in such a way that the suspension is not homogeneous anymore. Moreover, applying the no-slip boundary condition, i.e., vanishing of the momentum at the walls, causes fluid flow to give rise to a non-uniform velocity profile.

The linear increasing function of sedimentation velocity of colloids is fitted to the function $f(\phi)$ defined as $f(\phi) = a\phi + b$ and the parameters are obtained as $a = 0.15$ and $b = 0.019$.

In Fig. 4.7, the v_s of the systems which are considered in Fig. 4.6, including a system of length size $L_x = 100$ as a function of the number of colloids Nc are shown. Comparing the sedimentation velocity of the system with size $Lx = 100$ with the larger systems shows that it is increasing with a slope much larger than that for the system with $Lx = 1000$. One can see that increasing the number of colloids in our model of confined suspension will influence small systems more effectively because the confinement has a more important role in the behaviour of sedimentation velocity.

4.3 System with and without hydrodynamic interactions

We have considered the sedimentation velocity of colloids as a function of volume fraction in the previous section. In this section, we discuss the effect of hydrodynamic forces on the behaviour of the colloidal suspension as follows. Starting from the same initial conditions and parameter values, we perform simulation with and without HI, and by comparing the results for two cases, one can determine the effect of HI. In an MPC method, it is possible to "switch off" the HI by replacing the MPC solvent with a "random solvent". Two different approaches have been proposed to model a random solvent. According to [104], a random interchange of velocities of all fluid particles after each collision step provides a random solvent while the total momentum and energy is conserved, although the conservation of local momentum will naturally be violated.

The second approach, which is presented in [141], suggests a slightly different method in order to remove the HI. Here a random solvent can be achieved by assigning a velocity to every fluid particle directly from a random Gaussian distribution with a zero mean and a variance equal to $\sqrt{\frac{k_B T}{m_f}}$. In other words, stochastic rotation dynamics is replaced by a coupling between the system and a heat bath at the temperature T. In order to switch-off HI in our simulation,

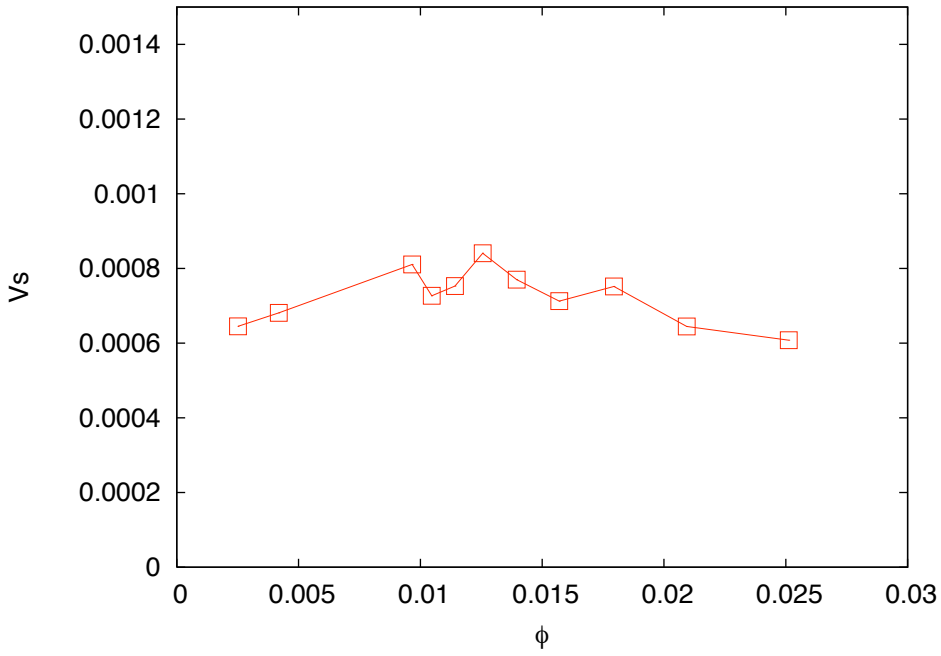

Figure 4.8: Sedimentation velocity as a function of volume fraction in the absence of hydrodynamic interaction.

we used each of the above two methods and obtain similar results in the two cases. In Fig. 4.8 the sedimentation velocity of colloids in absence of HI has been shown. This figure has been obtained for a number of colloidal particles $N_c = 2$, for a channel width of $L_y = 10$ and channel length changing from 100 to 1000. Here one finds that in the absence of HI, there is no correlation between the settling speed of colloids and volume fraction. By comparing this result with what we obtained in section (4.2), we conclude that an increase of sedimentation velocity of colloidal suspension with volume fraction in the narrow channel is an effect of hydrodynamic interactions in the system.

4.4 Variation of sedimentation velocity with field

The form of hydrodynamic interaction in the Eq.(4.6) is valid for systems with small Reynolds number [105, 142]. The Reynolds number is a dimensionless

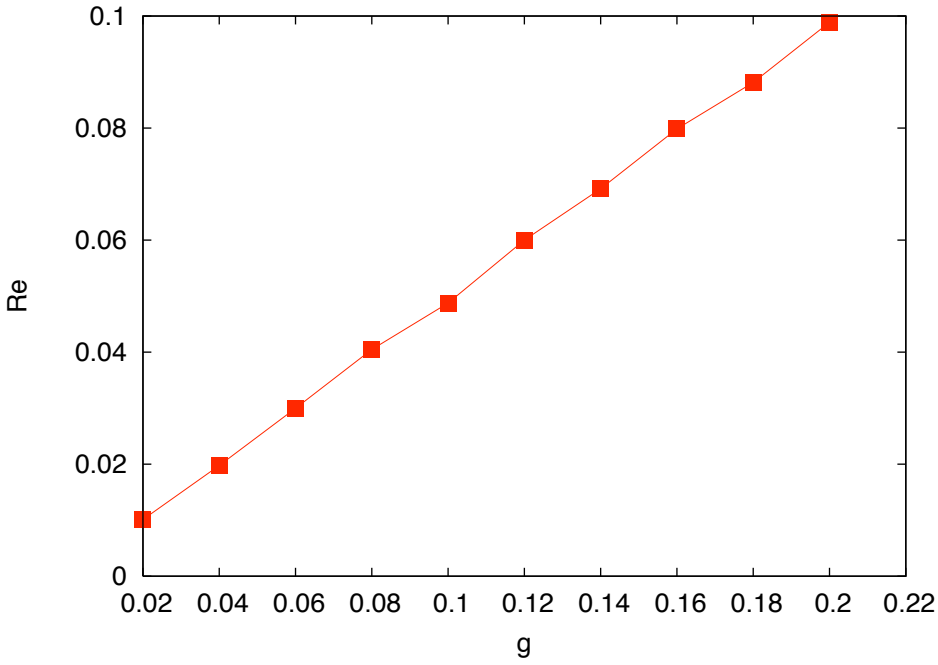

Figure 4.9: Reynolds numbers computed for fluid flow in a system of size 40×10 versus gravitational force with $N_c = 3$.

number which is given by the ratio of inertial forces to viscous forces, and consequently, quantifies the relative importance of these two types of forces for given flow conditions. A low Reynolds number means that the inertial forces are virtually absent and the viscous forces are dominant in the system. This gives rise to a laminar flow regime [143].

In order to choose a suitable range of values for the gravitational forces that give rise to a laminar flow, we calculate the Reynolds numbers for various fluid flow velocities in our sedimenting suspension model. For example, for a system of size 40×10 and number of colloids $N_c = 3$, where a gravitational force within the range of $[0.02, 0.2]$ has been applied, Re can be calculated from

$$Re = \frac{v\rho}{\eta/L} = \frac{vL}{\nu}, \tag{4.11}$$

where η is the dynamic fluid viscosity defined as $\eta = \rho\nu$, ρ is the fluid density, v is the mean velocity of fluid particles, L is the characteristic length of the system (here the width of the channel), and ν is the kinematic fluid viscosity

as in Eq.(3.16). The value of ν can be calculated using the parameters $\tau_c = 0.015, \rho = m_f n_f = 10$ and $\alpha = 90,^\circ$ for this system. In Fig. 4.9, the Reynolds numbers calculated from Eq.(4.11) are plotted as a function of g. We observe that the Reynolds numbers produced by the fluid flow within the specified g interval are small enough to ensure a laminar regime.

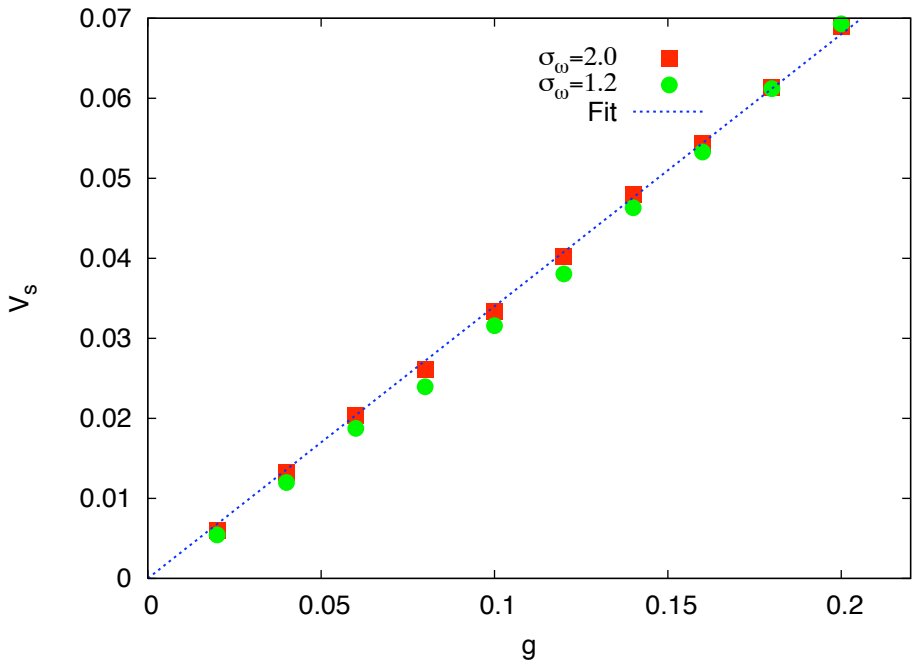

Figure 4.10: The sedimentation velocity as a function of the gravitational force for two values of cut-off diameter of the colloid-wall repulsive potential σ_w. The blue line shows a linear fit function with the slop of $s = 0.34$.

The average velocity of colloids, or sedimentation velocity, has also been determined within this force interval. For a single particle, the expression for the sedimentation velocity is given in Eq.(4.5) in terms of external force and parameters of the suspension. The sedimentation velocity of a single colloid is related to the gravitational force g by the mobility μ_0 as $v_s^0 = \mu_0 g$. For a collection of interacting colloids, μ_0 is replaced with the mobility tensor. The dynamics of

the particles are therefore given by the equations of motion [89,136,137,144,145]

$$v_i^s = \sum_j^N \mu_{ij}(X) F_j, \tag{4.12}$$

where μ is the translational part of the mobility matrices, which is typically is a function of the configuration $X = (R_1, ..., R_N)$ of all the colloidal particles. It describes the hydrodynamic interactions between particles and connects the forces acting on particles to the velocities they acquire in a given conguration. The forces F_j will be assumed to be constant and equal to F for all particles.

For our present example, the sedimentation velocity v_s of the colloidal particles is depicted in Fig. 4.10 as a function of the gravitational force g . It shows a perfect linear increase for $\sigma_w = 2.0$, the cut-off diameter of the colloid-wall repulsive potential. This is the value which we have chosen for all of our simulation systems. It is useful to compare this dependence of v_s on g with a case where the system is set to a reduced cut-off wall-colloid distance, which is $\sigma_w = 1.2$. The reduced value of the cut-off distance essentially enhances the movement of colloids in the direction perpendicular to that of sedimentation, but SFD is still obeyed by the colloidal particles. The v_s obtained for the latter case shows a small deviation from the linear fit function as expected.

To summarize, we have shown that the system has a mobility μ which is independent of g for both σ_w values and also that the value $g_c = 0.1$, which we have chosen for the gravitational force in our simulation so far, is within the range of a laminar flow.

4.5 Density discontinuity

We now investigate a density discontinuity on the macroscopic level for the colloidal suspension in an external field. For this purpose, we need a larger number of particles than we considered in earlier sections. We start the simulation with the initial position of colloids a close distance from each other. However this initial distance between successive particles is limited by the cutoff diameter of the repulsive potential of the colloids r_{cc}. We set the initial distance between

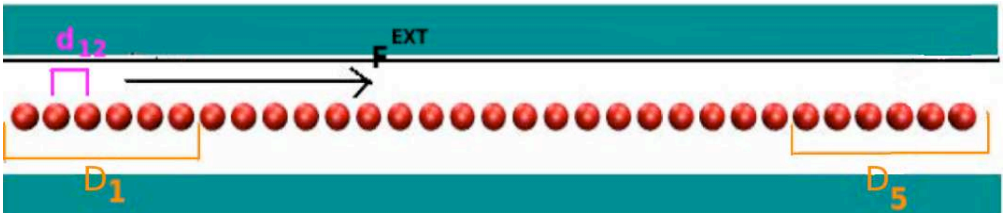

Figure 4.11: Colloidal particles are initially aligned in the channel a small distance from each other.

the centers of two neighboring colloids as $d_0 = 5.0$ in a system of size 300×10 and the number of colloids $N_c = 31$. The colloidal particles, which are aligned in the channel and located at small distances from each other form a chain. Fig. 4.11 shows one snapshot at time $t = 0$ of a movie obtained by recording the positions of particles in this simulation system. We label particles according to their positions along the channel, the leftmost particle has the lowest label (see Fig. 4.11). An external force $g = 0.1$ is applied to the 'colloid chain'. Fig. 4.14 shows another snapshot of the colloidal particles at time $t = 500$. A clustering of the group of particles initially located at the head of the system is observed which has a 'zigzag' shape (see Fig. 4.14), and subsequent snapshots show that the 'zigzag' shape will move to the middle and then to the tail of the particle chain. [1]

In order to have a more quantitative observation, average distances of colloids as a function of time are sketched in Fig. 4.12. Here 31 colloidal particles are distributed in 6 groups, every 5 consecutive colloids belong to one group with the distances d_{ij} (see Fig. 4.11). The distances D_i is defined as $D_i = \sum_{j=1}^{5} d_{ij}/5$, representing an average distance between 6 individual parts of the chain. This definition simplifies the calculations and also represents a coarse-grained picture of the system. The average distances D_i are depicted in Fig. 4.12 as a function of time. It is seen that distances D_i are increasing in time clearly for particles

[1] A similar behaviour in microfluidic crystals has been reported in [100]. Here water droplets are made at a T-junction between the water and oil channels. Thus a flowing 1D crystal of droplets that can move in 2D, has been obtained. It has been shown that the pack of moving droplets form the triangle-like traveling waves along the velocity of oil.

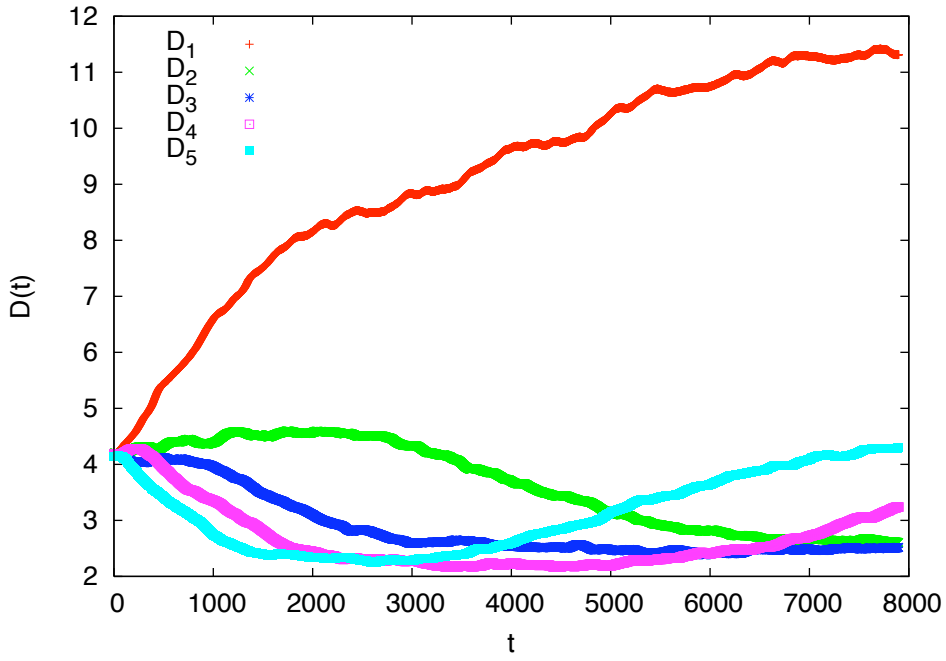

Figure 4.12: Average distances within groups of colloids versus time in a system in external force with the length $Lx = 300$.

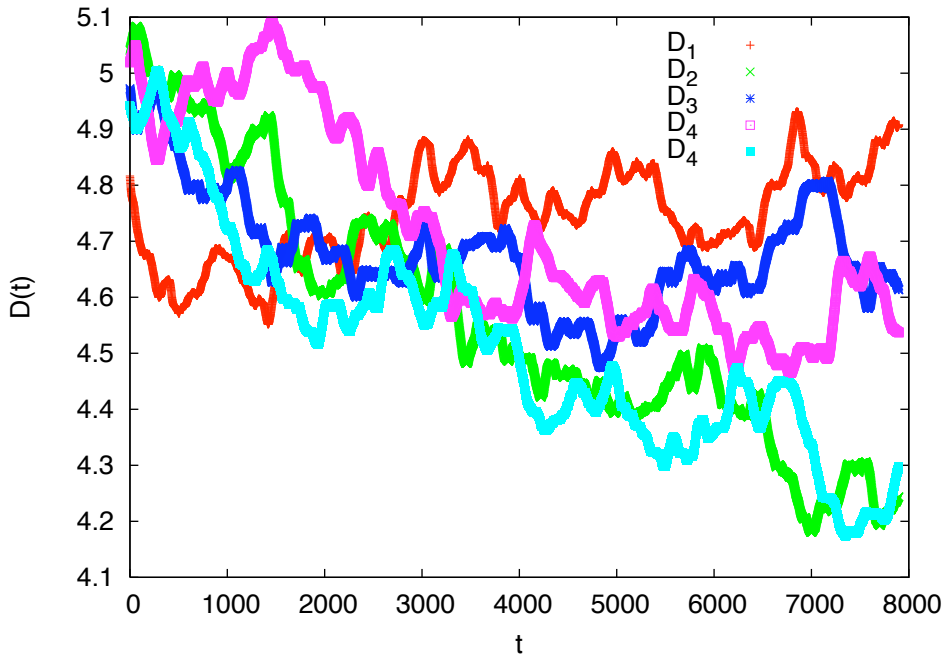

Figure 4.13: Average distances within groups of colloids versus time in a system without external force.

Figure 4.14: Colloids are making a zig-zag shape when they are moving due to an external force in a narrow channel.

placed at the head of the chain. One notices that the rate at which D_i increase varies monotonically with i. For example increasing rate of D_1 (located at the head of the chain) is maximum and that of D_5 (located at the tail) is minimum. However, this pattern is lost after a long time. Fig. 4.13 shows the results for an equivalent system but without any external force where no density discontinuity is expected. As it can be seen the average distances D_i are always fluctuating and show no systematic behaviour as in Fig. 4.12.

One may notice that the initial chain of the colloidal particles occupies only half of the length of the channel and the rest is empty (of colloidal particles). We consider this initial configuration as a density discontinuity at the macroscopic level. By considering the time evolution of successive distances between particles in Fig. 4.12, we realize that the initial discontinuity of the particle density is dissipating at the head of the chain and remains sharp at the tail. Since the lifetime of the shock increases when the number of particles N_c and the size L_x goes to infinity, we expect that the density discontinuity survives for longer time in these systems where the system is large enough.

4.6 Conclusions

In this chapter, our model of confined colloidal suspension in the presence of an external force has been investigated. The motion of colloidal particles in the presence of a gravitational force (sedimentation) is considered in particular. The dependence of the sedimentation velocity of colloidal particles on volume fraction is discussed. We varied the volume fraction by changing the size of the system. For two cases where either two or three colloids were involved, we observed that the sedimentation velocity increases with volume fraction. However, changing volume fraction by adjusting the length at the system may give rise to finite size effect for large volume fractions (and small system sizes). In order to avoid this effect, we kept the system large and changed the volume fraction by changing the number of colloids in the system. Here we found a linear increase of sedimentation velocity with volume fraction. Hence we found that within the range of volume fraction that we considered, our outcome is in contrast with the earlier studies that report the reduction of settling speed of colloidal suspension with the increase of the volume fraction. We interpreted this inconsistency as a result of the confined movement of the colloidal suspension in the system. Since sedimenting colloidal particles are placed in a narrow channel, they form a bead-like alignment of particles. This bead of colloidal particles affects the flow of the fluid in the direction of sedimentation and enhances the hydrodynamic forces. Increasing the number of colloids enhances this effect and hence yields a higher settling speed.

We compared the results obtained above for sedimentation velocity of colloids as a function of volume fraction with the case where the hydrodynamic interaction is absent. The hydrodynamic interaction is switched-off by modelling the fluid using a random-solvent algorithm. We found that when the hydrodynamic interaction is turned off in the system, the average settling speed will lose its correlation to the concentration of particles, i.e., there is no dependence of sedimentation velocity on volume fraction, in contrast with the case with HI as discussed in the previous paragraph.

We found that for the range of gravitational force are used, the Reynolds number is low enough to obtain a laminar flow regime. We obtained a linear increase of the sedimentation velocity of colloids as a function of gravitational force. This yields a constant mobility for the system and indicates that the fluid is in the laminar regime.

The collective behaviour of colloidal particles is considered in a case where the initial positions of colloidal particles are set such that they are placed very close to each other and hence represent a chain. We noticed the formation of the zig-zag shape in this chain of sedimenting colloidal particles in the channel. Calculating the average distances between two neighboring colloids showed that the distances between the particles located at the head of the chain increase faster than to those at the tail. This systematic behaviour disappears in the absence of an external force. From this observation, we conclude that this systematic trend of the coarse-grained averaged distances is a signature for an existence of shock in the system. However, obtaining a better understanding requires considering simulations in much larger systems with a much higher number of colloids which was not feasible because of the limitation of computing power.

5 Shock solution in two approaches

Shock solution

Here, our investigations concerning the shock solution, which are obtained using two approaches, are summarized. A shock is defined as a density discontinuity that is moving with a deterministic speed, determined by mass conservation. The Burgers equation specifies the spatial evolution of the macroscopic state of the reaction-diffusion systems. This equation is in general non-linear and exhibits shocks in some cases. This means that the solution of the macroscopic equations may develop a discontinuity even if the initial particle density is smooth. In other words, in these systems phase separation may occur. The shock therefore represents the interface between the two thermodynamically distinct phases. For the asymmetric exclusion process (ASEP), the time evolution of the particle density on the macroscopic Euler scale is described by the Burgers equation which may develop shocks.

In chapter 2, using an analytical approach, we determined the family of reaction-diffusion models with travelling shock solutions on the finite lattice. We found that the hydrodynamic equation is nonlinear and therefore admits shock solutions. These shocks are internally sharp and behave like collective single-particle excitations on the lattice scale. In other words, the shock represents a biased random walk. In section (2.4) where an exclusion process with binary degrees of freedom is considered, calculating the stationary current yielded Eq.(2.127). As derived in section (2.4)

$$J(\rho) = (p - q)\rho(1 - \rho), \tag{5.1}$$

which is basically the expression of current for the ASEP with the hopping rates p and q.

In our simulation model of colloidal suspension, we found a linear increase of sedimentation velocity of colloids as a function of density of colloidal particles in chapter 4. This is obtained in a co-moving reference frame. We have shown that this is also valid for the mean average velocity of colloids in the frame at rest (see Fig. 5.1).

Hence one can write the sedimentation velocity in a co-moving frame as

$$v_s = c\rho + c' - v_{cm}, \tag{5.2}$$

where c and c' are constant. Thus the expression for the current yields as

$$J(\rho) = \rho(c\rho + c' - v_{cm}). \tag{5.3}$$

which resembles Eq.(5.1) for ASEP where p set to $c/(v_{cm} - c')$ and q set to zero. In particular, note that $q = 0$ is valid for our SFD model. Hence the model can be considered as the ASEP model on a macroscopic level and can be coarse-grained by solving Burgers equation.

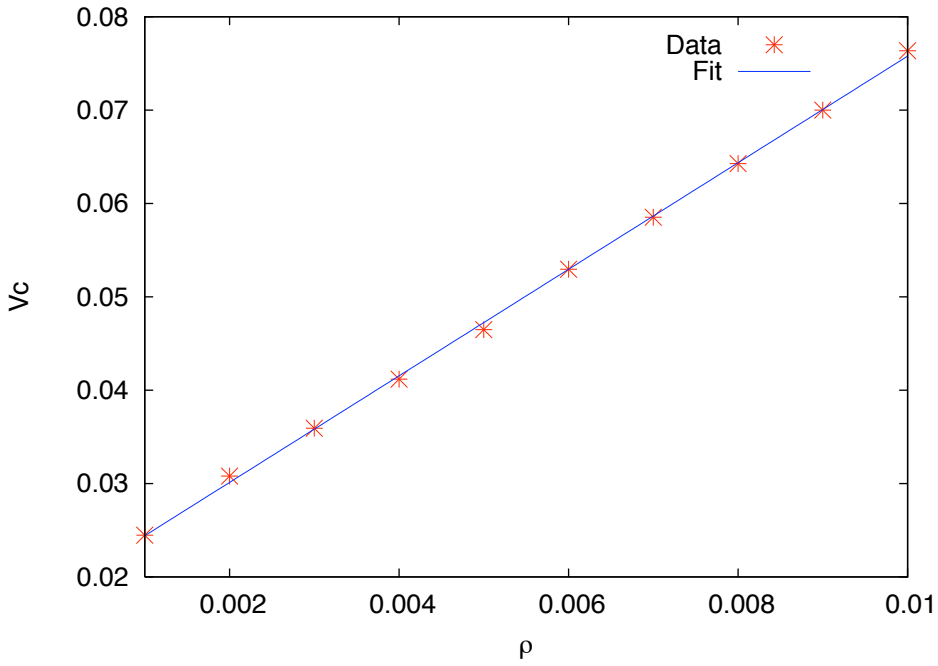

Figure 5.1: Average colloids velocity as a function of density of colloids for a system of size 100×10 in the reference frame at rest, which shows a linear increase. The data fitted to a function $f(\rho) = c\rho + c'$, where $c = 5.71$ and $c' = 0.019$.

The investigation for average distances of colloids (see section 4.5) showed that colloids tends to develop a density discontinuity. This can be a sign of the existence of a shock. However, it is not possible to obtain a sharp pattern

for a shock similar to that found in the lattice gas model in chapter 2. In the lattice gas model, the system has a product measure and it can support a sharp variation of density, but for colloidal suspension, this is not possible. To have a more macroscopic description, a larger numbers of colloidal particles should be considered. However, this would make our simulation very time consuming.

Bibliography

[1] W. B. Russel, D.A. Saville, and W. R. Schowalter. *Colloidal Dispersions*. Cambridge University Press, Cambridge, England, 1989.

[2] G.M. Whitesides and A.D. Stroock. *Phys. Today*, **54**:42, 2001.

[3] B. Alberts, D. Bray, A. Johnson, J. Lewis, M. Raff, K. Roberts, and P. Walter. *Essential Cell Biology*. Garland Publishing, New York, 1989.

[4] R. M. Barrer. *Zeolites and Clay Minerals as Sorbents and Molecular Sieves*. Academic Press, London, 1978.

[5] C. Bean. *Macroscopic Systems and Models, edited by G. Eisenmann, Membrances*. Marcel Dekker, New York, 1972.

[6] R. B. Jones. *J. Chem. Phys.*, **121**:483, 2004.

[7] S. Bhattacharya, J. Blawzdziewicz, and E. Wajnryb. *J. Fluid Mech.*, **541**:263, 2005.

[8] M. Zurita-Gotor, J. Blawzdziewicz, and E. Wajnryb. *J. Rheol.*, **51**:71, 2007.

[9] P. J. A. Janssen and P. D. Anderson. *Phys. Fluids*, **19**:043602, 2007.

[10] O. B. Usta, J. Butler, and A. J. C. Ladd. *Phys. Rev. Lett*, **98**:098301, 2007.

[11] Y. L. Chen, M. D. Graham, J. J. de pablo, G.C. Randall, M. Gupta, and P. S. Doyle. *Phys. Rev. E*, **70**:060901(R), 2004.

[12] P. Habdas and E.R. Weeks. *Curr. Opin. Colloid Interface Sci.*, **7**:196, 2002.

[13] D. G. Grier. *Curr. Opin. Colloid Interface Sci.*, **2**:264, 1997.

[14] E. R. Dufresne, D. Altman, and D. G. Grier. *Europhys. Lett.*, **53**:264, 2001.

[15] P. N. Segre, E. Herbolzheimer, and P. M. Chaikin. *Phys. Rev. Lett.*, **79**:2574, 1997.

[16] S. Khademi, J. O'Connell III, J. Remis, Y. Robles-Colmenares, L.J. Miercke, and R.M. Stroud. *Science*, **305**:1587, 2004.

[17] B. Cui, H. Diamant, B. Lin, and S. A. Rice. *Phys. Rev. Lett*, **92**:258301, 2004.

[18] A. Alvarez, E. Clement, and R. Soto. *Phys. Fluids*, **18**:083301, 2006.

[19] T. Beatus, T. Tlusty, and R. Bar-Ziv. *Nature Physc.*, **2**:743, 2006.

[20] M. Baron, J. Blawzdziewicz, and E. Wajnryb. *Phys. Rev. Lett.*, **100**:174502, 2008.

[21] Q-H. Wei, C. Bechinger, and P. Leiderer. *Science*, **287**:625, 2000.

[22] R. Arratia. *Ann. Prob.*, **11**:362, 1983.

[23] V. Kukla, J. Kornatowski, D. Demuth, H.Pfeifer I. Girnus, L.V.C Rees, S. Schunk, K. Unger, and J. Kärger. *Science*, **272**:702, 1996.

[24] C. Lutz, M. Kollmann, P. Leiderer, and C. Bechinger. *J. Phys. Condens. Matt.*, **16**:S4075, 2004.

[25] G. Coupier, M.S. Jean, and C. Guthmann. *Phys. Rev. E*, **73**:S4075, 2006.

[26] G.M. Schütz. *Int. J. Mod. Phys. B*, **11**:197, 1997.

[27] A. Basu and D. Chowdhury. *Physical Review E*, **75**:021902, 2007.

[28] T.E. Harris. *J. Appl. Prob.*, **2**:323, 1965.

[29] H. van Beijeren, K.W. Kehr, and R. Kutner. *Phys. Rev. B.*, **28**:5711, 1983.

[30] S. S. Nivarthi, A. V. McCormick, and H.T. Davis. *Chem. Phys. Lett.*, **229**:297, 1994.

[31] R. Radhakrishnan and K. E. Gubbins. *Phys. Rev. Lett.*, **79**:2847, 1997.

[32] K. Hahn and J. Kärger. *J. Phys. Chem. B.*, **5766**:102, 1998.

[33] A. Brzank and G.M. Schütz. *Appl. Catalysis A*, **288**:194, 2005.

[34] M. Kollmann and G. Nägele. *J. Chem. Phys.*, **113**:7672, 2000.

[35] M.-C. Miguel and R. pastor Satorras. *Europhys. Lett.*, **54**:45, 2001.

[36] M. P. Brenner. *Phys. Fluids*, **11**:754, 1999.

[37] G.M. Schütz. *J. Phys. A*, **36**:R339, 2003.

[38] G.M. Schütz. *Diffusion Fundamentals*, **2**:5, 2005.

[39] K. Nishinari, Y. Okada, A. Schadschneider, and D. Chowdhury. *Phys. Rev. Lett.*, **95**:118101, 2005.

[40] P. Fife. *Mathematical aspects of reacting and diffusing systems, Lecture Notes in Biomath.*, volume **28**. Springer, Berlin, 1979.

[41] T.M. Liggett. *Stochastic Interacting Systems: Voter, Contact and Exclusion Processes*. Springer, Berlin, 1999.

[42] G.M. Schütz. *Phase Transitions and Critical Phenomena*, volume **19**. C. Domb and J. Lebowitz (eds.) Academic, London, 2001.

[43] J. Krug. *Phys. Rev. Lett.*, **67**:1882, 1991.

[44] G. Schütz and E. Domany. *J. Stat. Phys.*, **72**:277, 1993.

[45] B. Derrida, M.R. Evans, V. Hakim, and V. Pasquier. *J. Phys. A.*, **26**:1493, 1993.

[46] A.B. Kolomeisky, G.M. Schütz, E.B. Kolomeisky, and J.P. Straley. *J. Phys. A.*, **31**:6911, 1998.

[47] V. Popkov and G.M. Schütz. *Europhys. Lett.*, **48**:257, 1999.

[48] D. Helbing. *Rev. Mod. Phys.*, **73**:1067, 2001.

[49] J.M. Burgers. *The Non Linear Diffusion Equation.* Reidel, Boston, 1974.

[50] C. Kipnis and C. Landim. *Scaling Limits of interacting particle systems.* Springer, Berlin, 1999.

[51] P.A. Ferrari, C. Kipnis, and E. Saada. *Ann. Prob.*, **19**:226, 1991.

[52] B. Derrida, J.L. Lebowitz, and E.R. Speer. *J. Stat. Phys.*, **89**:135, 1997.

[53] B. Derrida, S. Goldstein, J.L. Lebowitz, and E. R. Speer. *J. Stat. Phys.*, **93**:547, 1998.

[54] P.A. Ferrari and L.R.G. Fontes. *Probab. Theory Relat. Fields*, **99**:305, 1994.

[55] V. Belitsky and G.M. Schütz. *El. J. Prob.*, **7**:11, 2002.

[56] K. Krebs, F.H. Jafarpour, and G.M. Schütz. *New J. Phys.*, **5**:145, 2003.

[57] C. Pigorsch and G.M. Schütz. *J. Phys. A*, **33**:7919, 2000.

[58] M. Balazs. *J. Stat. Phys.*, **105**:511, 2001.

[59] A. Rákos and G.M. Schütz. *J. Stat. Phys.*, **117**:55, 2004.

[60] M. Balazs. *J. Stat. Phys.*, **117**:77, 2004.

[61] F. H. Jafarpour. *Physica A*, **358**:413, 2005.

[62] M. Arabsalmani and A. Aghamohammadi. *Phys. Rev. E*, **74**:011107, 2006.

[63] C.R. Doering, M.A. Burschka, and W. Horsthemke. *J. Stat. Phys.*, **65**:953, 1991.

[64] H. Hinrichsen, K. Krebs, and I. Peschel. *Z. Phys. B.*, page 105, 1996.

[65] D. Ben-Avraham. *Phys. Lett. A.*, **247**:53, 1998.

[66] M. Paessens and G.M. Schütz. *New. J. Phys.*, **6**:120, 2004.

[67] R. Glauber. *J. Math. Phys.*, **4**:294, 1963.

[68] O.J. O'Loan, M.R. Evans, and M.E. Cates. *Europhys. Lett.*, **42**:137, 1998.

[69] K. Nishinari, D. Chowdhury, and A. Schadschneider. *Phys. Rev. E*, **67**:036120, 2003.

[70] M. Dudzinski and G.M. Schütz. *J. Phys. A*, **33**:8351, 2000.

[71] Z. Nagy, C. Appert, and L. Santen. *J. Stat. Phys.*, **109**:623, 2002.

[72] J. de Gier and F.H.L. Essler. *Phys. Rev. Lett.*, **95**:240601, 2005.

[73] R.A. Fisher. *Ann. Eugenics*, **7**:353, 1937.

[74] J.L. Lebowitz, E. Presutti, and H. Spohn. *J. Stat. Phys.*, **51**:841, 1988.

[75] F. Tabatabaei and G.M. Schütz. *Phys. Rev. E.*, **74**:051108, 2006.

[76] F. Tabatabaei and G.M. Schütz. *Diffusion Fundamentals*, **4**:5.1, 2006.

[77] V. Privman. *Nonequilibrium Statistical Mechanics in One Dimension*. Cambridge, Cambridge University Press, 1997.

[78] G.M. Schütz, R. Ramaswamy, and M. Barma. *J. Phys. A.*, **29**:837, 1996.

[79] H. Spohn. *Large-Scale Dynamics of Interacting Particles*. Springer, Berlin, 1991.

[80] M. Robert and B. Widom. *J. Stat. Phys.*, **37**:419, 1984.

[81] M.R. Evans, S.N. Majumdar, and R.K.P. Zia. *J. Phys. A.*, **37**:L275, 2004.

[82] M.R. Evans, S.N. Majumdar, and R.K.P. Zia. *J. Stat. Phys.*, **123**:357, 2006.

[83] S. Katz, J. L. Lebowitz, and H. Spohn. *J. Stat. Phys.*, **34**:497, 1984.

[84] T. Antal and G.M. Schütz. *Phys. Rev. E*, **62**:83, 2000.

[85] J. F. Morris. *Phys. Fluids*, **13**:2457, 2001.

[86] J. Santana-Salona and J. L. Arauz-Lara. *Phys. Rev. Lett*, **87**:038302, 2001.

[87] M. E. Cates, K. Stratford, R. Adhikari, P. Stansell, J-C. Desplat, I. Pagonabarraga, and A. J. Wagner. *J. Phys.: Condens. Matter*, **16**:S3903, 2004.

[88] M. Hecht, J. Harting, T. Ihle, and H. J. Herrmann. *Phys. Rev. E*, **72**:011408, 2005.

[89] J. K. G. Dhont. *An introduction to the dynamics of colloids*. Elsevier, Amsterdam, 1996.

[90] J. L. Barrat and J.P. Hansen. *Basic Concepts For Simple Liquids*. Cambridge University Press, Cambridge, England, 2003.

[91] A. J. Archer. *J. Phys.: Condens. Matter*, **17**:1405, 2005.

[92] A. Malevanets and R. Kapral. *J. Chem. Phys.*, 110:8605, 1999.

[93] T. Ihle and D. M. Kroll. *Phys. Rev. E*, **63**:020201(R), 2001.

[94] A. Malevanets and R. Kapral. *J. Chem. Phys.*, 112:7260, 2000.

[95] Y. Inoue, Y. Chen, and H. Obashi. *J. Stat. Phys.*, **107**:85, 2002.

[96] H. Lee and R. Kapral. *Physica A*, **298**:56, 2001.

[97] J. T. Padding and A. A. Louis. *Phys. Rev. Lett.*, **93**:220601, 2004.

[98] R. Pesché, M. Kollmann, and G. Nägele. *Phys. Rev. E*, **64**:052401, 2001.

[99] R. Pesché and G. Nägele. *Phys. Rev. E*, **62**:5432, 2000.

[100] T. Beatus, T. Tlusty, and R. Bar-ziv. *Nature Phys.*, **2**:743, 2006.

[101] S. Bhattacharya, J. Blawzdziewicz, and E. Wajnryb. *Phys. Fluids*, **18**:053301, 2006.

[102] J. Pathak and K. B. Migler. *Langmuir*, **19**:8667, 2003.

[103] E. Allahyarov and G. Gompper. *Phys. Rev. E*, **66**:036702, 2002.

[104] N. Kikuchi, C. M. Pooley, J. F. Ryder, and J. M. Yeomans. *J. Chem. Phys.*, **119**:6388, 2003.

[105] M. Ripoll, K. Mussawisade, R. G. Winkler, and G. Gompper. *Europhys. Lett.*, **68**:106–112, 2004.

[106] K. Mussawisade, M. Ripoll, R. G. Winkler, and G. Gompper. *J. Chem. Phys.*, **123**:144905, 2005.

[107] M. Ripoll, K. Mussawisade, R. G. Winkler, and G. Gompper. *Phys. Rev. E*, **72**:016701, 2005.

[108] H. Löwen J. T. Padding, A. Wysocki and A. A. Louis. *J. Phys. Condens. Matter*, **17**:S3393, 2005.

[109] T. Ihle and D. M. Kroll. *Phys. Rev. E*, **67**:066706, 2003.

[110] D. J. Tritton. *Physical Fluid Dynamics*. Oxford science publications, Oxford, 1988.

[111] A. Lammura, G. Gompper, T. Ihle, and D. M. Kroll. *Europhys. Lett.*, **56**:319, 2001.

[112] T. Ihle, E. Tüzel, and D. M. Kroll. *Phys. Rev. E*, **70**:035701(R), 2004.

[113] B. J. Alder and T.E. Wainwright. *J. Chem. Phys.*, **27**:1208, 1957.

[114] B. J. Alder and T. E. Wainwright. *J. Chem. Phys.*, **31**:459, 1959.

[115] F. H. Stillinger and A. Rahman. *J. Chem. Phys.*, **60**:1545, 1974.

[116] J. A. McCammon and B. R. Gelin M. Karplus. *Nature*, **267**:585, 1977.

[117] M. P. Allen and D. J. Tildesely. *Computer Simulation in Chemical Physics*. Klumer Academic Publisher, Dordrecht, 1993.

[118] M. Kartunnen, A. Lukkarien, and I. Vattulainen. *eds, Novel Methods in Soft Matter Simulations, Lect. Notes Phys. 640*. Springer-Verlag, Berlin, 2004.

[119] R. Car and M. Parrinello. *Phys. Rev. Lett.*, **55**:2471, 1985.

[120] J. P. Hansen. *Theory of simple liquids*. Academic press, INC., London, 1986.

[121] J. D. Weeks, D. Chandler, and H. C. Anderson. *J. Chem. Phys.*, **54**:5237, 1971.

[122] T. Schweizer. *Molecurdynamik Simulationen von Ketten variabler Steifigkeit zwischen Grenzflächen*. Diplomarbeit, University of Ulm, 1996.

[123] R. Hentschke and R. G. Winkler. *J. Chem. Phys.*, **99**:5528, 1993.

[124] L. Verlet. *Phys. Rev.*, **159**:98, 1967.

[125] R. G. Winkler, V. Kraus, and P. Reineker. *J. Chem. Phys.*, **102**:9018, 1995.

[126] D. Frenkel and B. Smit. *Understanding Molecular Simulations*. Academic press, San Diego, 2002.

[127] M. Tuckermann, B. J. Berne, and G.J. Martyna. *J. Chem. Phys.*, **97**:1990, 1992.

[128] H. C. Anderson. *J. Chem. Phys.*, **72**:2384, 1980.

[129] R. L. Rowley P. S. Crozier. *Fluid Phase Equilibria.*, **193**:53, 2002.

[130] G. Bussi, D. Donadio, and M. M. Parrinello. *J. Chem. Phys.*, **126**:014101, 2007.

[131] L. D. Landau and E. M. Lifshitz. *Fluid Mechanics*. Pergamon Press, 1959.

[132] G. K. Batchelor. *J. Fluid. Mech.*, **52**:245, 1972.

[133] M. Rex and H. Löwen. *Eur. Phys. J. E*, **4**:10274, 2008.

[134] J. Happel and H. Brenner. *Low Reynolds Number Hydrodynamics*. Prentice-Hall, Englewood Cliffs, NJ, 1973.

[135] J. T. W. M. Tissen, J. Drenth J. G. E. M. Fraaije, and H. J. C. Berendsen. *Acta Coryst.*, **D50**:569, 1994.

[136] E. Wajnryba, P. Szymczak, and B. Cichocki. *J. Chem. Phys.*, **112** :2548, 2000.

[137] M. Reichert and H. Stark. *Phys. Rev. E.*, **69** :031407, 2004.

[138] M. Smoluchowski. *Proc. 5th Intern. Cong. Math.*, **2**:192, 1912.

[139] J. M. Burgers. *Proc. Kon. Nederl. Akad. Wet.*, **44**:1045, 1942.

[140] R. H. Davis. *Sedimentation of Small Particles in a viscous Fluid*. Computational Mechanics Publications, Southampton, 1996.

[141] M. Ripoll, R.G. Winkler, , and G. Gompper. *Eur. Phys. J. E*, **23** :349, 2007.

[142] V. Ramachandran, R. Venkatesan, G. Tryggvason, and H. S. Fogler. *J. Coll. Int. Sci.*, **229**:311, 2000.

[143] J. P. Matas, J. F. Morris, and É. Guazzeli. *Phys. Rev. Lett.*, **90**:014501, 2003.

[144] P. Szymczak and B. Cichocki. *Europhys. Lett.*, **59** :465, 2002.

[145] E. Wajnryba, P. Szymczak, and B. Cichocki. *Physica A.*, **335** :339, 2004.

Acknowledgments

I would like to express my gratitude to Prof. Gunter M. Schütz for the supervision of this thesis. He introduced me into the topic, gave many useful suggestions and was open to discussions.
Prof. Ulf-G. Meißner is thanked for his willingness to be the second referee for this work.
I thank the whole group of "IFF-Theory II" in research center Jülich for help and companionship. Foremost I wish to thank Prof. Roland Winkler for countless valuable discussions and useful suggestions. I would like to thank Sebastian Meßlinger for introducing me to the MPC simulation code. Also Dr. Hiroshi Noguchi and Sandra Frank are thanked for helping me about the simulation techniques.
My former office mate Dr. Rosemary Harris is acknowledged for many nice discussions and a pleasant atmosphere in our office.
During last year my office mate Dr. Sakuntala Chatterjee was the person that I could share ideas about physics and beyond. She is acknowledged also for reading the manuscript.
I would like to thank my husband Kourosh Rahmanizadeh for supporting me and also for interesting scientific discussions about my PhD projects. Without his support and sympathy I would not have been able to successfully complete my thesis.
I am deeply grateful to my parents who not only raised my interest in science but also provided support in every way.

Summary

Summary

In this thesis the systems in quasi-one-dimensional geometries using two different approaches is investigated. As the analytical approach, one-dimensional reaction-diffusion systems are investigated. The two-component models which satisfy some specified conservation laws are considered. It is found that three-states lattice gases with a single local conservation law can be classified into two families, one where the function is degenerate, i.e., takes the same value for two different states, another where the conserved quantity is a linear nondegenerate function of the occupation variable. This two groups of families are investigated in this work. For the first group, the hydrodynamic equation is obtained nonlinear and therefore admits shock solutions. For the second group, for open systems with different boundary fugacities, a complete list of models where the shock performs a biased random walk on the lattice is found.

As the second approach, a simulation method is used to model a suspension of colloidal particles in a narrow channel. To this end, a hybrid simulation scheme which couples a Molecular Dynamics simulation method to a MPC fluid, which is a coarse-grained model to describe fluid dynamics, is used. Then, the motion of colloidal particles in the presence of the gravitational force (sedimentation) is considered. The dependence of the sedimentation velocity of colloidal particles on volume fraction is discussed. The results which obtained for sedimentation velocity of colloids as a function of volume fraction are compared with the case without hydrodynamic interactions. The Reynolds numbers for a range of gravitational force are determined. A linear increase of the sedimentation velocity of colloids as a function of gravitational force is obtained. The formation of the zig-zag shape in the chain of sedimenting colloidal particles in the channel is noticed. A systematic behaviour of the average distances between successive colloids in the presence of the external force is showed. This behaviour is discussed being as a sign for developing a density discontinuity in the system.

The current density of colloidal particles is determined and existing shock solutions of the system in the two approaches, are discussed.